THIRD-ORDER NONLINEAR OPTICAL PROPERTIES OF CONJUGATED POLYMERS AND BLENDS

A Dissertation
Presented to
The Academic Faculty

by

San-Hui Chi

In Partial Fulfillment
of the Requirements for the Degree
Doctorate of Philosophy in the
School of Chemistry and Biochemistry

Georgia Institute of Technology
December 2009

THIRD-ORDER NONLINEAR OPTICAL PROPERTIES OF CONJUGATED POLYMERS AND BLENDS

Approved by:

Dr. Joseph W. Perry, Advisor
School of Chemistry and Biochemistry
Georgia Institute of Technology

Dr. Uwe Bunz
School of Chemistry and Biochemistry
Georgia Institute of Technology

Dr. Seth R. Marder
School of Chemistry and Biochemistry
Georgia Institute of Technology

Dr. Rick Trebino
School of Physics
Georgia Institute of Technology

Dr. Andrew Lyon
School of Chemistry and Biochemistry
Georgia Institute of Technology

Date Approved: November 6, 2009

To my parents, my brother, and Vince.

ACKNOWLEDGEMENTS

It seems just like yesterday that I arrived in the Hartsfield International Airport at 6 am, July 26th, 2003. Now, 3 am, October 18th, 2009, I am still awake and thinking how to express my deeply thanks to those people who made this thesis work possible.

I would like to show my deep gratitude to my advisor, Dr. Joseph Perry, for his trust, faith, and confidence in me. He has been always very supportive and understanding whenever I need his help and guidance for my research work. It has been a very enjoyable experience to learn after Joe and work with him, especially, when he shared some pieces of delicious Belgium chocolate with me during some meetings.

I would also like to thank Dr. Joel Hales for his mentorship, support, and friendship. When I started my research in Joe's group, I knew nothing about Nonlinear Optics and it was Joel who has guided me, very patiently, to explore the field of nonlinear optics, to learn the characterization techniques, and to study the nonlinear optical materials.

Besides research work, both Joe and Joel also have been set up very good examples for me to learn the skills in English presentation and writing. As a non-native English speaker, it was quite difficult for me to express myself. In these years, they both spent a lot of time correcting my English and showing me how to express my ideas and to tell the story. Especially, it was Joel who spent a tremendous amount of time to proof read my thesis and made my thesis read like English.

I would like to thank Dr. Seth Marder for his support in our collaboration research. I was quite intimidated and unconfident in myself at the first year in the

graduate school. One day, Seth told me: Be tougher. Since then, I started to realize that I have to be proactive if I want to have some achievement in my research and future career. After couple years, I found myself starting to learn his critical thinking and I started enjoying the conversation with him.

I would say, Joe, Joel, and Seth have been affected me a lot in developing my scientific attitude.

There are still many people I have to show my appreciation. I would like to thank Matteo Cozzuol, Matthew Sartin, Nisan Siegel, and Wojciech Haske for their support in my experiments and those beer-drinking parties. I also want to thank my girl friends, Wan-Ru Chen, Chen-Ju Lin, Shu-Chuan Lin, Xuan Zhang, and Xiaohong Zhang, for those wonderful girls nights and sharing my ups and downs during these years.

At the end, I want to give my deepest appreciation to my family for their full support. My parents have been constantly shipped my favorite snacks and Chinese Readers Digests from Taiwan and made me feel home in these years. My brother always chats with me on the messenger and sharing gossips. (I wish him the best for his graduate study in Heidelberg!) Vince has been supported me selflessly to pursue my dream in the research. Whenever I needed to work late in the lab or to work in the weekends, he always stayed with me to keep me accompanied. To my coming baby, thank you for being cooperative during my thesis writing!

TABLE OF CONTENTS

LIST OF TABLES

LIST OF FIGURES AND SCHEMES

LIST OF SYMBOLS

α_0	Linear absorption coefficient
$\tilde{\alpha}$	Hyperpolarizability
γ	2^{nd}-order hyperpolarizability
β	Two-photon absorption coefficient
c	Light speed in vacuum
σ	One-photon absorption cross section
δ	Two-photon absorption cross section
ε_0	Free-space permittivity
I	Intensity
L	Thickness (of sample)
λ	Wavelength
n_0	Linear refractive index
n_2	Nonlinear refractive index
N	number density
N_A	Avogadro number

$\Delta\phi$	nonlinearly-induced phase shift
ω	Frequency
A	Pre-exponential factor
τ	lifetime
τ_p	pulse width
ω_0	beam waist

SUMMARY

This thesis is concerned with the material processing, photophysical and third-order nonlinear optical responses, and applications of a set of conjugated polymers in the telecommunication regions.

Polyacetylene-based $\chi^{(3)}$ materials were chosen as candidates for all-optical signal and image processing. Substituted polyacetylenes were obtained using ring-opening metathesis polymerization of mono-substituted cyclooctatetraenes. Polymerization and processing conditions have been developed to generate thick, large-area films possessing large third-order nonlinearities in the telecommunication bands. The good optical quality of a 200 μm thick substituted polyacetylene film allowed for image correlation via off-resonant degenerated four-wave mixing with improved diffraction efficiency.

Poly(2-methoxy-5-(2-ethyl-hexyloxy)-(phenylene vinylene)) (MEH-PPV) and (6,6)-phenyl-C_{61}-butyric acid methyl ester (PCBM) composites showed strong nonlinear absorption and potential as optical limiters in the region of 700-900 nm. High optical quality, thick film of MEH-PPV:PCBM with the plasticizer dioctylphthalate (DOP) were made. Optical limiting of femtosecond and nanosecond pulses in the near infrared on these composites showed strong power suppression over a broad temporal regime. Femtosecond and nanosecond transient studies on the same thick MEH-PPV:PCBM:DOP composite films and the experimental results showed evidence for the photogeneration of radical ions as being responsible for the enhanced nonlinear absorption and strong optical suppression in the near infrared.

Dithienopyrrole-based donor-acceptor copolymers with narrow bandgap showed strong nonlinear absorption and potential as optical limiters in the telecommunication wavelengths. Molecular engineering was applied to manipulate the spectral overlap of two-photon absorption and subsequent nonlinear absorptions. Femtosecond transient spectroscopy showed near infrared transient absorption and 22 – 61% yields of photogenerated charge-transfer species depending on donor-acceptor coupling strength. Torsional fluctuations of the backbone structure potentially affected the excited state behavior. Evidence suggests that ultrafast relaxation occurs to ground state and to long-lived charge-transfer state from the initially excited state. The dispersion of nonlinear absorption measured using the Z-scan method revealed large two-photon absorption cross sections of these polymers in the telecommunication region. Large suppression of nanosecond pulses at 1064 nm was achieved.

CHAPTER 1

INTRODUCTION

1.1 π-Conjugated Polymers with Promising Third-Order Nonlinear Optical Properties for Photonic Applications

Since Alan MacDiarmid, Hideki Shirakawa, and Alan Heeger discovered conducting polyactylene in 1970's [1, 2], the novel properties of conjugated polymers have generated a tremendous amount of effort devoted to research involving the fundamental knowledge, synthesis, characterization, and application of this category of polymers. Due to the nature of the electronic configuration, conjugated polymers are enriched with unpaired π electrons that are highly delocalized along the conjugated backbones. (**Scheme 1.1**) Such enrichment of delocalized π electrons leads to semiconductor-like electrical and optical properties of conjugated polymers. Compared to the inorganic semiconductors, conjugated polymers possess the attractive mechanical properties and processing advantages of organics and are thus seen as promising candidates in the fields of organic photovoltaics [3] as well as various photonic applications [4-7].

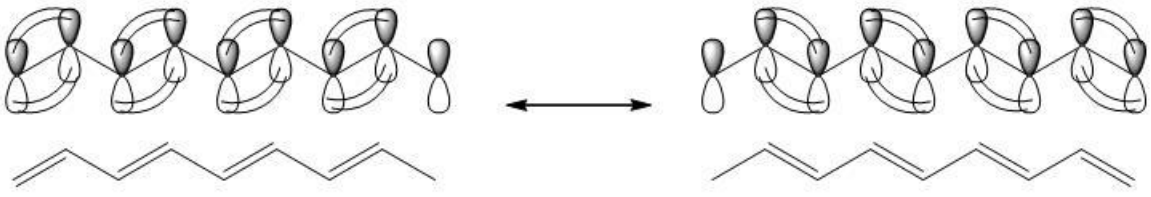

Scheme 1.1. Illustration of the resonant structures of a conjugated polymer backbone.

Several families of conjugated polymers such as polyacetylenes [7-12], poly(phenylene vinylene)s [13-15], polythiophenes [16], and poly(phenylene ethynylene)s [17] have been shown to possess promising third-order nonlinear optical properties for various photonic applications like all-optical switching, image recognition, and optical limiting. The performance of a conjugated polymer in photonic applications largely relies on its third-order nonlinear optical properties, such as the nonlinear refractive index and nonlinear absorption, which will be discussed in detail in Chapter 2.

Many approaches have been exploited to engineer the nonlinear optical response in conjugated polymers [4-6] including the extension of conjugation length [18], the incorporation of donors and/or acceptors to the conjugated backbone [19-21], and the increase in planarity of the conjugated backbone. A comparison between oligomers and conjugated polymers of phenylenevinylene was performed by Mathy et al. and it was evidenced that the magnitude of the third-order nonlinearities increases as the conjugation length increases until a saturation chain length of several tens of nanometers was achieved [18]. Marder and Perry et al. [19, 21] showed the incorporation of donors and acceptors into conjugated molecules could induce a charge redistribution upon photoexcitation resulting in exceptionally large third-order nonlinearities and two-photon absorption cross sections. Zhao et al. [22, 23]and Reinhardt et al. [24] showed that replacing conjugated linkers between donors and acceptors with electron rich and more polarizable bridge molecules such as thiophene units can also significantly enhance the third-order nonlinear optical properties.

1.2 Conjugated Polymers in All Optical Signal Processing Applications

With the growing knowledge of molecular design and engineering and material processing, many attempts invovling the development of organic or organic-inorganic hybrid devices for various photonic applications have been reported [4-7]. Here, a brief description of the main categories of all-optical signal processing applications and their figures-of-merit or specific material requirements will be given.

1.2.1 All-Optical Switching

In the past two decades, the need for ultrafast optical communication has boosted the research on all-optical switching that utilizes third-order nonlinear optical materials with large nonlinear refractive indices, n_2 [6, 26, 27]. For a nonlinear material to perform satisfactorily in all-optical switching applications, the figures of merit were defined as

$$W = \frac{n_2 I_0}{\alpha\lambda} > 1 \; and \; T = \frac{\beta\lambda}{n_2} < 1 \qquad \text{(Eq. 1.1)}$$

where α and β are the one-photon and two-photon absorption coefficients, respectively, I_0 is the operating light intensity, and λ is the wavelength. As indicated in the figures of merit, both one-photon and two-photon absorption can introduce losses in a switching device and are therefore limitations to the performance of the integrated nonlinear optical material. Conjugated polymers such as polyphenylenevinylenes [28] have been reported with attractive figures of merit in the telecommunications regions. Furthermore, several conjugated polymer-based or organic-inorganic hybrid switching devices have been reported [27, 28].

1.2.2 Free-Space Signal Processing: Image Correlation

The application of image correlation utilizes the phenomena of optical phase conjugation, which is a process that involves a reflected beam that retraces the phase factor and propagation direction of the original beam following interaction within a nonlinear medium. A common implementation of optical phase conjugation involves the use of degenerate four-wave mixing (**Scheme 1.2**), which will be further described in Chapters 2 and 3. In this experimental setup, beam 1 is impressed with a reference image, beam 2 is impressed with a single or set of object images, and beam 3 remains unmodified. If the three beams are focused into a nonlinear medium with appropriate spatial and temporal overlap, beam 4 will be diffracted out of the nonlinear medium and reflect the cross correlation of beam 1 and beam 2. When the reference and object images match, a strong cross correlation signal will be observed. Conjugated polymers, such as polyacetylene derivatives, have been implemented successfully as potential materials for image correlation in both visible and near IR (telecommunication) regions [7, 11].

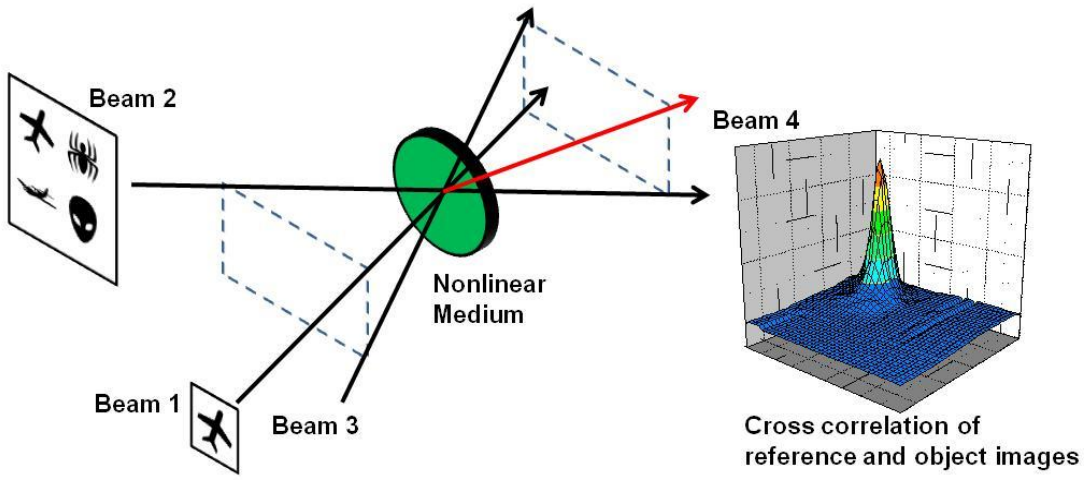

Scheme 1.2. Illustration of the setup of image correlation.

1.2.3 Optical Limiting

Along with the proliferation of the laser and the growth of laser tracking techniques, the need for an effective optical limiting system to protect human eyes and sensors is increasing. The essential requirements for OL materials are high linear transmission (T_0), low turn-on threshold (F_{Th}, defined here as the fluence where $T(F) = T_0/2$), high damage threshold, and large pulse energy suppression (S), which should be achieved over a wide spectral and temporal dynamic range (where S is defined as the reciprocal of nonlinear transmittance, T_F, just before the damage threshold). A figure-of-merit (FOM) for evaluating the pulse suppression performance of an optical limiter is defined here as $FOM = T_0S = T_0/T_F$.

Various third-order nonlinear processes, including nonlinear scattering, thermal nonlinearity, and nonlinear absorptions, have been utilized as potential passive optical limiting mechanisms due to their self-action nature. Research involving optical limiting (**Scheme 1.3**) started in the late 1960's by Geusic *et al.* [29] and Ralston *et al.* [30] with three-photon nonlinear absorption in inorganic semiconductors. In the early 1980's, organic materials were found to be new candidates in optical limiting systems. Van Stryland et al. demonstrated this at 1064 nm using self-focusing in CS_2 liquid to induce thermal nonlinearities and breakdown at high input fluences[31]. Blau *et al.* [32] , Perry *et al.* [33] and Shirk *et al.* [34] then utilized reverse saturable absorption, an effective third-order nonlinear response or $\chi^{(1)}$: $\chi^{(1)}$ process, in metal-centered porphyrin and phthalocyanine molecules. In 1995, Cha and Heeger *et al.* [16] first demonstrated the use of a fullerene-doped conjugated polymer (poly(3-octyl thiophene), P3OT) to enhance the nonlinear absorption via photo-induced charge transfer and free carrier absorption. Until

this point, the performance of most organic optical limiting systems was hindered by operating at wavelength regions in the vicinity of one-photon absorption causing strong linear transmission loss. Soon thereafter, Perry and Marder *et al.* [21, 35] and Prasad *et al.* [17, 36] initiated a series of studies developing organic conjugated molecules and polymers with large two-photon absorption cross sections. Furthermore, several demonstrations of enhanced optical limiting were achieved via two-photon absorption followed by subsequent excited state absorptions. Taking advantage of two-photon absorption, such optical limiting systems successfully retained higher linear transmittance at low input fluence than their one-photon absorption counterparts. At this point, a bis-donor stilbene system achieved 9X (9.5 dB) of suppression with FOM ~ 9 [21], which became the state-of-the art. Since then, few single-component optical limiting systems have been able to exceed the performance of this stilbene system until recently [37]. Hales *et al.* demonstrated a breakthrough with a temporally agile, broadband optical limiting system in the telecommunication region (1064-1550 nm) consisting of a lead bis(ethynyl)porphyrin polymer. A 60X (FOM ~ 54) suppression of femtosecond pulses as well as a 25X (FOM ~22) suppression of nanosecond pulses was achieved via two-photon absorption induced excited state absorptions which has likely become the current state-of-the art.

In addition to the many efforts spent on developing new nonlinear absorbing materials via molecular engineering[35, 38, 39], Perry et al. [40] and Van Stryland et al. [41] demonstrated that multi-component optical limiting systems could significantly improve the pulse-suppression capability. A tandem optical limiting system comprised of a nonhomogeneous distribution of nonlinear absorbing materials (blend films of indium

phthalocyanine and polymethal methacrylate) achieved 700X suppression of nanosecond pulses at 532 nm [40].

1.3 The Bottleneck of Device Application for Conjugated Polymers

Compared to low-molecular weight organic molecules, conjugated polymers are relatively insoluble and difficult to process due to their strong π-π interchain interactions [42-45]. Although approaches such as side-chain functionalization [46, 47] have been exploited for improved solubility of conjugated polymers, processing conjugated polymers to produce films with desirable optical quality for all-optical signal processing applications still remains an essential and difficult task. For applications such as image correlation and optical limiting, solid films with thicknesses of tens to hundreds of microns are required. Unfortunately, most conjugated polymers show significant scattering due to their semi-crystalline morphology as a result of strong π-π interchain interactions and therefore result in undesirable optical loss in such thick films. A common approach to process conjugated polymers into thick films is by implanting conjugated polymers into a guest-host system, in which the host is usually an optically inert polymer like polymethyl methacrylate or polycarbonate. However, the guest-host approach usually causes a dilution in the concentration of the optically active conjugated polymer and results in reduced nonlinear optical response as well as device performance.

1.4 Aim of this Thesis

This thesis comprises of a study of the processing, photophysical and nonlinear optical responses of a set of conjugated polymers and their potential applications. Substituted polyacetylenes were polymerized via a ring-opening metathesis polymerization method. The polymerization conditions were optimized to allow the fabrication of thick, optical quality polyacetylene films with large degenerate third-order nonlinearities which resulted in a successful demonstration of image correlation in the telecommunications spectral bands (1300 – 1550 nm). The composite of a poly(phenylene vinylene)-based conjugated polymer (MEH-PPV) and a C_{60} derivative (PCBM) were processed into optical quality thick films via the addition of a plasticizer. The nonlinear absorption of such ternary composite systems was enhanced via photo-induced charge transfer and the generation of free charge carriers. This composite was utilized in optical limiting applications (700 – 900 nm range) and showed strong power suppression over a broad temporal dynamic range. The suppression capability of this composite exceeded the best reported value for an optical limiting system in this spectral range to-date. Finally, a set of dithienopyrrole-based donor-acceptor conjugated co-polymers were investigated to understand the photophysics and nonlinear optical properties of these low-band gap materials. The results indicated structurally-related photophysical and nonlinear optical properties which might assist in the development of donor-acceptor based conjugate materials in the future. Furthermore, these low band-gap polymers showed potential as a new family of organic conjugated materials for photonic applications in the telecommunication spectral range.

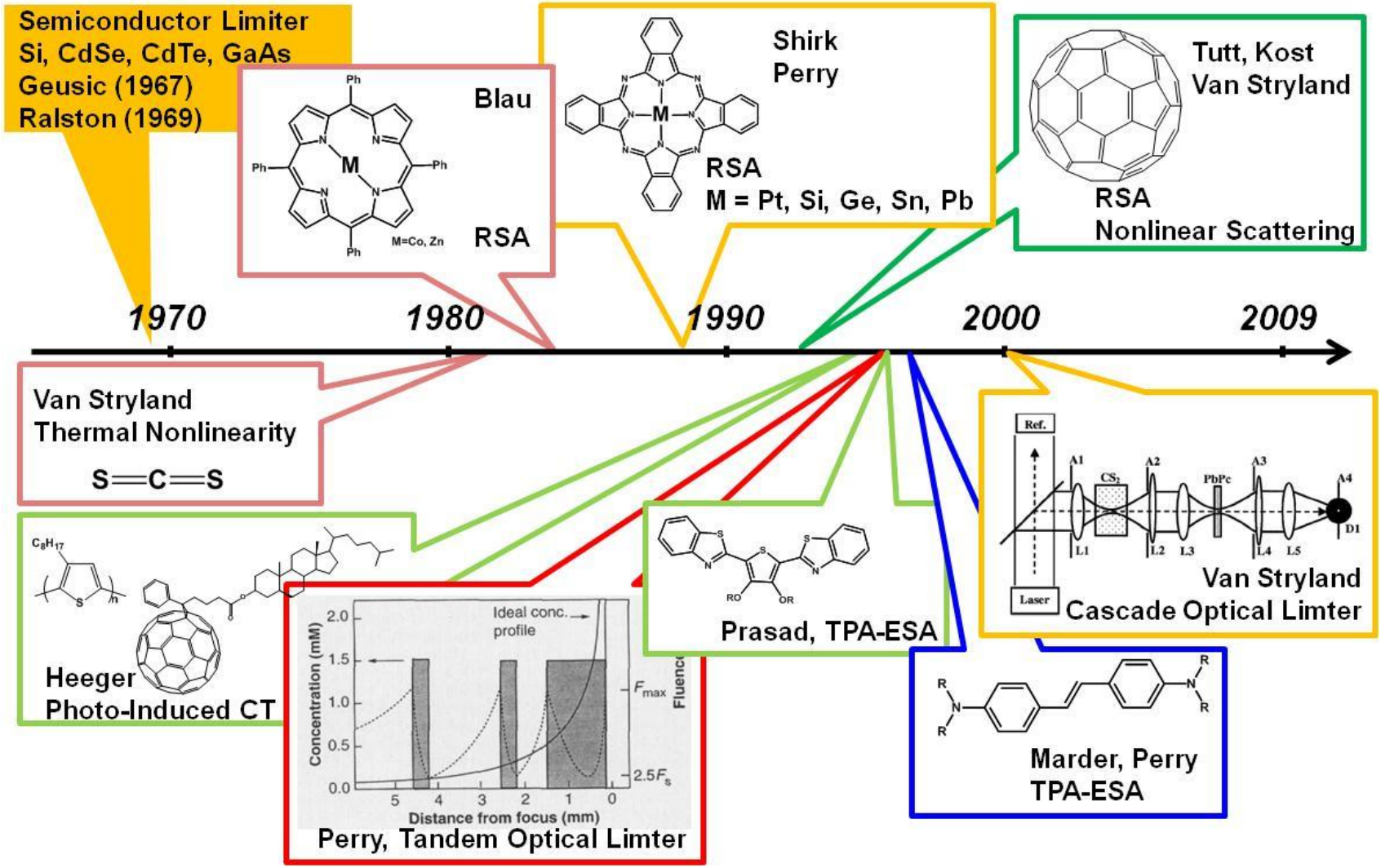

Scheme 1.3. Timeline of the development of optical limiting materials.

REFERENCES

[1] Chiang, C. K., Fincher, C. R., Park, Y. W., Heeger, A. J., Shirakawa, H., Louis, E. J., Gau, S. C. and MacDiarmid, A. G., "Electrical conductivity in doped polyacetylene," *Physical Review Letters* **39**, 1098-1101 (1977).

[2] Shirakawa, H., Louis, E. J., MacDiarmid, A. G., Chiang, C. K. and Heeger, A. J., "Synthesis of electrically conducting organic polymers: Halogen derivatives of polyacetylene, $(CH)_x$," *Chemical Communications*, 578-580 (1977).

[3] Brabec, C. J., Sariciftci, N. S. and Hummelen, J. C., "Plastic solar cells," *Advanced Functional Materials* **11**, 15-26 (2001).

[4] Spangler, C. W., "Recent development in the design of organic materials for optical power limiting," *Journal of Materials Chemistry* **9**, 2013-2020 (1999).

[5] Prasad, P. N. and Reinhardt, B. A., "Is there a role for organic materials chemistry in nonlinear optics and photonics?" *Chemistry of Materials* **2**, 660-669 (1990).

[6] Luther-Davies, B. and Samoc, M., "Third-order nonlinear optical organic materials for photonic switching," *Current Opinion in Solid State & Materials Science* **2**, 213-219 (1997).

[7] Halvorson, C., Hays, A., Kraabel, B., Wu, R. L., Wudl, F. and Heeger, A. J., "A 160-femtosecond optical-image processor based on a conjugated polymer," *Science* **265**, 1215-1216 (1994).

[8] Fann, W. S., Benson, S., Madey, J. M. J., Etemad, S., Baker, G. L. and Kajzar, F., "Spectrum of $\chi^{(3)}(-3\omega;\ \omega, \omega, \omega)$ in polyacetylene - an application of the free-electron laser in nonlinear optical spectroscopy," *Physical Review Letters* **62**, 1492-1495 (1989).

[9] Halvorson, C., Moses, D., Hagler, T. W., Cao, Y. and Heeger, A. J., "Frequency-dependence of 3rd-harmonic generation in cis-polyacetylene and transpolyacetylene - importance of the degenerate ground-state to nonlinear optical-response," *Synthetic Metals* **49**, 49-58 (1992).

[10] Halvorson, C., Hagler, T. W., Moses, D., Cao, Y. and Heeger, A. J., "Conjugated polymers with degenerate ground-state - the route to high-performance 3rd-order nonlinear optical-response," *Chemical Physics Letters* **200**, 364-368 (1992).

[11] Chi, S. H., Hales, J. M., Fuentes-Hernandez, C., Tseng, S. Y., Cho, J. Y., Odom, S. A., Zhang, Q., Barlow, S., Schrock, R. R., Marder, S. R., Kippelen, B. and Perry, J. W., "Thick optical-quality films of substituted polyacetylenes with large, ultrafast third-order nonlinearities and application to image correlation," *Advanced Materials* **20**, 3199-3203 (2008).

[12] Grubbs, R. H., Gorman, C. B., Ginsburg, E. J., Perry, J. W. and Marder, S. R., "New polymeric materials with cubic optical nonlinearities derived from ring-opening metathesis polymerization," *ACS Symposium Series* **455**, 672-682 (1991).

[13] Chung, S.-J., Maciel, G. S., Pudavar, H. E., Lin, T.-C., He, G. S., Swiatkiewicz, J., Prasad, P. N., Lee, D. W. and Jin, J.-I., "Two-photon properties and excitation dynamics of poly(*p*-phenylenevinylene) derivatives carrying phenylanthracene and branched alkoxy pendents," *Journal of Physical Chemistry A* **106**, 7512-7520 (2002).

[14] Frolov, S. V., Liess, M., Lane, P. A., Gellermann, W. and Vardeny, Z. V., "Exciton dynamics in soluble poly(*p*-phenylene-vinylene): Towards an ultrafast excitonic switch," *Phyiscal Review Letters* **78**, 4285-4288 (1997).

[15] Bader, M. A., Marowsky, G., Bahtiar, A., Koynov, K., Bubeck, C., Tillmann, H., Horhold, H. and Pereira, S., "Poly(*p*-phenylenevinylene) derivatives: New promising materials for nonlinear all-optical waveguide switching," *Journal of Optical Society of America B* **19**, 2250-2262 (2002).

[16] Cha, M., Saricftci, N. S., Heeger, A. J., Hummelen, J. C. and Wudl, F., "Enhanced nonlinear absorption and optical limiting in semiconducting polymer/methanofullerene charge transfer films," *Applied Physics Letter* **67**, 3850-3852 (1995).

[17] He, G. S., Weder, C., Smith, P. and Prasad, P. N., "Optical power limiting and stabilization based on a novel polymer compound," *IEEE Journal of Quantum Electronics* **34**, 2279-2285 (1998).

[18] Mathy, A., Ueberhofen, K., Schenk, R., Gregorius, H., Garay, R., Mullen, K. and Bubeck, C., "Third-harmonic-generation spectroscopy of poly(*p*-phenylenevinylene): A

comparison with oligomers and scaling laws for conjugated polymers," *Physical Review B* **53**, 4367-4376 (1996).

[19] Albota, M., Beljonne, D., Bredas, J. L., Ehrlich, J. E., Fu, J.-Y., Heikal, A. A., Hess, S. E., Kogej, T., Levin, M. D., Marder, S. R., McCord-Maughon, D., Perry, J. W., Rockel, H., Rumi, M., Subramaniam, G., Webb, W. W., Wu, X. L. and Xu, C., "Design of organic molecules with large two-photon absorption cross sections," *Science* **281**, 1653-1656 (1998).

[20] Ooba, N., Tomaru, S., Kurihara, T., Kaino, T., Yamada, W., Takagi, M. and Yamamoto, T., "Enhancement of third-order optical nonlinearity of poly(aryleneethynylene)s by introducing an intramolecular charge transfer interaction into their π-conjugation.," *Japanese Journal of Applied Physics* **34**, 3139-3141 (1995).

[21] Ehrlich, J. E., Wu, X. L., Lee, I. Y. S., Hu, Z. Y., Rockel, H., Marder, S. R. and Perry, J. W., "Two-photon absorption and broadband optical limiting with bis-donor stilbenes," *Optics Letters* **22**, 1843-1845 (1997).

[22] Zhao, M. T., Singh, B. P. and Prasad, P. N., "A systematic study of polarizability and microscopic 3rd-order optical nonlinearity in thiophene oligomers," *Journal of Chemical Physics* **89**, 5535-5541 (1988).

[23] Zhao, M. T., Samoc, M., Singh, B. P. and Prasad, P. N., "Study of 3rd-order microscopic optical nonlinearities in sequentially built and systematically derivatized structures," *Journal of Physical Chemistry* **93**, 7916-7920 (1989).

[24] Reinhardt, B. A., Brott, L. L., Clarson, S. J., dillard, A. G., Bhatt, J. C., Kannan, R., Yuan, L. X., He, G. S. and Prasad, P. N., "Highly active two-photon dyes: Design, synthesis, and characterization toward application," *Chemistry of Materials* **10**, 1863-1874 (1998).

[25] Marder, S. R., Beratan, D. N. and Cheng, L.-T., "Approaches for optimizing the first electronic hyperpolarizability of conjugated organic molecules," *Science* **252**, 103-106 (1991).

[26] Samoc, A., Samoc, M., Woodruff, M. and Lutherdavies, B., "Tuning the properties of poly(p-phenylenevinylene) for use in all-optical switching," *Optics Letters* **20**, 1241-1243 (1995).

[27] Hochberg, M., Baehr-Jones, T., Wang, G. X., Shearn, M., Harvard, K., Luo, J. D., Chen, B. Q., Shi, Z. W., Lawson, R., Sullivan, P., Jen, A. K. Y., Dalton, L. and Scherer, A., "Terahertz all-optical modulation in a silicon-polymer hybrid system," *Nature Materials* **5**, 703-709 (2006).

[28] Koynov, K., Goutev, N., Fitrilawati, F., Bahtiar, A., Best, A. and Bubeck, C., "Nonlinear prism coupling of waveguides of the conjugated polymer MEH-PPV and their figures of merit for all-optical switching," *Journal of Optical Society of America B* **19**, 895-898 (2002).

[29] Geusic, J. E., Singh, S., Tipping, D. W. and Rich, T. C., "3-photon stepwise optical limiting in silicon," *Physical Review Letters* **19**, 1126-1128 (1967).

[30] Ralston, J. M. and Chang, R. K., "Optical limiting in semiconductors," *Applied Physics Letters* **15**, 164-166 (1969).

[31] Soileau, M. J., Williams, W. E. and Vanstryland, E. W., "Optical power limiter with picosecond response-time," *IEEE Journal of Quantum Electronics* **19**, 731-735 (1983).

[32] Blau, W., Byrne, H., Dennis, W. M. and Kelly, J. M., "Reverse saturable absorption in tetraphenylporphyrins," *Optics Communications* **56**, 25-29 (1985).

[33] Perry, J. W., Mansour, K., Marder, S. R., Perry, K. J., Alvarez, D. and Choong, I., "Enhanced reverse saturable absorption and optical limiting in heavy-atom-substituted phthalocyanines," *Optics Letters* **19**, 625-627 (1994).

[34] Shirk, J. S., Lindle, J. R., Bartoli, F. J., Hoffman, C. A., Kafafi, Z. H. and Snow, A. W., "Off-resonant 3rd-order optical nonlinearities of metal-substituted phthalocyanines," *Applied Physics Letters* **55**, 1287-1288 (1989).

[35] Perry, J. W., Barlow, S., Ehrlich, J. E., Heikal, A. A., Hu, Z. Y., Lee, I. Y. S., Mansour, K., Marder, S. R., Rockel, H., Rumi, M., Thayumanavan, S. and Wu, X. L., "Two-photon and higher-order absorptions and optical limiting properties of bis-donor substituted conjugated organic chromophores," *Nonlinear Optics* **21**, 225-243 (1999).

[36] He, G. S., Xu, G. C., Prasad, P. N., Reinhardt, B. A., Bhatt, J. C., Mckellar, R. and Dillard, A. G., "2-photon absorption and optical-limiting properties of novel organic-compounds," *OPTICS LETTERS* **20**, 1930-1930 (1995).

[37] Hales, J. M., Cozzuol, M., Screen, T. E. O., Anderson, H. L. and Perry, J. W., "Metalloporphyrin polymer with temporally agile, broadband nonlinear absorption for optical pulse suppression in the near infrared," *Optics Express* **17**, 18478-18488 (2009).

[38] Marder, S. R., Perry, J. W., Bourhill, G., Gorman, C. B., Tiemann, B. G. and Mansour, K., "Relation between bond-length alternation and 2nd electronic hyperpolarizability of conjugated organic-molecules," *Science* **261**, 186-189 (1993).

[39] Kogej, T., Beljonne, D., Meyers, F., Perry, J. W., Marder, S. R. and Bredas, J. L., "Mechanisms for enhancement of two-photon absorption in donor-acceptor conjugated chromophores," *Chemical Physics Letters* **298**, 1-6 (1998).

[40] Perry, J. W., Mansour, K., Lee, I. Y. S., Wu, X. L., Bedworth, P. V., Chen, C. T., Ng, D., Marder, S. R., Miles, P., Wada, T., Tian, M. and Sasabe, H., "Organic optical limiter with a strong nonlinear absorptive response," *Science* **273**, 1533-1536 (1996).

[41] Hernandez, F. E., Yang, S., Van Stryland, E. W. and Hagan, D. J., "High-dynamic-range cascaded-focus optical limiter," *Optics Letters* **25**, 1180-1182 (2000).

[42] Moon, Y. B., Rughooputh, S. D. D. V., Heeger, A. J., Patil, A. O. and Wudl, F., "X-ray-scattering study of the conversion of poly(para-phenylene vinylene) precursor to the conjugated polymer," *Synthetic Metals* **29**, E79-E84 (1989).

[43] Moon, Y. B., Cao, Y., Smith, P. and Heeger, A. J., "X-ray-scattering from crystalline polyaniline," *Polymer Communications* **30**, 196-199 (1989).

[44] Klavetter, F. L. and Grubbs, R. H., "Polycyclooctatetraene (polyacetylene) - synthesis and properties," *Journal of the American Chemical Society* **110**, 7807-7813 (1988).

[45] Fincher, C. R., Chen, C. E., Heeger, A. J., Macdiarmid, A. G. and Hastings, J. B., "Structural determination of the symmetry-breaking parameter in trans-(CH)x," *Physical Review Letters* **48**, 100-104 (1982).

[46] Hide, F., DiazGarcia, M. A., Schwartz, B. J., Andersson, M. R., Pei, Q. B. and Heeger, A. J., "Semiconducting polymers: A new class of solid-state laser materials," *Science* **273**, 1833-1836 (1996).

[47] Kobayashi, M., Colaneri, N., Boysel, M., Wudl, F. and Heeger, A. J., "The electronic and electrochemical properties of poly(isothianaphthene)," *Journal of Chemical Physics* **82**, 5717-5723 (1985).

CHAPTER 2

THIRD-ORDER NONLINEAR OPTICAL RESPONSES AND CHARACTERIZATION TECHNIQUES

The subject of this chapter is an illustration of several characterization techniques for third-order nonlinear optical properties employed in this dissertation work. A qualitative introduction of the third-order nonlinear optical response will be first described. Third-order nonlinear optical phenomena such as intensity-dependent refractive index (nonlinear refractive index), two-photon absorption, and effective third-order nonlinear optical processes will then be described. Finally, several characterization techniques used in this dissertation work, including degenerate four-wave mixing, Z-scan, power-dependent nonlinear transmission (optical limiting) and time-resolved pump-probe measurement, will be discussed.

2.1 Third-Order Nonlinear Optical Response

When an atom or a molecule[†] interacts with an input electromagnetic field (or optical field), the field induces a displacement of electron density from the nucleus and creates an induced dipole, μ. (**Scheme 2.1**) The scale of displacement or the magnitude of induced dipole depends on the molecule's intrinsic property: polarizability. The interaction between a molecule and the input optical field can be expressed as

$$\boldsymbol{\mu}(\omega) = \tilde{\alpha}\boldsymbol{E}(\omega), \qquad \text{(Eq. 2.1)}$$

[†] It must be noted that the description here, technically, is about the dipole induced in a single atom. Since a molecular response is an ensemble average of these atomic responses, the description here is also applied to a molecular system.

where $\boldsymbol{\mu}$ and $\boldsymbol{E}$ are the frequency-dependent vector quantities of induced dipole and optical field and α is the polarizability of the molecule. The optical field at frequency ω can be further written as

$$\mathbf{E}(t,r) = \frac{1}{2}\sum_{\omega}\{\mathbf{A}_{\omega}(r)exp(-i\omega t) + c.c.\} \quad \text{(Eq. 2.2)}$$

where $\mathbf{A}_{\omega}$ is a complex field amplitude including information such as the polarization of the field.

For some molecular systems, the interaction of a molecule with an input optical field can greatly depend on the intensity of the field. Under exposure to an intense field, which can be produced by a source such as laser, the displacement of the electron cloud responds nonlinearly to the field and the oscillation of the induced dipole becomes anharmonic. In this nonlinear regime, the strong interaction between the molecule and the field results in the generation of new fields or modification of the properties of the original fields. Under these conditions, it becomes impossible to obtain an exact solution for $\boldsymbol{\mu}$ and the total induced dipole is usually expressed as a Taylor series expansion in $\boldsymbol{E}$,

$$\boldsymbol{\mu} = \boldsymbol{\mu_0} + \tilde{\alpha}^{(1)}\boldsymbol{E} + \frac{1}{2!}\tilde{\alpha}^{(2)}\boldsymbol{E}\cdot\boldsymbol{E} + \frac{1}{3!}\tilde{\alpha}^{(3)}\boldsymbol{E}\cdot\boldsymbol{E}\cdot\boldsymbol{E} + \cdots, \quad \text{(Eq. 2.3)}$$

where $\boldsymbol{\mu_0}$ is the permanent dipole and $\tilde{\alpha}^{(1)}$, $\tilde{\alpha}^{(2)}$, and $\tilde{\alpha}^{(3)}$ are first-, second-, and third-order polarizabilities, respectively. The first-order polarizability, $\tilde{\alpha}^{(1)}$, is also called the linear molecular polarizability. The second-order polarizability, only exhibits non-zero values in noncentrosymmetric molecular systems [1]. The third-order polarizability, $\tilde{\alpha}^{(3)}$, also known as γ, exists in all molecular systems without any symmetry restriction. The third-order polarizability is also related to the nonlinear refractive index and nonlinear absorption, terms that will be discussed later. It must be noted that, in Eq. 2.3, the involved optical fields can have different frequencies which can

result in many different nonlinear optical phenomena [2]. Since the focus of this thesis is on the degenerate third-order nonlinear optical properties, only degenerate phenomena will be discussed and other third-order nonlinear processes will be ignored.

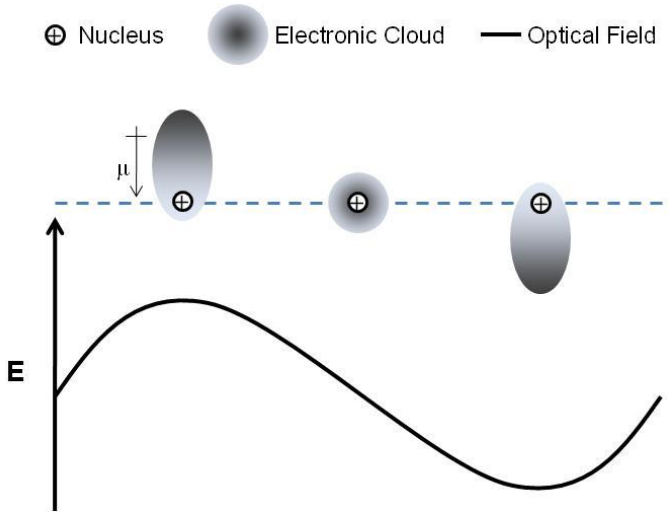

Scheme 2.1. The oscillatory motion of the electron cloud about its nucleus in the presence of an applied optical field [1].

2.1.1 Relationship between Microscopic and Macroscopic Parameters

In a condensed molecular medium, the polarization of an individual molecule is affected by the polarization of the surrounding molecules. Therefore, the responses observed in most third-order nonlinear optical experiments usually reflect the macroscopic nonlinearity, i.e. $\chi^{(3)}$. To relate the macroscopic and microscopic quantities, the macroscopic polarization **P** can be written as

$$\mathbf{P} = N\langle \boldsymbol{\mu} \rangle, \qquad \text{(Eq. 2.4)}$$

where *N* is the number density of microscopic dipoles per unit volume. Likewise, the macroscopic polarization can also be expanded as

$$\mathbf{P} = \mathbf{P_0} + \chi^{(1)}\boldsymbol{E} + \frac{1}{2!}\chi^{(2)}\boldsymbol{E}\cdot\boldsymbol{E} + \frac{1}{3!}\chi^{(3)}\boldsymbol{E}\cdot\boldsymbol{E}\cdot\boldsymbol{E} + \cdots \qquad \text{(Eq. 2.5)}$$

where $\chi^{(n)}$ is denoted as the *n*-th order susceptibility. Using equations 2.3 – 2.5, the relationship between the microscopic polarizability $\tilde{\gamma}$ and macroscopic susceptibility $\chi^{(3)}$ can be written as

$$\chi^{(3)} = NL(\omega)^4\langle\tilde{\gamma}\rangle \quad \text{(Eq. 2.6)}$$

$$L(\omega) = \frac{n(\omega)^2+2}{3} \quad \text{(Eq. 2.7)}$$

where $L(\omega)$ is the Lorentz local field factor used to account for the difference between macroscopic fields (the magnitude of fields in a vacuum) and microscopic fields (the local or effective electric field) due to the polarizability in the surrounding medium.

2.1.2 Units of $\chi^{(3)}$

In this thesis, the units of $\chi^{(3)}$ are given in cgs units expressed as *esu* or $cm^2 statvolt^{-2}$. The conversion to SI units is

$$\chi^{(3)}[m^2V^{-2}, SI] = \left(\frac{4\pi}{9} \times 10^{-8}\right)\chi^{(3)}[cm^2 statvolt^{-2}, esu] \quad \text{(Eq. 2.8)}$$

2.2 Third-Order Nonlinear Optical Phenomena

As previously mentioned, the real and imaginary parts of $\chi^{(3)}$ are related to the nonlinear refractive index (n_2) and two-photon absorption coefficient (β) that lead to the phenomena of nonlinear refraction (NLR) and two-photon absorption (2PA). Both NLR and 2PA are degenerate third-order nonlinear processes, i.e. related to $\chi^{(3)}(-\omega;\omega,-\omega,\omega)$. In a material possessing large third-order nonlinearity, the incident optical field will induce modifications in the material's optical properties which, in turn,

cause changes in the phase or amplitude of the incident field itself. Due to such self-action effects, NLR and 2PA have been utilized in many photonic applications such as all-optical signal processing [3-7].

2.2.1 Nonlinear Refraction: Intensity-Dependent Refractive Index

The nonlinear refractive index (n_2) can be related to the real part of $\chi^{(3)}(-\omega;\omega,-\omega,\omega)$ and written as

$$n_2 = \frac{3}{4\varepsilon_0 n_0(\omega)^2 c}\mathrm{Re}\left[\chi^{(3)}(-\omega;\omega,-\omega,\omega)\right] \quad \text{(Eq. 2.9)}$$

where ε_0 is the free-space permittivity, $n_0(\omega)$ is the linear refractive index at frequency ω, and c is the speed of light in vacuum [1]. The units of n_2 are m^2/W. This quantity manifests itself as a change in the refraction of a material that is dependent on the input intensity:

$$n = n_0 + n_2 I. \quad \text{(Eq. 2.10)}$$

The change in refractive index induces a phase change in the incident optical field and this phase change is intensity-dependent:

$$\Delta\phi = \frac{2\pi}{\lambda_0} n_2 I L \quad \text{(Eq. 2.11)}$$

where L is the length of the nonlinear material and λ_o is the wavelength of the optical field. This intensity-dependent phase change can affect the field propagation in space by speeding up or retarding the phase front and causing certain propagation effects such as self-focusing and self-defocusing [1]. For example, as a Gaussian beam propagates within a nonlinear material the induced phase change will reflect the spatial distribution of the beam intensity and result in a phase front curvature. If n_2 is positive, this phase

curvature acts like a convex lens and the beam tends to focus. If n_2 is negative, this phase curvature acts like a concave lens and the beam tends to diverge.

2.2.2 Two-Photon Absorption

Two-photon absorption is a process by which an optical transition between two real states is achieved by the simultaneous absorption of two photons [8]. The absorption of the first photon will induce some perturbation to the wave function of a lower excited state. If the second photon is absorbed before the perturbation fades away, a transition to a higher excited state can be accomplished. The lifetime of the perturbation is very short so the photon fluxes must be large enough to give a reasonably high probability that the two photons can be absorbed before the perturbation vanishes; thus, only power levels typically achieved with a laser beam can generate this nonlinear process. Therefore, even though the theory of multiphoton absorption was proposed in 1931 by Maria Göppert-Mayer , the phenomenon of 2PA was not observed until the invention of the laser, some 30 years later [2].

The magnitude of 2PA of a material can be represented as a 2PA coefficient (β) or cross section (δ). Just like the nonlinear refractive index, the 2PA coefficient is a macroscopic quantity and can be related to the imaginary part of $\chi^{(3)}(-\omega;\omega,-\omega,\omega)$ and is written as [1]

$$\beta = \frac{3\omega}{2\varepsilon_0 n_0(\omega)^2 c^2}\,\mathrm{Im}\left[\chi^{(3)}(-\omega;\omega,-\omega,\omega)\right] \qquad \text{(Eq. 2.12)}$$

where the units of β are m/W; furthermore, β can be written as a term in the overall absorption coefficient,

$$\alpha = \alpha_0 + \beta I, \qquad \text{(Eq. 2.13)}$$

where α_0 is the linear absorption coefficient. The microscopic term associated with 2PA is its cross section, δ, and it can be related to the microscopic third-order polarizability

$$\delta = \frac{1}{6}\frac{3L(\omega)^4\hbar\omega^2}{2\varepsilon_0 n_0(\omega)^2 c^2}\mathrm{Im}[\gamma(-\omega;\omega,-\omega,\omega)] \quad \text{(Eq. 2.14)}$$

where the units of δ are $m^4 \cdot s \cdot photon^{-1}$. The conversion between β and δ is

$$\delta = \beta E_{ph}/N. \quad \text{(Eq. 2.15)}$$

The effect of β is to induce an intensity-dependent attenuation of the amplitude of an incident optical field as it propagates through a 2PA medium. The intensity attenuation via 2PA can be described as a function of propagation distance in the *z* direction [2]

$$\frac{\partial I}{\partial z} = -(\alpha_0 I + \beta I^2) \quad \text{(Eq. 2.16)}$$

and

$$T = \frac{I(L)}{I_0} = \frac{T_0}{1+I_0\beta I L_{eff}} \quad \text{(Eq. 2.17)}$$

where $T_0 = exp(-\alpha_0 L)$ is the linear transmission, L is the length of the 2PA sample, and $L_{eff} = (1- exp(-\alpha_0 L))/ \alpha_0$ is the effective sample length. This nonlinear amplitude attenuation can participate in optical limiting, which has been briefly introduced in chapter 1. The quadratic dependence of 2PA on the intensity of the incident field results in features other than just nonlinear attenuation of light. As an example, this quadratic dependency makes 2PA occur only within a small volume near the waist of a focused laser beam which allows for improvement of axial and radial spatial resolution in applications such as 3D optical data storage and optical bio-imaging [9].

2.2.3 Effective $\chi^{(3)}$ Phenomena ($\chi^{(1)}$:$\chi^{(1)}$ processes) – Excited State Absorption

In third-order nonlinear optical processes, if one of the involved optical frequencies is near resonance with an electronic transition of a material, linear absorption will take place and give a path to populate the excited states. If the incident field is strong, the excited states can be significantly populated. In material systems like semiconductors or conjugated polymers, the density of excited states is high and the excited electron can make a further transition to other higher lying states before it relaxes back to the ground state. Thus, a series of sequential transitions between individual real states (**Scheme 2.2**) can occur and cause a cumulative $\chi^{(1)}$ process that is often referred to as a $\chi^{(1)}$:$\chi^{(1)}$ process or effective $\chi^{(3)}$ process [1].

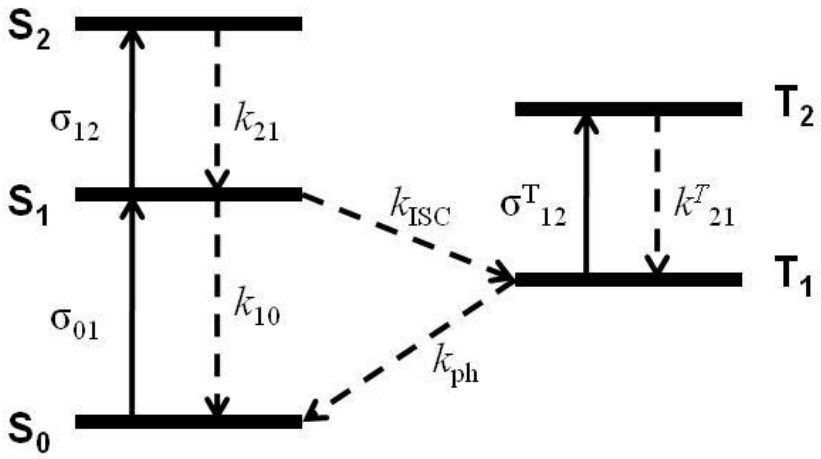

Scheme 2.2. Schematic state diagram of a five-level system illustrating the transition between the ground state and singlet and triplet excited states.

In scheme 2.2, the five-level state diagram illustrates the transitions between the ground state (S_0) and singlet and triplet excited states. Such transitions will cause population redistribution between the ground and excited states. The population of the

excited state is dependent on the number density of initial state population and the cross section (σ) of the transition between two states. For linear absorption from S_0 to S_1, the absorption coefficient (which is related to the imaginary part of $\chi^{(1)}$) is $\alpha_0 = \sigma_{01} N_0$ where N_0 is the population of ground state as well as the total population before excitation [1]. If only the transition between S_0 to S_1 and S_1 to S_2 is considered, upon excitation, a certain amount of population (ΔN) will leave the ground state and transfer to the S_1 state. Thus, the effective absorption coefficient will become [1]

$$\alpha_{eff} = \sigma_{01}(N_0 - \Delta N) + \sigma_{12}\Delta N = \sigma_{01} N_0 + (\sigma_{12} - \sigma_{01})\Delta N \qquad \text{(Eq. 2.18)}$$

and Eq. 2.18 can be written in an analogous way to Eq. 2.13 as [1]

$$\alpha_{eff} = \alpha_0 + (\sigma_{12} - \sigma_{01})\Delta N = \alpha_0 + \Delta\alpha. \qquad \text{(Eq. 2.19)}$$

Since ΔN is intensity dependent, Eq. 2.19 presents an intensity-dependent absorption that is similar to the nonlinear absorption process described previously. Depending on the relative sizes of the cross sections, different nonlinear absorption behavior can be observed. If $\sigma_{12} < \sigma_{01}$, the α_{eff} decreases as the intensity increases. This process is known as saturable absorption which is essentially ground state bleaching and leads to increased transmittance at high intensity. On the other hand, if $\sigma_{12} > \sigma_{01}$ the α_{eff} increases as the intensity increases. This mechanism is known as reverse saturable absorption (RSA) which will result in a decreased transmittance at high intensity. In addition to saturable absorption and RSA, in some systems like semiconductors and conjugated polymers, the photoexcitation can lead to a charge generation and separation leading to free charge carriers [10]. The population of charge carriers is also intensity dependent and these charge carriers can also play roles in the total or effective absorption

process. It must be noted that these excited state absorptions are pulse-width dependent due to the intrinsic lifetime (relaxation) of the individual states/carriers.

All these processes mentioned above can cause the modification of input light intensity. Saturable absorption is broadly utilized in a laser cavity for passive Q-switching and mode locking [2] while RSA and charge carrier absorption is of great interest in optical limiting [11, 12], which is one of the applications focused on in this thesis and will be addressed extensively in chapters 4 and 5.

2.3 Characterization Techniques

In this dissertation work, degenerate four-wave mixing (DFWM) [1, 13] and Z-scan [14-16] techniques were used to characterize the third-order nonlinear response of several conjugated polymers. Power-dependent nonlinear transmission or optical limiting was used to test the performance of target materials for optical limiting applications. A time-resolved pump-probe technique (transient absorption spectroscopy) was used to characterize the photophysical response and related nonlinear optical properties. Furthermore, since different excited state absorptions have different relaxation times, optical limiting and transient absorption measurements were performed using different pulsewidths (nanosecond and femtosecond) to monitor pulsewidth dependent nonlinear absorption and various photophysical processes in different temporal regimes.

2.3.1 Measuring Third-Order Nonlinear Optical Properties

2.3.1.1 Degenerate Four-Wave Mixing

Degenerate four-wave mixing (DFWM) is a commonly used technique in the laboratory to determine the third-order nonlinearity and the temporal response of a medium [1, 13]. DFWM investigates the same nonlinear polarization term, i.e. $\chi^{(3)}(-\omega;\omega,-\omega,\omega)$, that is related to the intensity dependent refractive index. This process involves three spatially distinguishable beams to produce a fourth beam that has a different propagation direction than the original beams. During the DFWM process, the condition of momentum conversation has to be satisfied:

$$\overrightarrow{k_1}+\overrightarrow{k_2}+\overrightarrow{k_3}+\overrightarrow{k_4}=0. \qquad \text{(Eq. 2.20)}$$

The geometry for the DFWM experiments used in this study is the "forward scattering" configuration (FS-DFWM) (**Scheme 2.3**) [13]. Three beams (1, 2 and 3) are focused on the sample and the induced beam 4 exits the medium. The three incident beams are arranged in such a geometry that each beam originates from the corner of a box and, because of the momentum conservation, the induced fourth beam will propagate along the remaining corner to satisfy the phase matching condition. The intensity of beam 4 is related to the magnitude of $\chi^{(3)}$ according to the following [8]:

$$I_4 = I_1 I_2 I_3 \frac{9\omega^2\left|\chi^{(3)}(-\omega;\omega,-\omega,\omega)\right|^2 L^2}{16c^4 n_0(\omega)^4 \varepsilon_0^2} = mI_1 I_2 I_3, \qquad \text{(Eq 2.21)}$$

$$\text{where } m = \frac{9\omega^2\left|\chi^{(3)}(-\omega;\omega,-\omega,\omega)\right|^2 L^2}{16c^4 n_0(\omega)^4 \varepsilon_0^2}. \qquad \text{(Eq 2.22)}$$

This result is found under the assumption that there is no linear absorption. Using this equation and the approach described below, the magnitude of $\chi^{(3)}$ can be determined.

DFWM is a referential technique. A reference with a known third-order nonlinearity must be used to properly extract the magnitude of $\chi^{(3)}$ of a target sample. As indicated in Eq 2.22, the detected signal intensity of beam 4 is dependent on the product of the three incident field intensities. If the incident fields have identical intensities, one would expect, for a third-order nonlinear response, the output signal to exhibit a cubic power-dependency on the incident intensity. An example is given in chapter 3 (figure 3.5) showing the power-dependent DFWM measurements of a slab of fused silica and a film of substituted polyacetylene. In a DFWM experiment, references with known values of $\left|\chi^{(3)}(-\omega;\omega,-\omega,\omega)\right|$ must be used to properly extract the magnitude of $\chi^{(3)}$ of a target sample by using the following relation, based on Eq. 2.22 [1]:

$$\left|\chi^{(3)}_{sample}\right| = \left|\chi^{(3)}_{ref}\right| \left(\frac{m_{sample}}{m_{ref}}\right)^{1/2} \frac{L_{ref}}{L_{sample}} \left(\frac{n_{sample}}{n_{ref}}\right)^{2}. \qquad \text{(Eq 2.23)}$$

Table 2.1 lists several reported references that were used in DFWM measurements as well as the Z-scan technique which is described in detail below. Furthermore, DFWM can also be used to investigate the temporal response of $\chi^{(3)}$. This can be achieved by introducing an optical delay to one of the three incident pulses. The cross correlation of these three pulses will map out the temporal response of the nonlinear material.

The drawbacks of the DFWM technique are its inability to discriminate between the real and imaginary parts of $\chi^{(3)}$ and its relatively complicated optical layout [1]. The optical layout is shown in **Scheme 2.4**. With such a complex layout, it is very difficult and time-consuming for one to perform wavelength-dependent or dispersion studies of nonlinear optical responses by DFWM.

In the DFWM setup used in this dissertation work, a 1 kHz repetition rate Ti:Sapphire regenerative amplifier (Spitfire, Spectra-Physics) operating at 800 nm

generated the excitation wavelength (from 1150 – 1550 nm, ~75 fs HW1/e) following passage through an optical parametric amplifier (OPA-800C, Spectra-Physics). The excitation beam was then split into three beams. The intensity of each beam was modified using a polarizer-waveplate pair to obtain the same input intensity. The input energy was measured by an Ophir® PE9 pyroelectric head energy meter (for energy range of 200 nJ and above) or a PD300-IR power meter (for energy range of 300 nJ and below). The three beams were focused inside the sample with special attention paid to good spatial and temporal overlap. The generated fourth beam was then collected and detected by a GaAs photoreceiver (Model#2033, NewFocus). These signals were passed through Boxcar integrator units (SR250, Stanford Research Systems) and the processed signals were acquired using a data acquisition card (6025E, National Instruments) and a home-built Labview® program. Each data point was averaged over 250 shots. For power-dependenet measurements, the input energies were varied using a computer-controlled half-waveplate rotator (PR50-PP, Newport Corporation) in conjunction with a polarizer. A motorized translation stage was used to vary the temporal delay of beam 1 to obtain the crosscorrelation signal and a temporal resoponse of the sample.

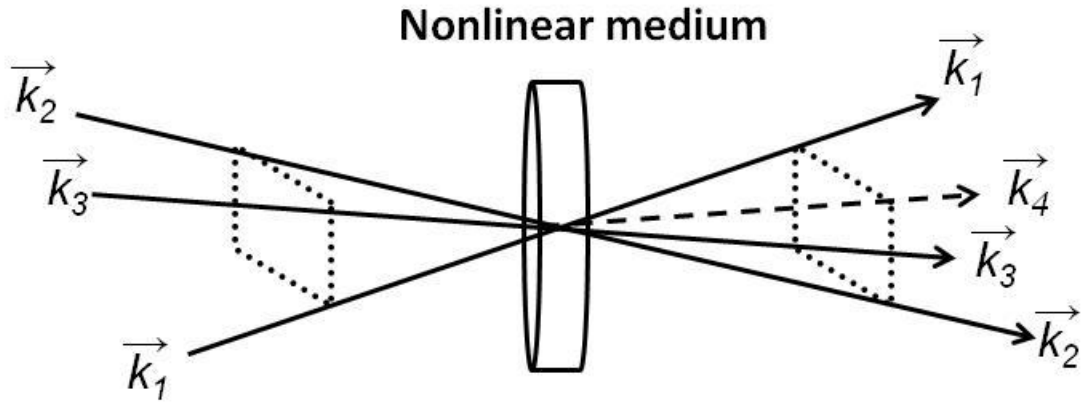

Scheme 2.3. Forward-scattering geometry for DFWM.

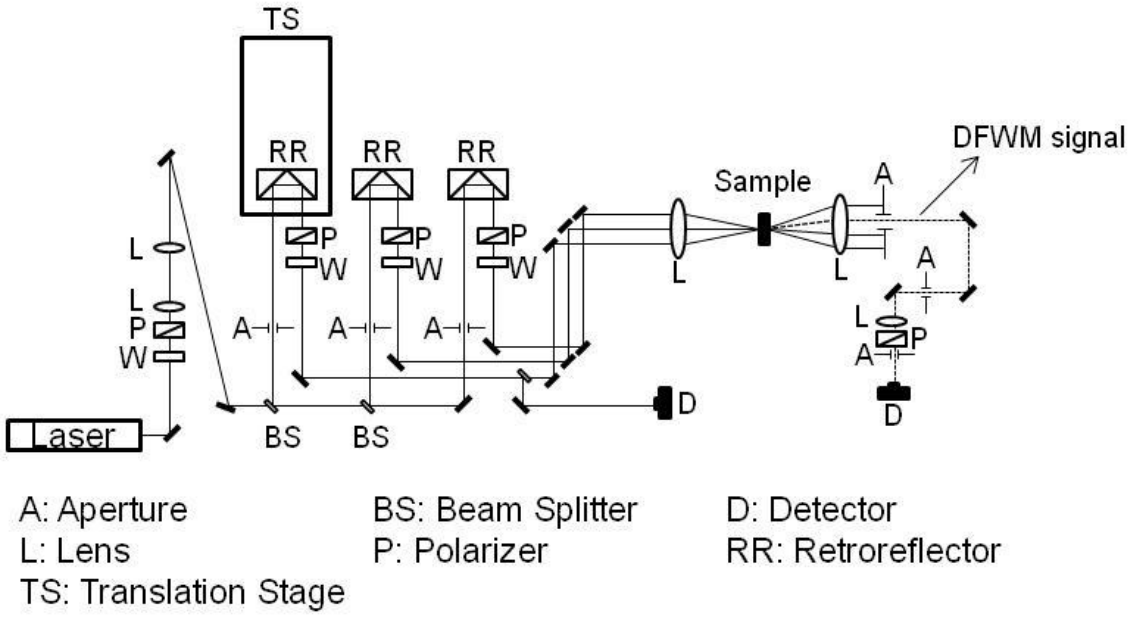

Scheme 2.4. Optical layout for a DFWM [1].

Table 2.1. Nonlinear optical properties of references.

Samples	λ [nm]	Thickness [μm]	n_0	n_2 [m^2/W]	β [m/W]	Ref.
Fused Silica	1300	1000	1.45	2.63×10^{-20}		[17]
	1550		1.45	2.63×10^{-20}		
ZnSe	1300	1016	2.468	1.34×10^{-18}		[5, 18, 19]
	1550		2.457	1.18×10^{-18}		
ZnS	1300	1016	2.278	6.14×10^{-19}		[19]
	1550		2.271	5.77×10^{-19}		
GaAs	1300	410	3.41	4.10×10^{-18}	1.77×10^{-10}	[18, 20-23]
	1550		3.374	2.29×10^{-17}	9.03×10^{-11}	

2.3.1.2 Z-scan

The Z-scan method is a standard technique for nonlinear optical material measurements and was used throughout this dissertation work because of the relative simplicity of its optical layout and the ease at which nonlinearities can be extracted from the acquired data [8, 14-16]. The Z-scan technique was developed to simultaneously measure the magnitude of both the nonlinear refraction (NLR) and nonlinear absorption (NLA). The sign of the nonlinear refractive index (n_2) can also be obtained at the same time. The geometry ofthe Z-scan optical layout is shown **in Scheme 2.5**. The basic idea of Z-scan is to utilize the self-focusing and self-defocusing phenomena, described above, to determine the magnitude of nonlinear refraction and to use the aforementioned nonlinear attenuation to determine the strength of nonlinear absorption. As shown in scheme 2.5, a sample is placed on a motorized stage and moved along the direction of the beam propagation (Z-axis). Using a single focused laser beam, the transmittance of the

beam after passage through a medium and a subsequent aperture is determined as a function of sample position (closed-aperture Z-scan). Assuming a material with a positive nonlinear refractive index, if the sample is started at a large negative value of Z and is moved closer to the focus, self-focusing is induced because of the increased irradiance. Self-focusing moves the focus closer to the lens and leads to greater beam divergence in the far field and reduced transmittance through the aperture. Consequently, when the medium is moved pass the focus, self-focusing collimates the beam and the transmittance through the aperture is increased. In Scheme 2.5, the sketch of the transmitted signal (D3/D1) at various Z-positions is illustrated for a medium with a positive nonlinear refractive index. The nonlinear phase change (and consequently the nonlinear refractive index) can be determined by the difference in peak and valley transmittance ($\Delta T_{PV} = T_P - T_V$), that is [15, 16]

$$\Delta T_{PV} \cong 0.406(1-S)^{0.27}|\Delta\phi| \qquad \text{(Eq 2.23)}$$

$$\text{where } \Delta\phi = \frac{2\pi}{\lambda} n_2 I_0 L_{eff} \qquad \text{(Eq 2.24)}$$

and S is the transmittance of the aperture, I_0 is the irradiance at the waist (Z = 0), and $L_{eff} = (1\text{-}e^{-\alpha 0 L})/\alpha_0$. If the aperture is removed and all the transmitted light is collected (open-aperture Z-scan), NLA can be determined. The sketch of the transmitted signal (D2/D1) at various z-positions in Scheme 2.5 shows how the nonlinear absorption increases as the sample moves closer to the focus due to the larger irradiance. The nonlinear absorption can be determined by

$$\Delta T(z) \approx \frac{q_0}{2\sqrt{2}} \frac{1}{1+\frac{z^2}{z_0^2}} \qquad \text{(Eq. 2.25)}$$

$$\text{Where } q_0 = \beta I_0 L_{eff} \qquad \text{(Eq. 2.26)}$$

and z_0 is the Rayleigh range of the beam.

Although Z-scan is a relatively easy and simple technique to implement, its signal-to-noise ratio is not as good as DFWM. Z-scan is very sensitive to beam distortion introduced by the sample's surface roughness or inhomogeneities. Even though Z-scan is an absolute technique that doesn't require a reference sample like DFWM, using references can help provide a useful control giving further validity to the extracted nonlinearity. Furthermore, since most femtosecond laser systems are sensitive to environmental instability, such as temperature fluctuations, using a reference detector (D1 in Scheme 2.5) to monitor and normalize the transmittance received on the signal detectors (D2 and D3 in Scheme 2.5) is critical. Also, it must be noted that Z-scan technique is sensitive to all types of nonlinearities; in other words, this technique provides no discrimination between different nonlinear processes [15, 16]. It is very important to pay extra attentions to determine the origin of the nonlinearity. Performing multiple energy scans usually can provide an indication of the existence of higher nonlinearities. If the measured nonlinearity is dependent with the excitation intensity, it indicates other higher nonlinear process, such as $\chi^{(5)}$, exists. Using an additional characterization technique, such as DFWM, can also give an indication of the origin of the nonlinearity.

In this dissertation work, Z-scan measurements were performed at several excitation wavelengths (700-1550 nm). The excitation wavelengths were generated by a 1 kHz repetition rate Ti:Sapphire regenerative amplifier (Spitfire, Spectra-Physics) operating at 800 nm following passage through an optical parametric amplifier (450-2290 nm, ~75 fs HW1/e, TOPAS, Spectra-Physics). The excitation beam was focused by a lens with focal length of 150 mm. The beam waist (45-55 μm) was measured by knife-

edge scans and the beam was determined to be Gaussian in shape ($1.0 < M^2 < 1.1$). The Rayleigh range was determined to be 3.5-6 mm. The pulse width was estimated by an autocorrelator (Positive Light). Reference scans on 1-mm slabs of fused silica, ZnSe, and ZnS were performed prior to data measurements on the sample to generate a correction factor to account for potential bias in the experimental data that may be caused by non-ideal beam quality.

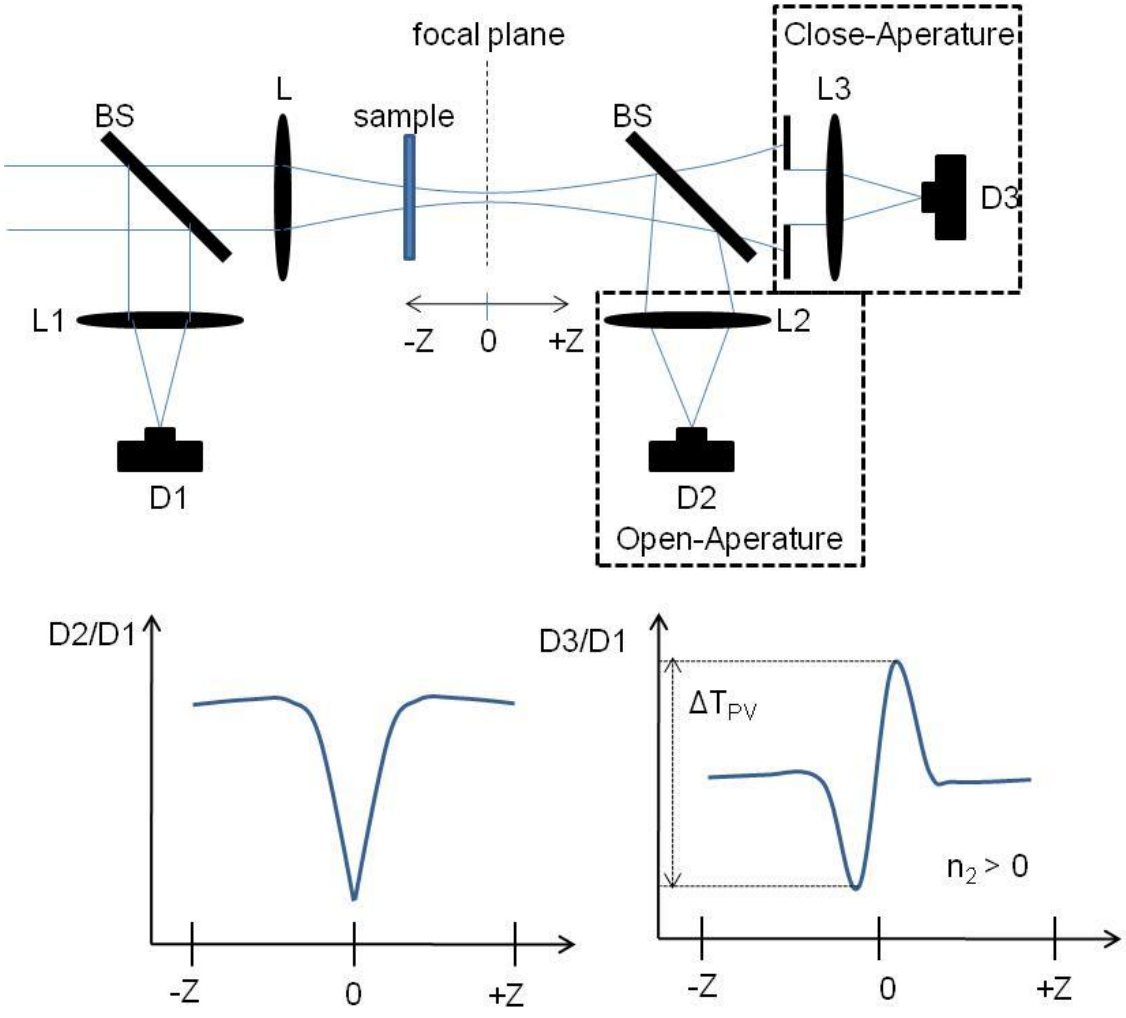

Scheme 2.5. The optical setup for femtosecond z-scan measurements.

2.3.1.3 Power-Dependent Nonlinear Transmission (Optical Limiting)

The apparatus for optical limiting has a similar optical layout as the open-aperture Z-scan, but instead of moving the sample along the Z direction the sample is fixed at a particular z-position. The change in nonlinear absorption is then monitored as a function of the intensity of the incident beam by varying the input pulse energy (see **Scheme 2.6**).

For femtosecond optical limiting, the same setup as femtosecond Z-scan was used but the focusing geometry was changed to F/20 and the repetition rate was reduced to 50 Hz to eliminate cumulative effects such as thermal nonlinearities. For nanosecond optical limiting, the excitation wavelength used was from the idler beam of an optical parametric oscillator (~4ns HW1/e, MOPO-PO, Spectra-Physics) generated by a Q-switched Nd:YAG laser (10 Hz, Quanta-Ray PRO-250-10, Spectra-Physics). The excitation beam was chopped at 1 Hz to eliminate cumulative effects. The focusing geometry was F/5 and the collection geometry was F/2 to ensure total collection of the exiting beam. The beam waist (15-25 μm HW1/e^2) was measured using a pinhole scan. The input energy was measured by an Ophir® PE9 pyroelectric head energy meter. Computer-controlled half-waveplate rotators (PR50-PP, Newport Corporation) in conjunction with polarizers were used to control the input energy. Two sample geometries were used in nanosecond optical limiting. In the bulk optical limiting measurements, the samples were solid films or solutions in a glass cuvette with a 1mm optical path length. For solution measurements, the focus was placed at the middle of the cuvette's path length. For film measurements, the sample was placed 1mm in front of the focus and the beam radius was slightly different than in solution measurements (i.e. 30-45 μm HW1/e^2). The second sample geometry involved a microcapillary waveguide with

18 mm length. In this setup, the microcapillary (20 μm in diameter, $n_{cladding}$ = 1.44, Polymicro Technologies) was filled with a solution of nonlinear material. The input beam was coupled into the microcapillary with a 10× objective and the exit beam was collected with a 20× objective. The benefit of using the microcapillary is to extend the length of nonlinear interaction with a constant beam radius, since the Rayleigh ranges in bulk optical limiting measurements are typically only a few mm's.

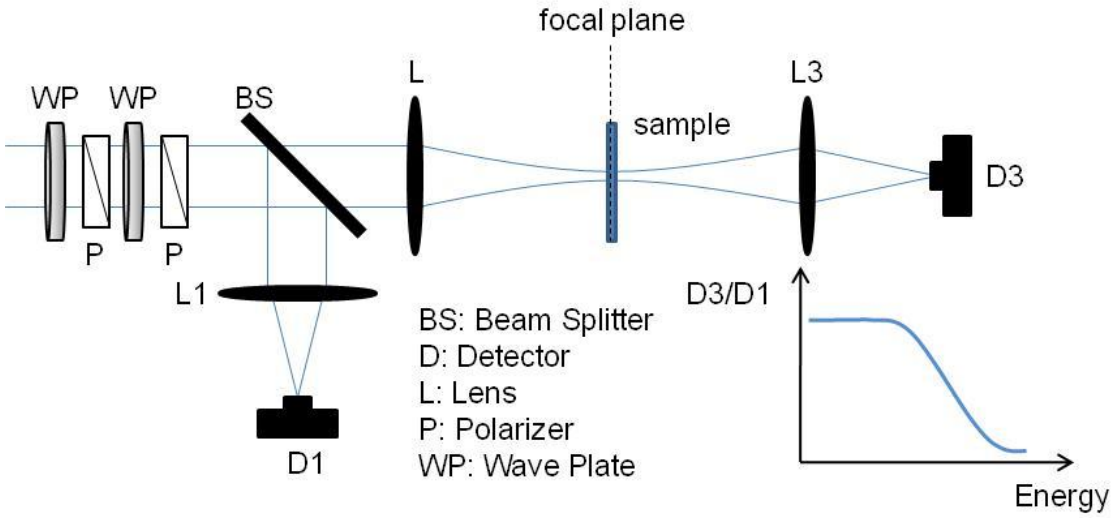

Scheme 2.6. The optical setup of optical limiting.

2.3.2 Characterizing Photophysical Properties: Transient Absorption Spectroscopy

Transient absorption spectroscopy has been used as a powerful tool to understand the photophysical respone of an excited molecule including the excited state absorption spectra and the temporal dynamic of various photo-induced transient species. Transient absorption spectroscopy is a pump-probe technique. The basic principle of transient absorption spectroscopy is to excite the target molecule with a strong pump pulse and then to interrogate the photo-induced transient species with a weak, broadband probe pulse. By varying the temporal delay of the probe pulse, the absorption of the transient species can be monitored at different delays, and therefore the temporal dynamics of the transient species can be determined. As previous mentioned, excited states have different lifetimes and therefore different impulse response are needed for excited state transitions. Thus, using pump pulses with different pulse widths, one will be able to resolve a wide rang of excited state dynamics. For example, using a femtosecond-pulsed pump beam, fast relaxation processes such as internal conversion or intersystem crossing can be resolved, while nanosecond pulses usually don't have sufficient temporal resolution. In chapter 4 and chapter 5, both femtosecond- and nanosecond- pulsed transient absorption spectroscopy were employed to understand the photophysical response of poly(phenylene vinylene) and dithienopyrrole-based copolymers. In these systems, fast photo-induced charge transfer dynamics were observed by femtosecond transient absorption and long-lived triplet absorption was observed by nanosecond transient absorption.

Femtosecond transient absorption spectra were acquired with a commercial pump-probe spectroscopy system (Ultrafast Systems, Helios) (see **Scheme 2.7**). The excitataion wavelengths (pump) were generated in the same way as the femtosecond Z-

scan mentioned previously. The probe beam was based on white-light continuum (WLC) generated by splitting a portion (~5%) of the regenerative amplifier (Spitfire, Spectra-Physics) and focusing into an appropriate crystal. The probed signals were collected by a fiber optic cable coupled to a multichannel spectrometer with a Silicon (spectral range 400-900 nm) or InGaAs (spectral range 800-1600 nm) sensor. The measureable delay time window extended up to 3.2 ns. The pump beam was chopped at 500 Hz to obtain, sequentially, the reference WLC spectra (without pump) and the signal spectra (with pump) which allowed for the generation of the transient (ΔOD) spectra. Each data point was averaged for 1.5 seconds. The instrument response function (~200 fs) and the chirp correction function for WLC (applied to all data sets) were determined by measuring the solvent response of carbon tetrachloride. For solution measurements, the optical pathlength of the quartz cuvette used was 2 mm and the solution was stirred continuously throughout the acquisition.

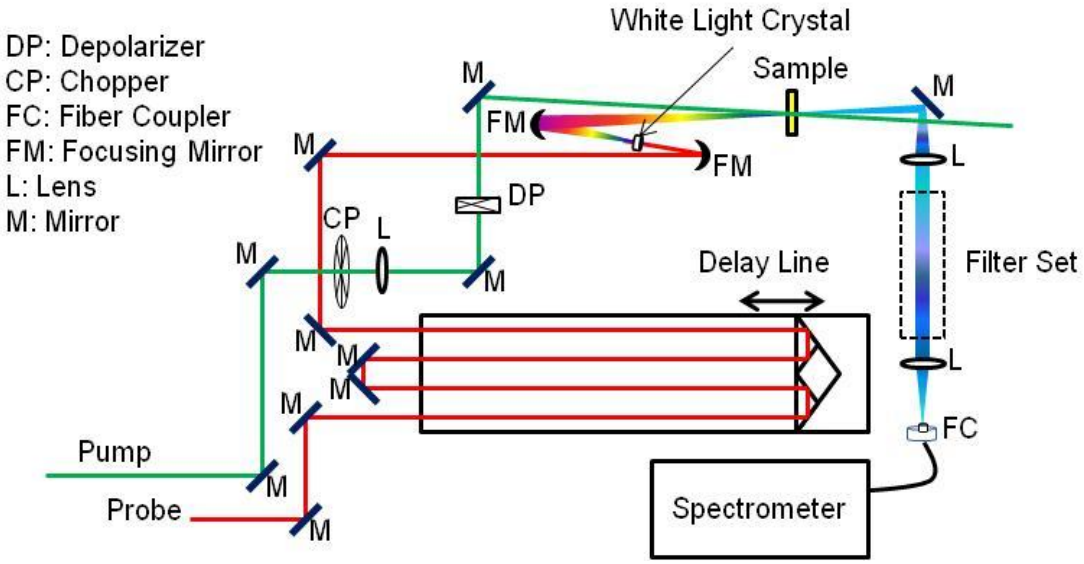

Scheme 2.7. The optical layout of femtosecond transient absorption spectrometer.

Nanosecond pump-probe measurements were carried out with the same laser source described for nanosecond optical limiting. The probe beam was white light produced by a tungsten-halogen bulb supplied with a 240W Oriel 69931 radiometric power supply (Newport Oriel, Irvine, CA). The pump and probe were overlapped at angle of approximately 15° as they passed through the sample. For transient kinetic measurements, the white light was focused on an Acton SpectraPro 2150i monochrometer (Princeton Instruments, Trenton, NJ) set to the selected probing wavelengths. The light was collected by a HCA-S-200M-Si (spectral range 320-1000 nm) or a HCA-S-200M-IN (spectral range 900-1700 nm) photodiode (Femto, Berlin, Germany) and the signal was recorded on a Tektronix 300MHz oscilloscope (Richardson, Texas). Solutions were contained in 1 cm path-length quartz cuvettes and were stirred continuously.

The transient data was analyzed by global fitting at multiple wavelengths with the function of

$$\Delta OD = y_0 + A_1 e^{-(t-t_0)/\tau_1} + A_2 e^{-(t-t_0)/\tau_2} + A_3 e^{-(t-t_0)/\tau_3} \qquad \text{(Eq. 2.7)}$$

where A is the amplitude of a transient absorbing species with lifetime of τ, and y_0 is the offset. The sign of amplitude indicates the type of excited state process. For example, if saturable absorption, ground state bleaching, or stimulate emission occurs, a negative sign of amplitude will be observed. In femtosecond transient spectra, the presence of an offset usually indicates the existance of a long-lived species like a triplet excited state. Nanosecond transient measurements with deoxygenated and oxygenated solutions confirmed the presence of triplet excited state species and reconstruction of the absorption spectra and temporal dynamics of these species became possible.

REFERENCES

[1] Hales, J. M. and Perry, J. W., "Organic and polymeric third-order nonlinear optical materials," in *Introduction to organic electronic and optoelectronic materials and devices*, Sun, S.-S. and Dalton, L. R., eds. (CRC Press, Boca Raton, FL, 2008).

[2] Sutherland, R. L., *Handbook of nonlinear optics* (Marcel Dekker, New York, NY, 1996).

[3] Hochberg, M., Baehr-Jones, T., Wang, G. X., Shearn, M., Harvard, K., Luo, J. D., Chen, B. Q., Shi, Z. W., Lawson, R., Sullivan, P., Jen, A. K. Y., Dalton, L. and Scherer, A., "Terahertz all-optical modulation in a silicon-polymer hybrid system," *Nature Materials* **5**, 703-709 (2006).

[4] Chi, S. H., Hales, J. M., Fuentes-Hernandez, C., Tseng, S. Y., Cho, J. Y., Odom, S. A., Zhang, Q., Barlow, S., Schrock, R. R., Marder, S. R., Kippelen, B. and Perry, J. W., "Thick optical-quality films of substituted polyacetylenes with large, ultrafast third-order nonlinearities and application to image correlation," *Advanced Materials* **20**, 3199-3203 (2008).

[5] Major, A., Yoshino, F., Aitchison, J. S., Smith, P. W. E., Sorokin, E. and Sorokina, I. T., "Ultrafast nonresonant third-order optical nonlinearities in znse for photonic switching at telecom wavelengths," *Applied Physics Letters* **85**, 4606-4608 (2004).

[6] Bader, M. A., Marowsky, G., Bahtiar, A., Koynov, K., Bubeck, C., Tillmann, H., Horhold, H. and Pereira, S., "Poly(*p*-phenylenevinylene) derivatives: New promising materials for nonlinear all-optical waveguide switching," *Journal of Optical Society of America B* **19**, 2250-2262 (2002).

[7] Koynov, K., Goutev, N., Fitrilawati, F., Bahtiar, A., Best, A. and Bubeck, C., "Nonlinear prism coupling of waveguides of the conjugated polymer MEH-PPV and their figures of merit for all-optical switching," *Journal of Optical Society of America B* **19**, 895-898 (2002).

[8] Sheik-Bahae, M. and Hasselbeck, M. P., "Third-order optical nonlinearities," in *OSA Handbook of Optics* (Optical Society of America, 2000).

[9] Strickler, J. H. and Webb, W. W., "Three-dimensional optical data storage in refractive media by two-photon point excitation," *Optics Letters* **16**, 1780-1782 (1991).

[10] Saricftci, N. S., Smilowitz, L., Heeger, A. J. and Wudl, F., "Photoinduced electron transfer from a conducting polymer to buckminsterfullerene " *Science* **258**, 1474-1476 (1992).

[11] Cha, M., Saricftci, N. S., Heeger, A. J., Hummelen, J. C. and Wudl, F., "Enhanced nonlinear absorption and optical limiting in semiconducting polymer/methanofullerene charge transfer films," *Applied Physics Letter* **67**, 3850-3852 (1995).

[12] Hales, J. M., Cozzuol, M., Screen, T. E. O., Anderson, H. L. and Perry, J. W., "Metalloporphyrin polymer with temporally agile, broadband nonlinear absorption for optical pulse suppression in the near infrared," *Optics Express* **17**, 18478-18488 (2009).

[13] Kuebler, S. M., *Studies of the third-order nonlinear optical properties of materials by degenerate four-wave mixing* (Thesis, St. Catherine's College, University of Oxford, Oxford, 1997)

[14] Balu, M., Hales, J., Hagan, D. J. and Van Stryland, E. W., "White-light continuum z-scan technique for nonlinear materials characterization," *Optics Express* **12**, 3820-3826 (2004).

[15] Van Stryland, E. W. and Sheik-Bahae, M., eds. *Z-scan technique for nonlinear materials characterization* (Marcel Dekker, New York, NY, 1998).

[16] Van Stryland, E. W. and Sheik-Bahae, M., "Z-scan measurements of optical nonlinearities," in *Characterization techniques and tabulations for organic nonlinear materials*, Kuzyk, M. and Dirk, C., eds. (Marcel Dekker, New York, NY, 1998), pp. 655-692.

[17] Milam, D., "Review and assessment of measured values of the nonlinear refractive-index coefficient of fused silica," *Applied Optics* **37**, 546-550 (1998).

[18] Hutchings, D. C. and Wherrett, B. S., "Theory of the dispersion of ultrafast nonlinear refraction in zincblende semiconductors below the band-edge," *Physical Review B* **50**, 4622-4630 (1994).

[19] Krauss, T. D. and Wise, F. W., "Femtosecond measurement of nonlinear absorption and refraction in CdS, ZnSe, and ZnS," *Applied Physics Letters* **65**, 1739-1741 (1994).

[20] Villeneuve, A., Yang, C. C., Stegeman, G. I., Ironside, C. N., Scelsi, G. and Osgood, R. M., "Nonlinear absorption in a GaAs wave-guide just above half the band-gap," *IEEE Journal of Quantum Electronics* **30**, 1172-1175 (1994).

[21] Dinu, M., Quochi, F. and Garcia, H., "Third-order nonlinearities in silicon at telecom wavelengths," *Applied Physics Letters* **82**, 2954-2956 (2003).

[22] Hutchings, D. C. and Wherrett, B. S., "Theory of anisotropy of 2-photon absorption in zincblende semiconductors," *Physical Review B* **49**, 2418-2426 (1994).

[23] Hurlbut, W. C., Lee, Y. S., Vodopyanov, K. L., Kuo, P. S. and Fejer, M. M., "Multiphoton absorption and nonlinear refraction of GaAs in the mid-infrared," *Optics Letters* **32**, 668-670 (2007).

CHAPTER 3

THICK, OPTICAL-QUALITY FILMS OF SUBSTITUTED POLYACETYLENES WITH LARGE, ULTRAFAST THIRD-ORDER NONLINEARITIES AND APPLICATION TO IMAGE CORRELATION

3.1 Abstract

Polyacetylene-based $\chi^{(3)}$ materials were synthesized by ring-opening metathesis polymerization (ROMP) of liquid phase precursors such as *n*-butyl-cyclooctatetraene and *sec*-butyl-cyclooctatetraene. The substituent on the monomer prevents the formation of crystalline domains during polymerization, thereby improving the amorphous morphology of the polymer in a solid-state neat film and the film's corresponding optical transparency. Different polymerization conditions were employed to optimize the monomer-to-polymer conversion efficiency and the population of long-chain conjugated polymers as well as the film's nonlinearity and transparency. The principal variations were choice of polymerization initiators, introduction of coordinating ligands (hexafluoro-*t*-butanol and tetrahydrofuran), and adjustment of the initiator-to-monomer ratio. The introduction of coordinating ligands to modulate the concentration of active initiators suggests a practical route to control the polymerization conditions and consequently polymer processing without the necessity of managing complicated organometallic syntheses. As a result, optical-quality films of substituted polyacetyelenes were fabricated with large $\chi^{(3)}$ of up to 2.1×10^{-10} esu in the near-infrared

(1150 – 1550 nm). Thick films (200 μm) of such materials provided large diffraction efficiencies (~0.1% at 100 MW/cm^2 for 1300 nm and ~1% at 1 GW/cm^2 for 1550 nm) and allowed the demonstration of ultrafast image-correlation applications.

3.2 Introduction

Processable organic materials with large, ultrafast third-order susceptibilities, $\chi^{(3)}$, could enable all-optical signal processing (AOSP) applications through either fabrication of large-area thick films or integration into hybrid organic/silicon photonic devices [1-4]. Conjugated polymers, such as polyacetylene, have been shown to exhibit large optical nonlinearities upon application of intense electromagnetic fields [2]. Despite these nonlinearities, many conjugated polymers are inadequate for photonic applications because they lack sufficient processability, or form films with significant crystallinity [5] or inhomogeneous morphologies [6] resulting in poor optical quality. For example, although films of unsubstituted polyacetylene have been found to possess large third-order susceptibilities [7-9], they also exhibit extensive crystallinity [10], resulting in poor optical quality and large scattering losses [11]. A more processable soluble diester polyacetylene derivative has been reported [1]; however, only thin films have been produced from this material and the bulky side groups can be anticipated to lead to a reduced nonlinear response through a dilution effect. The diester polyacetylene was successfully used in an image-correlation application performed using degenerate four-wave mixing (DFWM) in the visible region with resonant excitation, although the diffraction efficiency was relatively low, due mainly to the limited interaction length.

Ring-opening metathesis polymerization (ROMP) provides for the facile synthesis of a great variety of unsaturated polymers [12]. The ROMP method (**Scheme 3.1**) utilizes an organometallic alkylidene-based initiator (e.g., ruthenium-based Grubbs initiators [13-15] or 4-coordinate tungsten- and molybdenum-based Schrock initiators [16-18]) to polymerize strained-ring olefin monomers [6, 19]. The ROMP process allows for *in-situ* polymerization of liquid-phase monomers, which allows facile processing of neat films [11] as well as potential integration of the resulting polymers into micro- or nanostructured photonic devices. Moreover, this method is amenable to independent optimization of monomers and initiators to improve processing conditions, optical quality of films, and the third-order susceptibility of the resulting conjugated polymers.

In this chapter, the synthesis and processing of substituted polyacetylene obtained using ROMP of mono-substituted cyclooctatetraene (R-COT) monomers are reported. Polymerization and processing conditions have been developed that have led to thick (2 – 200 μm), large-area (> 1 cm^2) films possessing good optical transparency and large third-order nonlinearities in the near-infrared (NIR) region, including the telecommunication bands. Dispersion of third-order nonlinearities of poly(*n*-butyl-COT) films were studied by DFWM and Z-scan techniques throughout the 1150-1550 nm range. The good optical quality of a 200 μm thick poly(*n*-butyl-COT) film allowed for DFWM-based image correlation under off-resonant excitation conditions to be performed with improved diffraction efficiency relative to that obtained using the diester polyacetylene derivative mentioned above; the resulting diffracted signals were strong enough to be captured with a standard VIDICON detector. Furthermore, a demonstration of integrating poly(*n*-butyl-COT) into a microstructured 3D photonic crystal via *in situ* polymerization was achieved.

ROMP

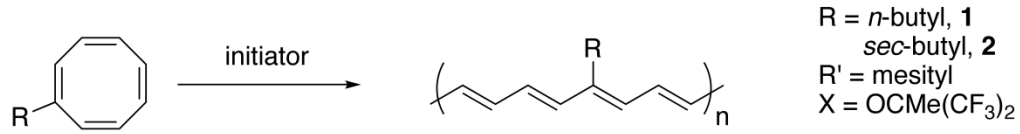

Initiators

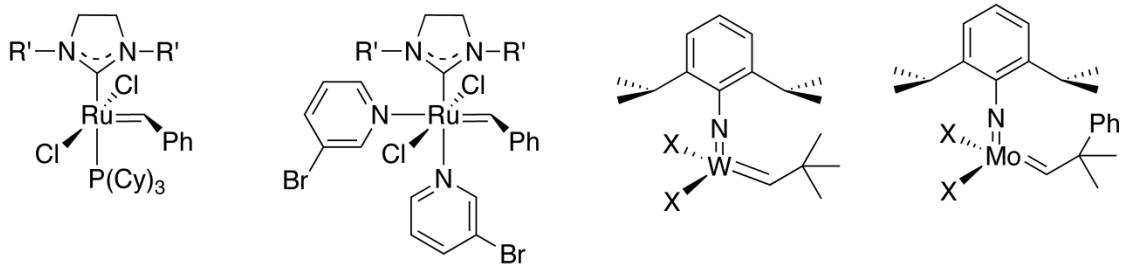

3 **4** **5** **6**

Scheme 3.1. Ring opening metathesis polymerization of mono-substituted cyclooctatetraene and structures of organometallic initiators used. Monomers **1** and **2** as well as intiator **3** were synthesized by Dr. Jian-Yang Cho and Dr. Susan Odom in Seth Marder group in the School of Chemistry and Biochemistry at the Georgia Institute of Technology. Initiator **5** was synthesized in Richard Schrock group in the Department of Chemistry at the Massachusetts Institute of Technology.

3.3 Background: Issue and Approach

The aforementioned morphology and crystallinity of unsubstituted polyacetylene films leads to optical scattering and limits the ability to perform optically-based processes. The to overcome such issues one can combine the use of side groups on monomers along with the control of ROMP via initiators, solvents, and additives to favor the formation of amorphous materials with reduced optical losses. It has been evidenced that the use of alkyl-substituted COT (**1** or **2**) instead of unsubstituted COT as the monomer leads to an amorphous polymer film morphology that exhibits reduced optical scattering [11], presumably due to side groups disrupting π-π stacking type aggregation.

On the other hand, efforts to control the process of ROMP have been mostly limited to molecular engineering through complicated organometallic syntheses. Based on a discussion with Professors R. H. Grubbs and R. R. Schrock, previous research in their groups suggested it was possible to use a co-solvent with electron-donating additives or ligands to interfere with the activity of ROMP initiators via the coordination to the center, electron-deficient transition metals. The hope was that such additives/ligands would provide a means to modulate the concentration of active initiators thereby allowing control of the polymerization conditions and consequently polymer processing and morphology. In this section, a brief description of ROMP, ROMP initiators, and electron-donating ligands that will affect the activity of the initiators is given.

3.3.1 Ring-Opening Metathesis Polymerization (ROMP)

The research of ROMP, as one kind of olefin metathesis, started in the 1950's. ROMP is a chain-growth type living polymerization and its initiation depends on the ring strain of monomer. In ROMP, metal initiators are used to perform the [2+2] cyclo-addition and redistribution of C=C double bonds. ROMP of strained-ring olefin monomers, such as R-COT, offers a convenient approach to synthesize unsaturated polymers like polyacetylene. The polymerization generally consists of several different steps (reactions) as illustrated in **Scheme 3.2**. After the reaction is initiated, the organometallic initiators usually stay connected to the double bonds of the cyclic monomers or acyclic polymers throughout the entire polymerization. Thus, chain transfer reaction can occur along with polymerization. Chain transfer can lead to a diverse polymer chain length distribution (inter-molecular) or can give rise to cyclic

oligomers (intra-molecular) such as benzene, thereby inhibiting the formation of long chain polymers. Since such a large number of reactions play roles in ROMP, the prediction and control of the behavior of the polymerization is usually difficult.

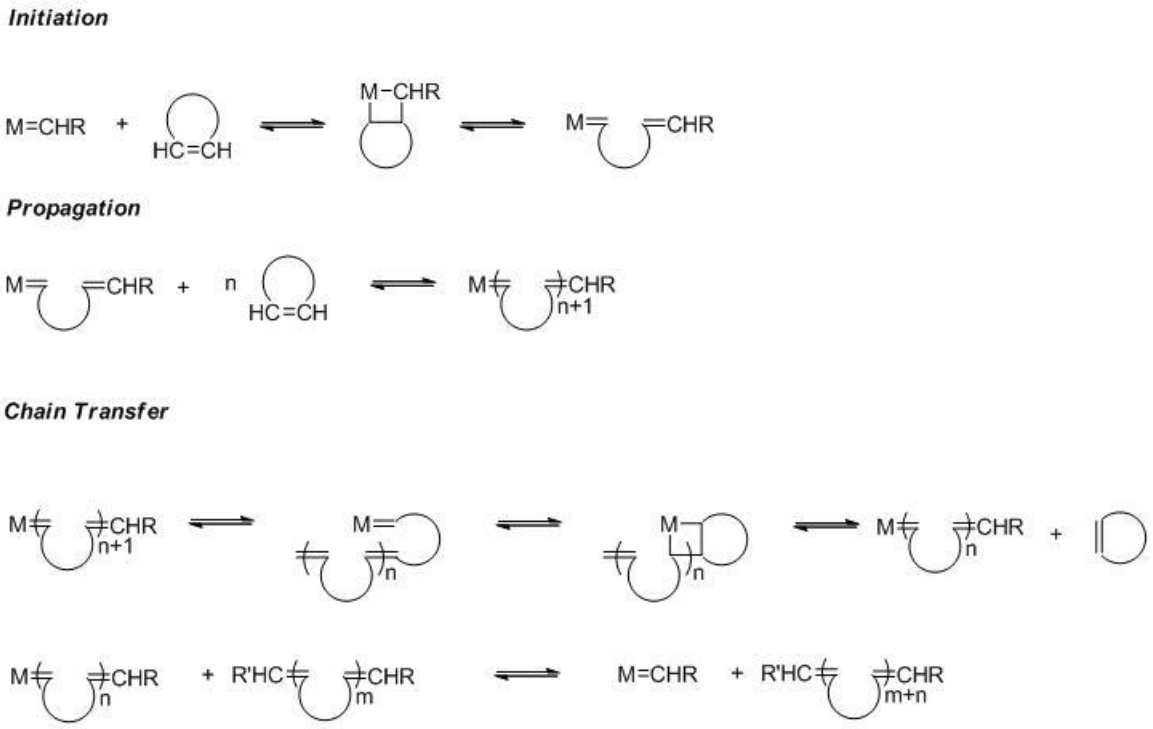

Scheme 3.2. Reactions in ring opening metathesis polymerization.

3.3.2 ROMP Initiators

The development of ROMP and other olefin metathesis reactions is tied to the research of various metathesis initiators. The research of metathesis initiators started with transition metal salts such as WCl_6. However, the application of these transition metal salts was limited due to their incompatibility with most functional groups and the difficulties in control over these initiators. In the 1970s, Chauvin proposed the metal

alkylidene-based mechanism for olefin metathesis [20]. Since then many efforts were attempted by researchers to synthesis these metal alkylidene initiators and to understand their reaction mechanisms. In the late 1980s, Schrock and Grubbs developed the highly active molybdenum and tungsten alkylidenes (**5** and **6**) [16-18, 21]. However, these initiators are highly sensitive to oxygen and moisture and intolerant to a number of functional groups such as aldehydes and alcohols [22]. Depending on the electron-donating strength of these functional groups, they can either form weak but competitive binding to the active, electron-deficient metal center and deactivate the initiator, or attack directly to the metal center and switch off the active species.

Different from these molybdenum and tungsten based initiators, ruthenium-based initiators were found to be very tolerant with the presence of alcohol, water and other polar functional groups [23]. Through a series of systematic improvements on the synthesis, activity, and functional group tolerance of ruthenium-based initiators, a set of trihexylphosphine (PCy_3) containing ruthenium initiators (including initiator **3**) were developed with improved activity and environmental stability [14]. Initiator **3**, especially, has superior activity for low-strained or sterically hindered olefin monomers and extraordinary half-life time, although the initiation and rate of conversion is slower compared to its siblings such as initiator **4** [13, 24, 25].

3.3.3 Electron-Donating Ligands and their Influence on Initiators

Many studies on electron-donating ligands and their influence on initiators have been reported by Christopher Gorman in his dissertation [26], as well as the possibility of using electron-donating ligands (Lewis bases) to obtain some degree of "*tailorability on*

rates of initiation and propagation and some effect control". A group of graduate students in R. H. Grubbs' research group synthesized a series of Schrock-type tungsten and molybdenum initiators (**5** and **6**) with an additional 5th electron-donating ligand directly bonded to the center metal and studied the properties of these modified initiators [26-28]. Floyd Klavetter showed weak binding ligands (e.g. THF) can dissociate (dissociation constant ~ 6.5×10^{-2} mol/l) from the center metal in solution at room temperature [28]. Jerome Claverie compared the strength of various ligands (**Scheme 3.3**) and showed the initiator activity is reduced by weak binding ligands (e.g. THF) and completely blocked by strong binding ligands (e.g. pyridine) [27]. Studies in R. R. Schrock's group also showed similar results, and gave evidence that the competing reactions between weakly or partially bonded ligands (e.g. quinuclidine) and monomers occurs at NMR time scales [29-31]. Based on this previous research, it was suggested that the use of proper ligands to compete with monomers could be a route to tailor the rate of polymerization and to obtain some degree of control without pursuing complicated organometallic synthesis.

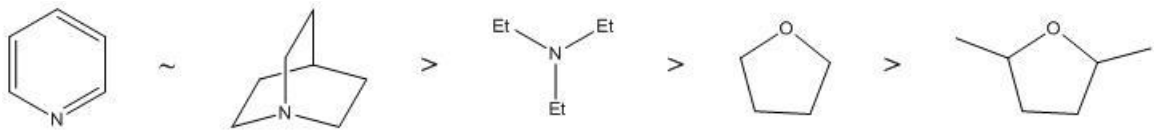

Scheme 3.2. Ligand strength scale for initiator **5**.

3.4 Results and Discussion

3.4.1 Comparison of Poly(R-COT)s Prepared Using Different Experimental Conditions

A variety of experimental conditions was employed for the polymerization of the R-COTs including different combinations of monomer/initiator and their respective molar ratios, as well as the inclusion or omission of a co-solvent or coordinating ligands. The monomer-to-initiator ratios were initially selected based on literature values [6, 26, 32]. Detailed results on the physical and optical properties of the resulting films for given processing conditions are listed in **Table 3.1** while the corresponding Vis-NIR absorption spectra are shown in **Figure 3.1**. It should be noted that all results reported in Table 3.1 were determined from measurements on multiple films (the statistical precision of the values was estimated to be ± 15%) each fabricated with the same batch of monomer and initiator. Since initiator **3** possessed only a 30% conversion efficiency for monomer **1**, initiator **4** was then investigated since it reacts more aggressively than **3** [24], and increasing the conversion efficiency might result in a larger population of long, conjugated polymer chains and a concomitant increase in nonlinearity. However, the polymerization of monomer **1** with initiator **4** resulted in films with no discernible increase in $|\chi^{(3)}|$ and very poor optical quality. To improve on these results, two approaches were undertaken: the amount of initiator used was decreased and a bulkier monomer (*sec*-butyl-COT **2** instead of *n*-butyl-COT **1**) was used. For the first approach, decreasing the amount of initiator resulted in a slight reduction in $|\chi^{(3)}|$ and little improvement in optical quality. For the second approach, the optical quality was improved but the measured nonlinearity was only half that of a poly(*n*-butyl-COT) film

synthesized with same monomer-initiator ratio. It should also be noted that the use of 1:1 mixtures of the monomers **1** and **2** with initiators **3** or **4** showed no dramatic improvement in the combination of optical quality and nonlinearity. It was reasoned that while the bulkier nature of the *sec*-butyl-COT monomer resulted in moderate improvement in optical quality, this characteristic also played a role in reducing the optical nonlinearity through a dilution effect. In accordance with the goal of identifying films that provided an optimal combination of these two qualities, the *n*-butyl-COT monomer was chosen for subsequent studies.

The next approach that was undertaken was to test Schrock-type tungsten and molybdenum initiators (**5** and **6**). It has been reported in the literature that the polymerization of COT using **5** with monomer-initiator ratio of 150:1 results in optimal films in terms of molecular weight and polydispersity index [26]. With the monomer-initiator ratio of 150:1, initiator **6** did not fully polymerize monomer **1,** possibly due to decomposition of the initiator prior to termination of polymerization, while initiator **5** reacted aggressively and the resulting polymer solidified within 10 seconds, which left insufficient time for film processing. Further increases of the amount of initiator **6** (or equivalently decreasing the monomer/initiator ratio), allowed for the fabrication of several varieties of poly(*n*-butyl-COT) films but their resulting nonlinearities were less than 5×10^{-11} esu (see Table 3.1). On the other hand, poly(*n*-butyl-COT) films polymerized with initiator **5** (at 150: 1 monomer-initiator ratio) gave larger nonlinearities but poor optical quality, which is likely due to the aggressive exothermic polymerization that can lead to an inhomogenous morphology. Overall, the activities of the ROMP initiators towards *n*-butyl and *sec*-butyl COT derivatives were found to increase in the

following order: Mo-based **6** < Ru-based **3** < Ru-based **4** < W-based **5**; these observations are consistent with previous reports of the relative ROMP activities of the initiators [13, 24].

The activity of the W initiator, **5**, was found to be so high that the time to gelation[‡] is impractically short for fabrication of films [26]. Thus, in order to improve the processability of the polymer solutions prior to gelation and the morphology of resulting films, the addition of moderately coordinating ligands (tetrahydrofuran – THF, and 1,1,1,2,2,2-hexafluoro-*tert*-butanol – HFB) were introduced to tailor the activity of initiator **5** and to have control over the rate of polymerization [6, 31]. Various molar ratios of initiator **5** and monomer **1** (including 150:1) and the coordinating ligands were examined. With an excess of THF (> 2 equiv.), an increase in the time to gelation and a decrease of the nonlinearity were observed. Furthermore, the average nonlinearity is higher with the use of HFB compared to without HFB. However, the best compromise between solution processability, film morphology and the resulting nonlinearity was obtained with the use of HFB and a small amount (less than 1 equiv.) of THF (see Table 3.1).

With the goal of producing films appropriate for later use in image-correlation experiments, particular polymerization conditions were identified that resulted in facile processing of thick films (i.e., longer times to gelation) which possessed good optical quality[§] and large $\chi^{(3)}$. While initiators **4** and **6** produced serviceable films in this regard,

---

[‡]The time to gelation was defined, somewhat arbitrarily, as the point after which the viscosity had increased to an extent that it was prohibitively difficult to transfer the polymerizing liquid mixture from the mixing vial to the glass substrate.

[§] The optical quality of the films was gauged both by the optical losses observed in the Vis-NIR absorption spectra, specifically in the 1300 – 1550 nm regime, as well as the

these films exhibited the lowest nonlinearities of all the initiators examined (Table 3.1) and resulted in films of poor and moderate optical quality, respectively. Initiators **3**, **5**, and THF/HFB-coordinated **5** produced films with reasonably large nonlinearities however, the short gelation times obtained with uncoordinated **5** made film fabrication difficult and the resulting films showed poor optical quality. Films produced with **3** and THF/HFB-coordinated **5** exhibited all of the desired qualities; however, while films from the THF/HFB-coordinated initiator **5** possessed approximately twice the nonlinearity of those of **3** (Table 3.1), initiator **3** produced films with better morphology (see **Figure 3.2**, lower right) resulting in superior optical quality (Fig. 3.2, left).

It should be also noted that other factors have been observed to affect the polymerization rate, conversion yield, and nonlinearity of the polymers. These include environmental contaminants, such as moisture, which can degrade the initiator, and impurities, such as mono-substituted cyclooctatriene (a potential side product during monomer synthesis), that can lead to reduced conjugation length due to the presence of saturated units in the polymer chain.

---

amount of distortion observed on a laser beam (operating in the same spectral region) after passing through film. This provided some measure of both the optical scattering losses associated with crystallinity of the films as well as their overall morphology.

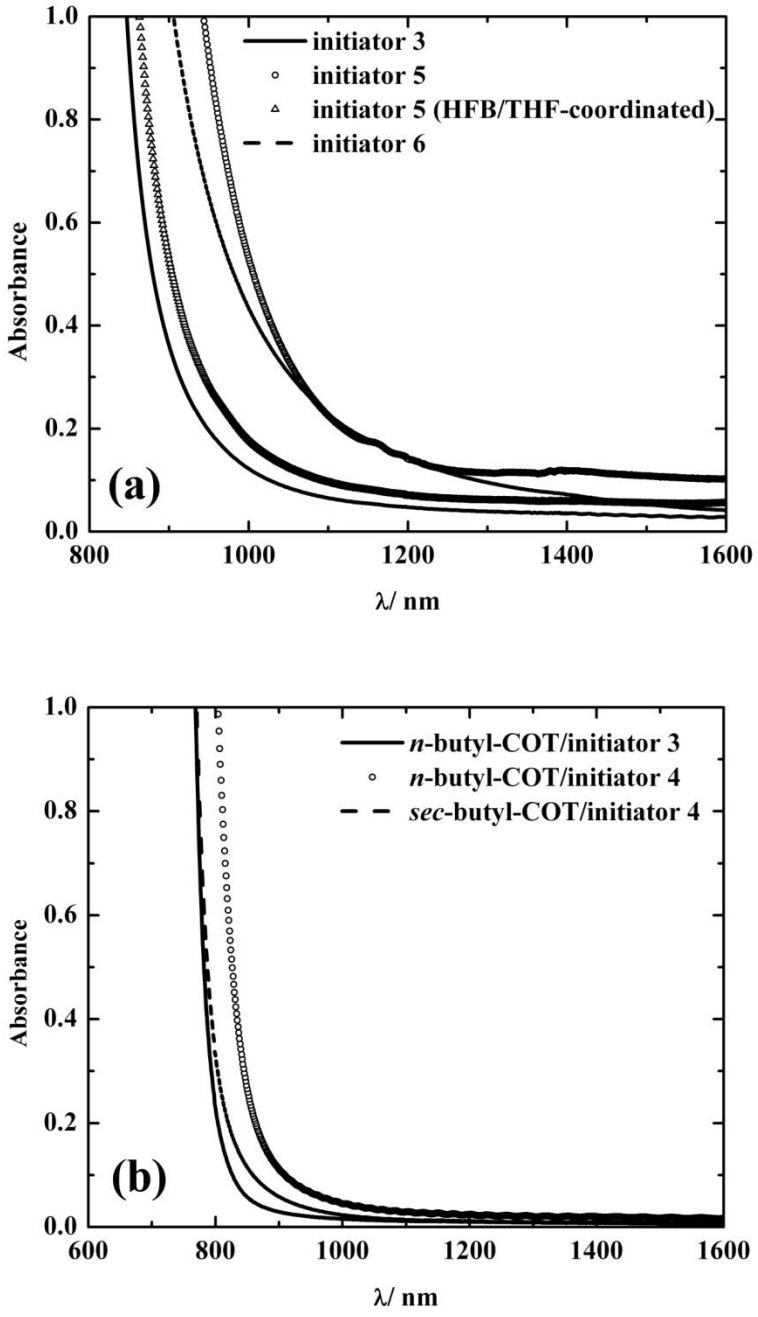

Figure 3.1. Absorption spectra of poly(R-COT) films made with different monomer and initiator systems. (a) 25 m thick poly(*n*-butyl-COT) films made with initiator **3** (500:1), **5** (150:1), HFB/THF-coordinated **5** (150:1), and **6** (50:1). (b) 15 m thick poly(*n*-butyl-COT) films made with initiators **3** (500:1) and **4** (450:1) and poly(*sec*-butyl-COT) films made with initiator **4** (450:1).

Table 3.1. Third-order nonlinearities at 1300 nm of poly(R-COT)s derived from various ROMP initiators and COT monomers. The instrumental accuracy and statistical precision associated with the $|\chi^{(3)}|$ values were both estimated to be ± 15%.

Monomer	**Initiator**	**Ratio**[d]	**Processing Window**[f]	**Thickness [μm]**	**Bandedge [nm]**	$\|\chi^{(3)}\|$ **[esu]**	**Optical quality**[h]
1[a]	**3**	500:1	~30 mins	25	854	9.8×10^{-11}	good
	4	450:1	~5 mins	15	(945)[g]	8.3×10^{-11}	poor
		900:1	~5 mins	15	851 (918) [g]	6.5×10^{-11}	poor
		1660:1	~5 mins	15	(887) [g]	5.1×10^{-11}	poor
	5	150:1	~10 secs	25	915	13×10^{-11}	poor
	HFB/THF-coordinated **5**[c]	150:1	~30 secs	25	860	21×10^{-11}	moderate - good
	6	50:1	~5 mins	25	880	4.3×10^{-11}	moderate
		100:1	~5 mins	25	831	1.5×10^{-11}	moderate
		150:1[e]	-	-	-	-	-
2	**4**	450:1	~5 mins	15	772	3.8×10^{-11}	moderate
1/2[b]	**3**	500:1	~30 mins	25	774	2.2×10^{-11}	good
	4	450:1	~5 mins	15	799	7.2×10^{-11}	moderate

[a] Several batches of *n*-butyl-COT were used. [b] *n*-butyl-COT : *sec*-butyl-COT = 1:1 (molar ratio). [c] HFB:THF : initiator **5** = 1:0.1:1 (molar ratio). [d] monomer-to-catalyst molar ratio. [e] The mixture of monomer and initiator **6** remained as transparent, dark red, viscous fluid after 4 days, which suggests the initiator might be decomposed before finishing polymerization. [f] The length of processing time window is based on the time to gelation. [g] The bandedges in the parentheses were measured with 200 μm thick films. [h] These trends can be qualitatively observed in the Vis-NIR absorption spectra shown in Figure 3.1, however film morphology observed via laser beam distortion following passage through a film also played a role in the determined optical quality.

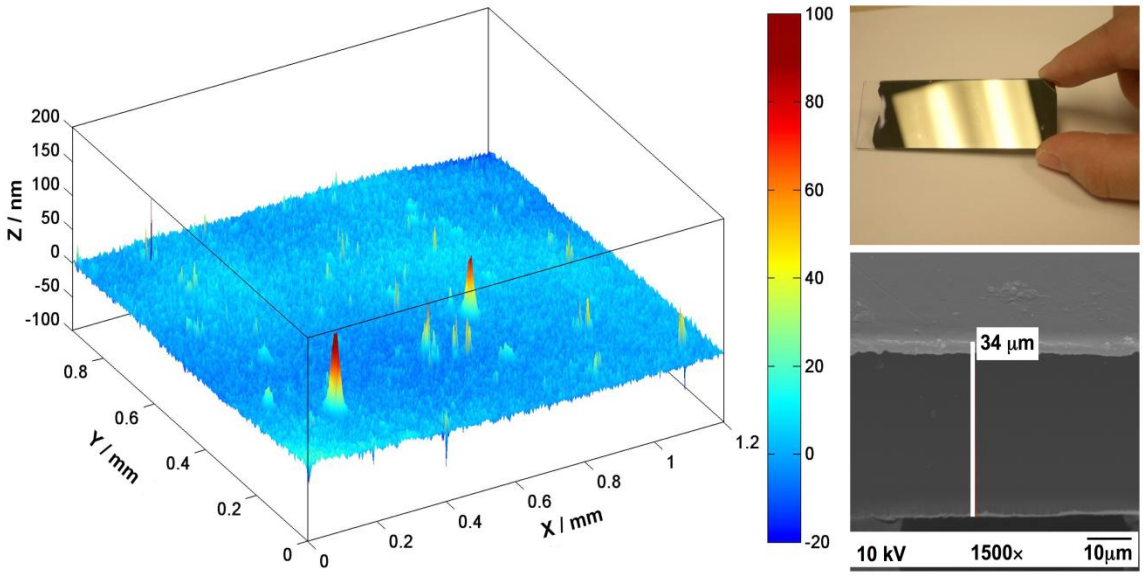

Figure 3.2. Representative topographical and morphological characterization of *in situ* polymerized poly(*n*-butyl-COT) films on glass substrates obtained using initiator **3**. (Left) Optical profilometer image of the film surface which reveals an RMS roughness of ~10 nm despite some surface impurities. (Lower right) SEM image of the cross-section of the film revealing an amorphous morphology. (Upper right) Photograph of a 1 inch × 3 inch area film showing its highly reflective nature.

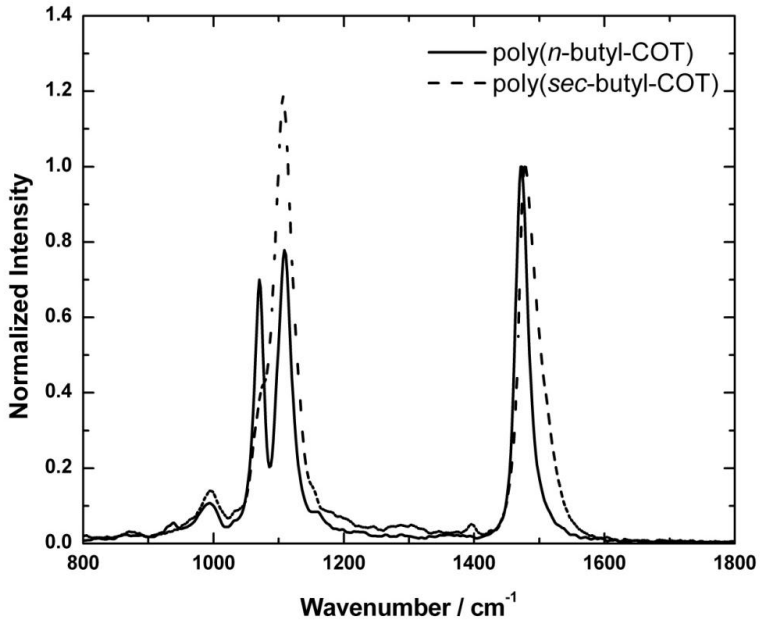

Figure 3.3. Typical resonance Raman spectra of poly(R-COT); C=C stretching at 1470-1480 cm^{-1} and C-C stretching at 1100-1110 cm^{-1}.

3.4.2 Physical and Linear Spectral Properties of Substituted Polyacetylenes

As described in the Experimental Details (see below), the thicknesses of the polymer films could be readily controlled in the range from 2 to 200 μm, and large-area (> 1 cm^2) films could easily be achieved (see Figure 3.2, upper right). The poly(R-COT) films were found to possess linear refractive indices varying from 2.1 to 2.2 at 1300 nm, depending on the film composition, consistent with the expected high polarizability of long polyene chains. Strong linear absorption in the visible wavelength region and intense C=C stretching vibrational bands around 1470 cm^{-1} in the resonance Raman spectra (**Figure 3.3**) are also indicative of long-chain, *trans*-dominated, polyacetylene [33-36]. The absorption band-edge positions of 25 μm thick poly(*n*-butyl-COT) and poly(*sec*-butyl-COT) films ranged from 750 to 950 nm, the spectral cut-offs being dependent on the particular polymerization conditions employed. (Figure 3.1)

Poly(R-COT)s synthesized with different monomers and catalysts showed the typical Raman spectra of *trans*-polyacetylene with C=C stretching vibrational frequencies at 1470 cm^{-1} and C-C stretching frequencies around 1100 cm^{-1} (Figure 3.3). No *cis*-polyacetylene features (908, 1247, and 1541 cm^{-1}) [37] were observed in the spectra, which indicated a dominant contribution from the *trans* content. According to previously reported experimental and theoretical studies [33-35], a reduction in vibrational frequency occurs concomitantly with decreasing band gap energy and increasing polymer conjugation length. Therefore, the resonant Raman spectra determined for the synthesized poly(R-COT)s here suggested that the films contained a significant population of long chain conjugated polymers which possessed associated band gap energies approaching 1.8 eV, a value predicted for a polyacetylene polymer with infinite conjugation length.

3.4.2.1 Correlation Between Raman Intensity, Absorption Band Edge, and $|\chi^{(3)}|$

For poly(R-COT) films of similar thickness and fabricated with the same type of monomer/catalyst combination, it should be noted that a strong correlation was found between the band-edge position, the intensity of the C=C stretching Raman signal, and the $\chi^{(3)}$ values for the various films measured. **Figure 3.4** depicts this correlation for a number of different 25 μm thick poly(*n*-butyl-COT) films fabricated using catalyst **3**. The recipe for the polymerization process differed slightly from film to film by the batch of catalyst or monomer used as well as the inclusion of solvent with the monomer/catalyst mixture. Figure 3.4a shows the $|\chi^{(3)}|$ values of the films versus their respective band edges. The band edges were determined simply by the intersection of two lines extrapolated from the fast rising edge of the absorption band and the long wavelength baseline (see Figure 3.1). Figure 3.4b shows the $|\chi^{(3)}|$ values versus the intensities of the C=C stretching resonant Raman signal located at 1470-1480 cm^{-1} (see Figure 3.3). These intensities have been normalized to the peak value. The fitting lines reveal linear correlations for both sets of observables. This linear correlation is likely the result of the varying concentration of long, conjugated polymer chains present in each film that would be expected to play a dominant role in the band edge position, resonance Raman intensity, and nonlinearity. These results provided a reliable, semi-quantitative means to predict the nonlinearity of a film through simple spectroscopic measurements and consequently allowed for a more rapid optimization route for film nonlinearity following variation of a particular constituent or processing condition.

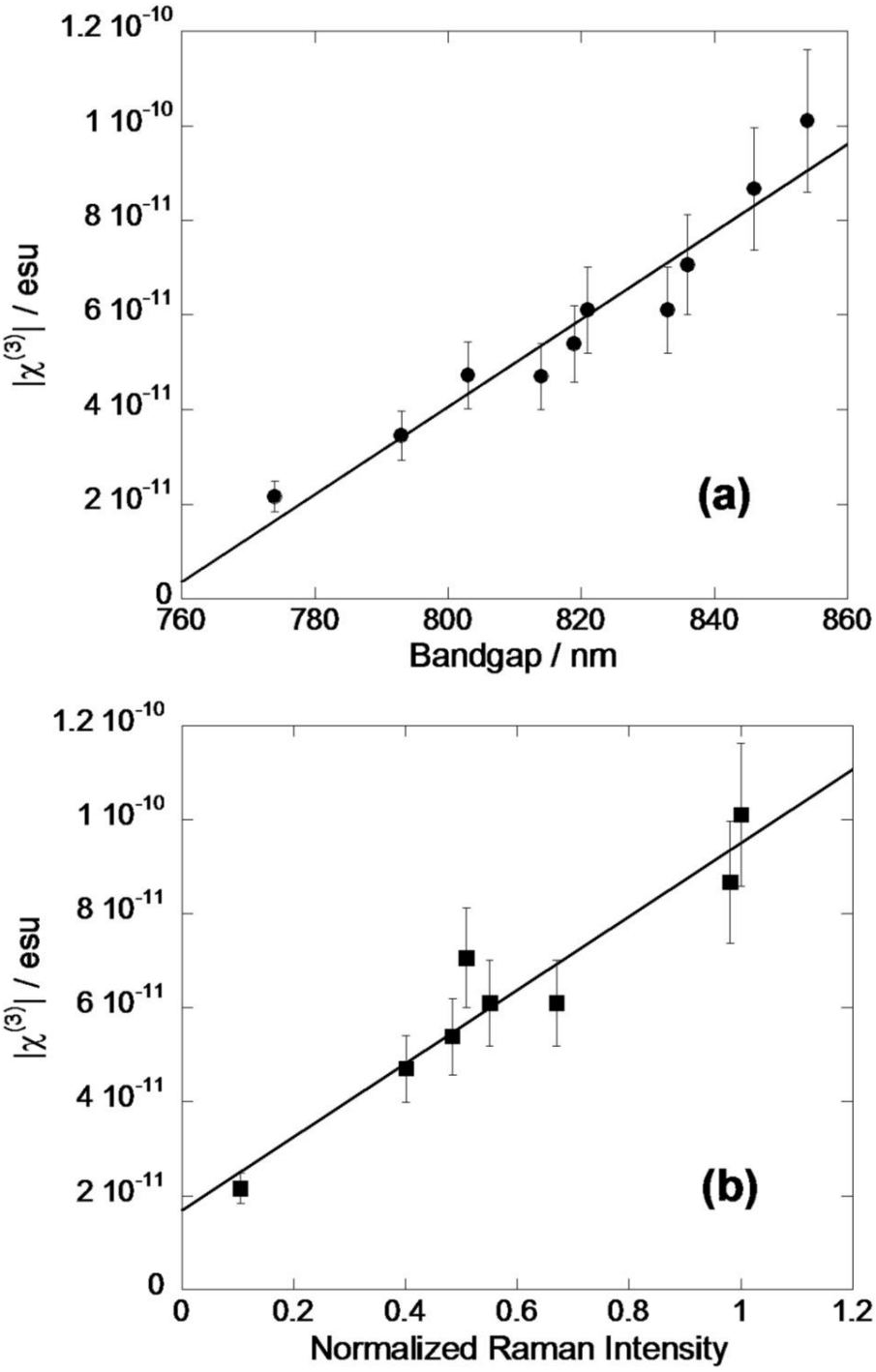

Figure 3.4. Correlation plots for 25 μm thick poly(*n*-butyl-COT) films fabricated using initiator **3** employing a variety of different processing conditions: (a) $|\chi^{(3)}|$ versus band edge position and (b) $|\chi^{(3)}|$ versus normalized resonance Raman intensity. The solid lines denote linear curve fittings to the data. Error bars associated with the $|\chi^{(3)}|$ values are estimated at ± 15%.

3.4.2.2 Determining Optical Losses of Poly(*n*-butyl-COT) Films

The overall optical losses of poly(*n*-butyl-COT) films synthesized with initiator **3** were determined from absorption spectra on the hermetically sealed, sandwiched films of 100 – 200 μm thickness. First, the absorption spectra of 2 – 5 μm thick, sandwiched poly(*n*-butyl-COT) films (fabricated using catalyst **3**) were measured and their average optical densities, $OD_{thin,\lambda}$, at 1300 nm and 1550 nm were used to correct for the reflection losses due to the air-glass-polymer interfaces in thicker films (≥ 25 μm), $OD_{correct,\lambda} = OD_{thick,\lambda} - OD_{thin,\lambda}$. The transmission losses, in *dB*, of individual films with different thicknesses, *L*, were calculated based on the corrected optical densities, $dB = 10 \times OD_{correct,\lambda} / L(cm)$. The transmission losses of over 100 different films with thicknesses ranging from 25 to 200 μm were calculated. For 100 – 200 μm thick films, the average losses were found to be 41 ± 11 dB/cm at 1300 nm and 22 ± 7 dB/cm at 1550 nm. For films with thicknesses below 100 μm, reflection losses dominated and the thin sample absorption correction resulted in large errors. Accordingly, these films were not included in the final loss determination.

3.4.3 Dispersion of Degenerate Third-Order Nonlinear Optical Properties

The study of wavelength-dependent dispersion of degenerate third-order nonlinear optical properties of poly(R-COT) was guided by Dr. Joel M. Hales. All poly(R-COT) films were found to possess large optical nonlinearities with ultrafast temporal response (<100 fs) throughout the NIR, consistent with non-resonant $\chi^{(3)}(-\omega;\omega,-\omega,\omega)$ values. Polarization-dependent DFWM measurements as well as careful fitting to Z-scan data

also support a non-resonant third-order nonlinearity. This is consistent with the large detuning of the excitation wavelengths from the lowest energy one-photon electronic resonance. Furthermore, the experimentally measured phase of $\chi^{(3)}$ across the NIR is also relatively small, which is also consistent with two-photon resonances not being a major contributor to the nonlinear response. Evidence of the large ultrafast nonlinearities of poly(R-COT) films is given in **Figure 3.5**. Figure 3.5 shows the power-dependent response of the DFWM signal for both a slab of fused silica and a poly(*n*-butyl-COT) film. At similar signal magnitudes, there is a 30× reduction in drive intensity and a 20× reduction in interaction length for the poly(*n*-butyl-COT) film, which reflects a nonlinearity for the film that is nearly four orders-of-magnitude greater than that of fused silica. Both power dependencies show a slope of ~3 as expected for a non-resonant third-order nonlinearity. The power-dependent response DFWM signal for the poly(n-butyl-COT) film becomes slightly hypocubic at higher intensities as evidenced in Figure 3.5a. This is a result of increased nonlinear absorption resulting in reduced driving intensities. Figure 3.5b shows the temporal dependence of the DFWM signal for the two samples. In both cases, the response is limited only by the temporal duration of the laser pulses suggesting the temporal response is << 100 fs.

Films of poly(*n*-butyl-COT) showed different values of $|\chi^{(3)}|$ at 1300 nm depending on the initiator used; the values increased in the following sequence: **6** < **4** < **3** < **5** < THF/HFB-coordinated **5** (see Table 1 for complete values). Films possessing good optical quality produced with **3** and THF/HFB-coordinated **5** had nonlinearities of 9.8×10^{-11} and 2.1×10^{-10} esu, respectively. These $|\chi^{(3)}|$ values compare favorably with non-resonant nonlinearities for other conjugated polymers [1]. It should be noted that

larger third-order nonlinearities in this spectral region have been found for trans-polyacetylene prepared by the Shirakawa method (see Reference [7]). However, these nonlinearities were determined via third-harmonic generation measurements and therefore reflect $\chi^{(3)}(-3\omega;\omega,\omega,\omega)$. This nonlinearity is known to be enhanced through both two- and three-photon resonance enhancement. These values would therefore be reduced accordingly for non-resonant values of $\chi^{(3)}(-\omega;\omega,-\omega,\omega)$ as reported herein. Furthermore, the dispersion of the nonlinearity was determined in the NIR using the Z-scan method and the values of the magnitude and phase[4] of $\chi^{(3)}$ for a representative film are shown in **Table 3.2**. Two points can be gleaned from these data. The first is that the existence of phase angles less than 30 degrees implies that nonlinear refraction dominates nonlinear absorption throughout most of the NIR region for these films. Second, the dispersion is relatively weak in the 1300 – 1550 nm region but shows evidence of a possible two-photon resonance around 1150 nm. Finally, the values for n_2 and β at 1300 nm for the film produced with THF/HFB-coordinated catalyst **5** were determined to be 1.5×10^{-16} m^2/W and 6.8×10^{-10} m/W, respectively. These values are significantly larger than those of either silicon or gallium arsenide [38], semiconductors that are typically utilized as $\chi^{(3)}$ materials in this spectral regime.

[4] The magnitude and phase of $\chi^{(3)}$ are related to its real and imaginary components (determined by the Z-scan technique) as follows: $|\chi^{(3)}| = [\mathrm{Re}(\chi^{(3)})^2 + \mathrm{Im}(\chi^{(3)})^2]^{1/2}$ and $\phi = \arctan[\mathrm{Im}(\chi^{(3)})/\mathrm{Re}(\chi^{(3)})]$. This can be equivalently expressed as $\mathrm{Re}(\chi^{(3)}) = |\chi^{(3)}|\bullet\cos\phi$, $\mathrm{Im}(\chi^{(3)}) = |\chi^{(3)}|\bullet\sin\phi$. The $\mathrm{Re}(\chi^{(3)})$ is associated with nonlinear refraction while the $\mathrm{Im}(\chi^{(3)})$ is associated with nonlinear absorption. Conversion from the Re/Im components of $\chi^{(3)}$ to the nonlinear refractive index (n_2) and the two-photon absorption coefficient (β) can be found in Reference 1.

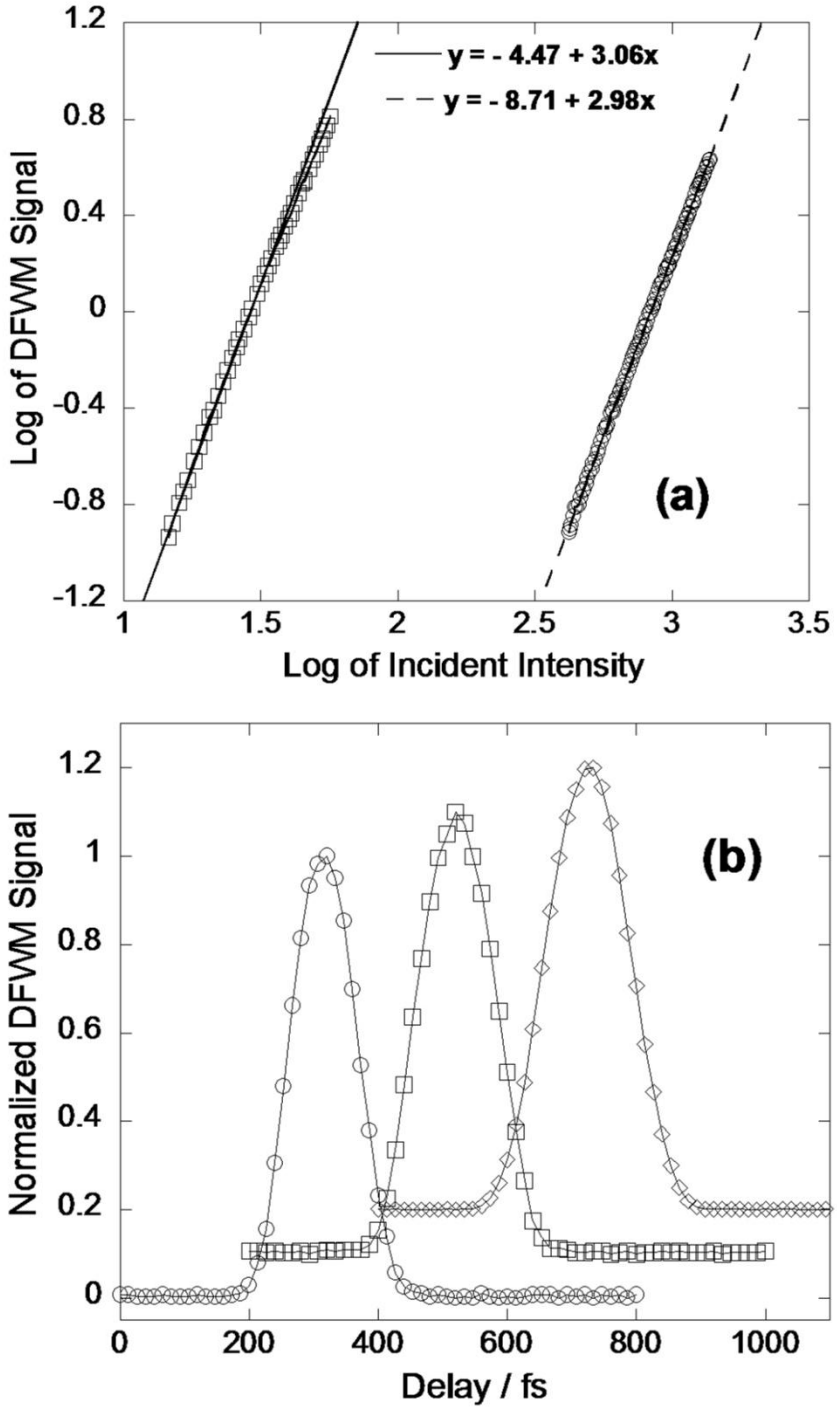

Figure 3.5. (a) Power dependence of DFWM signal for 540 μm slab of fused silica (circles) and 25 μm thick poly(*n*-butyl-COT) film (squares) using initiator **3** as denoted in Table 3.1. Lines denote linear fits to data. (b) Time-resolved DFWM signals for 540 μm slab of fused silica (open circles) and the same polyacetylene film at two different intensities (0.5 GW/cm^2, squares; 2.5 GW/cm^2, triangles). Lines are given as guides for the eye and plots are offset in x and y for ease of viewing.

Table 3.2. Dispersion of $\chi^{(3)}$ and ϕ [a] for selected wavelengths throughout the NIR region for poly(*n*-butyl-COT) film.[b]

λ [nm]	**1150**	**1300**	**1450**	**1550**
$\lvert\chi^{(3)}\rvert$ [esu]	16.7×10^{-11}	9.8×10^{-11}	8.0×10^{-11}	6.7×10^{-11}
ϕ	51°	26°	17°	20°

[a] ϕ is the phase of $\chi^{(3)}$. [b] Film prepared using initiator **3**.

3.4.4 Application to Image Correlation

A particular AOSP application, for which such large area films are suitable, is optical correlation for image recognition. Pattern or image recognition performed in the optical domain can be significantly faster than the same process performed in the electronic domain due to its parallel nature. It has long been known that DFWM can be exploited to perform image recognition [39]. Furthermore, employing a material with an ultrafast nonlinearity allows for the possibility of extremely rapid optical pattern recognition, which could play a significant role in the development of security verification [40], facial recognition [1], and artificial intelligence in general. The success of this application is predicated on a large diffraction efficiency which itself is dependent on the drive intensity, sample length and material nonlinearity [1]. Facile processing through ROMP using initiator **3** (chosen for the superior optical quality of the resulting films) permitted fabrication of 200 μm thick poly(*n*-butyl-COT) films which, in the DFWM geometry, were found to generate substantial diffraction efficiencies at moderate drive intensities using off-resonant excitation: ~0.1% at 100 MW/cm^2 for 1300 nm and ~1% at 1 GW/cm^2 for 1550 nm. These results represent sizable improvements compared

to other conjugated polymers [1] that have been used for DFWM, due in part to both the large nonlinearity and increased interaction length of the poly(*n*-butyl-COT) films.

These sizable diffraction efficiencies permitted demonstration of imaging and image recognition experiments using the aforementioned 200 μm thick poly(*n*-butyl-COT) films. This demonstration was performed by Dr. Shuo-Yen Tseng and Dr. Canek Fuentes-Hernandez from Professor Bernard Kippelen's research group at the School of Electrical and Computer Engnineering. For the imaging experiments, 1 mm diameter circular apertures encoded the beams used as the impulse response, $h(\mathbf{r})$, and reconstruction, $r(\mathbf{r})$, functions [41]. The letter characters, approximately 3.5 mm × 3.5 mm in size, comprising the word "GATECH" were sequentially encoded onto the object beam $g(\mathbf{r})$. The DFWM signal, which is proportional to the convolution, $|r(\mathbf{r}) \otimes h(\mathbf{r}) \otimes g(\mathbf{r})|^2$,[42] was then captured at the rear focal plane of the imaging system. As shown in **Figure 3.6a**, clear imaging with a signal-to-noise ratio (SNR) ≥ 2 was observed despite the relatively large extent of the impulse and reconstruction apertures. The finite size of these apertures produced a smoothing effect by acting as a low-pass filter for the angular spectrum of the input fields at the sample position. While the spatial resolution could be improved with the use of smaller apertures, in our setup this reduces the transmitted power, yielding smaller diffraction efficiencies and signals comparable with the uncorrelated scattering from the fundamental beams hence producing SNR ~ 1.

Image recognition was then implemented by replacing the impulse response, $h(\mathbf{r})$, with the image of an airplane and by sequentially encoding $g(\mathbf{r})$ with different images, as shown in Figure 3.6b. In an image-recognition experiment, a positive correlation

corresponds to the strongest signal around the image's zero-order component (**r** = 0). As can be demonstrated [42], this is expected for the autocorrelation of the impulse response, which can be obtained through a convolution if $g(\mathbf{r}) = h^*(-\mathbf{r}) = h(-\mathbf{r})$, where the complex conjugate can be dropped since *h* is real. As shown in Fig. 3.6b, the autocorrelation signal, proportional to $|r(\mathbf{r}) \otimes h(\mathbf{r}) \otimes h(-\mathbf{r})|^2$, yields a larger signal around the zero-order component compared to the one obtained if the original airplane is rotated 90° or if the original airplane is replaced with the image of a different airplane.

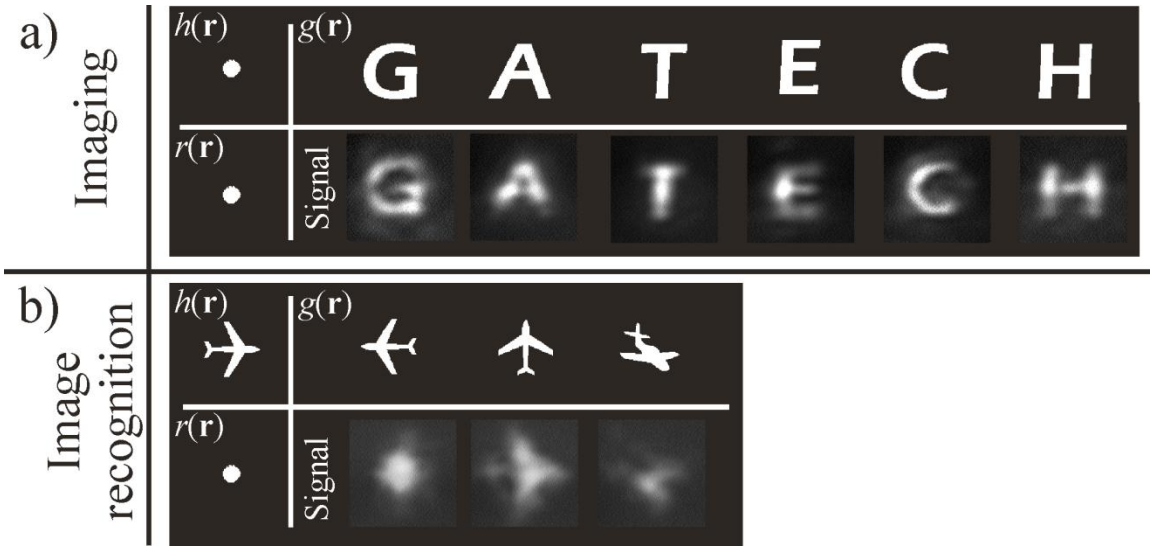

Figure 3.6. Image correlation using DFWM in a 200 μm thick poly(*n*-butyl-COT) film prepared using initiator **3**. a) Imaging obtained through DFWM. b) Image recognition demonstration. In all cases, 1 mm diameter circular apertures were used. This experiment was performed by Dr. Canek Fuentes-Hernandez and Dr. Shuo-Yen Tseng in Bernard Kippelen group in the School of Electronics and Computer Engineering at the Georgia Institute of Technology

3.4.5 Demonstration of *in situ* Polymerization for Photonic Microstructure Integration

As mentioned previously, ROMP with a liquid-phase monomer can potentially allow the integration of poly(R-COT) into nano- or micro-structured photonic devices such as a photonic crystal (PC). Photonic crystals (PC) are relatively new types of optical materials with a periodic refractive index where a photonic band gap (PBG) is formed and has the ability to selectively block the transmission of electromagnetic (EM) waves [43, 44]. PCs can be fabricated through multi-photon lithography, electron-beam direct writing, or self-assembly [45, 46]. The location of the PBG or the wavelength of maximum reflectance is determined by the size and refractive index of each component in the structure as well as the nature of the periodicity itself [47]. By fabricating a PC using nonlinear optical (NLO) materials with large nonlinear refractive indices in the region of the PBG, the location of the PBG and consequently the propagation of light can then be controlled by varying the incident intensity. To fabricate a NLO material-based PC, a prospective approach is to infiltrate NLO materials into an existing PC template; however, this approach is usually limited by the solubility and processability of the available NLO material. The development of ROMP of poly(R-COT) described above showed that polymer films can be synthesized *in situ* with a liquid phase mixture of monomers and initiators with or without solvent. Thus, it should be possible to draw the liquid, reacting mixture of monomers and initiators into the microstructure of a PC by capillary force.

The slow polymerization of *n*-butyl-COT with initiator **3** allows the mixture to remain as a low viscosity liquid throughout the infiltration process. The preliminary

demonstration of infiltration of poly(R-COT) into microstructure PCs via *in situ* polymerization was carried out by an undergraduate researcher, Meng Kang.[5] In this work, the PC templates were synthetic opals made from silica microspheres via self assembly. The monomer-to-initiator equivalent ratio was ~450:1 and the initiator was pre-dissolved in spectral grade dichloromethane to a concentration of 0.1M. While low-weight molecules still dominated and the solution mixture remained fluid, the mixture was infiltrated into the PC by capillary action. **Figure 3.7** shows the scanning electron microscope image of an infiltrated opal film with microspheres of diameter 700 nm. In Figure 3.7, spheres covered by polymer shown darker color due to the electronic charging effect. As shown in the figure, the poly(*n*-butyl-COT) had penetrated to different depths of the opal film indicating good infiltration, as opposed to just coating the surface. As seen in the cross section, polymer formed bee-comb-like frame structures (light color) when the spheres were removed. However, the infiltration also showed signs of disturbed microstructures, which might lead to broaden reflection bands and reduced reflectivity. (**Figure 3.8**) The PBG location or peak reflection wavelength (λ_{max}) is determined by

$$\lambda_{\max} = \left(\frac{8}{3}\right)^{1/2} D\left(n_{sphere}^2 V_{sphere} + n_{void}^2 V_{void} - \sin^2\phi\right)^{1/2} \qquad \text{(Eq. 3.1)}$$

where D is the diameter of the structural spheres, n is the refractive index of the sphere or the void, V is the volume fraction of the sphere or void, and ϕ is the light incident angle. For a face-center-cubic packed opal film made of silica microspheres (D = 700 nm, n_{sphere}

[5] Meng Kang enrolled in the Research Experience for Undergraduate (REU) program held by the Center of Material Development and Information Technology Research (MDITR) in the summer of 2008. She is currently a biomedical and mechanical engineering dual major at Duke University.

= 1.37, V_{sphere} = 0.74), with normal incidence, the reflection peaks were calculated, according to Eq. 3.1, to be at ~1468 nm and ~1860 nm with air (n = 1.0) and poly(n-butyl-COT) (n = 2.2) filling the void spaces, respectively. In figure 3.8, the transmission and reflection peaks were measured to be at 1389 nm and 1689 nm for air and poly(n-butyl-COT) filled PCs. The difference in the measured peak positions compared to the calculated ones is mainly due to the packing defects present in the periodic structures. For the poly(n-butyl-COT)-infiltrated PCs, the disturbance of the packing of microspheres during infiltration and the volume shrinkage after polymerization led to a larger deviation in the peak position.

Following these experiments, the possibility of *in situ* polymerization of poly(n-butyl-COT) in a microstructured photonic crystal had been demonstrated. Many challenges still need to be overcome for the research on NLO material-based PCs to become a practical reality. These challenges include (1) fabricating defect-free photonic crystals, (2) strengthening PC template structures to overcome disturbance during infiltration, (3) developing a methodology to remove PC templates without degrading or damaging the NLO materials, and so on. Nevertheless, this preliminary work still showed the excellent potential of poly(n-butyl-COT) and *in situ* ROMP in photonic device integration and applications.

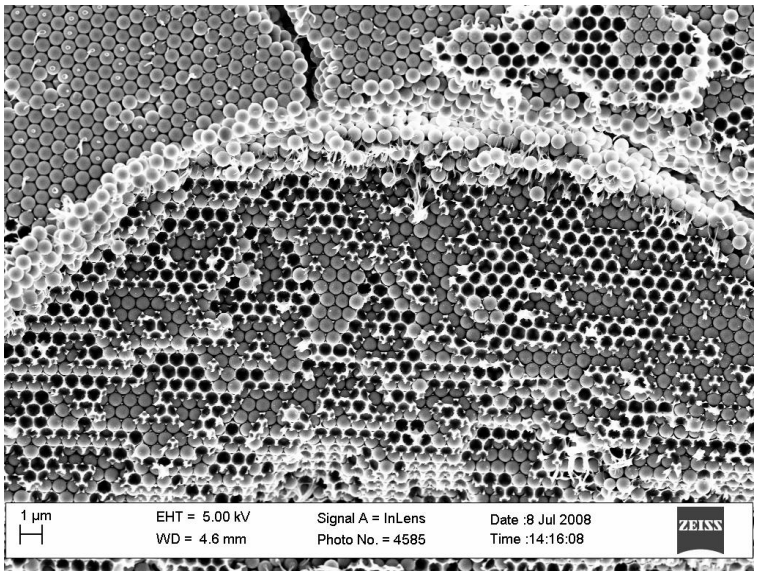

Figure 3.7. SEM image of the poly(n-butyl-COT) infiltrated synthetic opal (*D* = 700 nm).

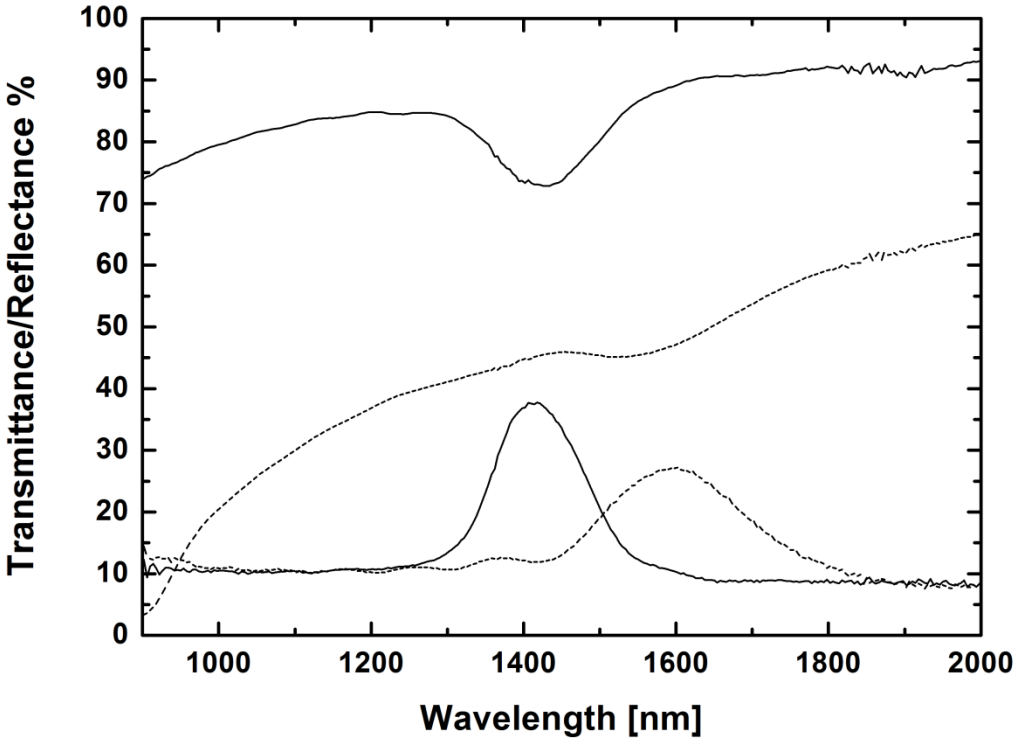

Figure 3.8. Transmission and reflection spectra of a 25-µm thick synthetic opal (D = 700 nm) with air (solid) and poly(*n*-butyl-COT) (dashed) filled void.

3.5 Summary

The controlled polymerization of polyacetylene-based $\chi^{(3)}$ materials via ROMP to form thick, large-area, optical-quality films and have discussed their linear and nonlinear optical properties in the telecommunication region is reported. The polymerization can be controlled by choice of ROMP initiator or by addition of coordinating solvents, thereby facilitating the processing and optimization of the optical properties of the resulting polymers. Furthermore, the films exhibited ultrafast (< 100 fs), large third-order susceptibilities ($\chi^{(3)}$ as large as 2.1×10^{-10} esu) throughout the NIR telecommunications band (1300 – 1550 nm). Thick films of such polymers resulted in large DFWM diffraction efficiencies thereby permitting the demonstration of the free-space AOSP application of image recognition. Furthermore, reasonably small optical losses (for short path length devices, ~ 1 mm) and the potential for *in situ* polymerization suggest that photonic waveguide applications are feasible for such materials.

3.6 Experimental Details

3.6.1 Material Synthesis and Polymerization

The chemical structures of the monomers and initiators used in this work are shown in Scheme 1. Mono-substituted cyclooctatetraenes (R-COT), *n*-butyl- (**1**) and *sec*-butyl-COT (**2**), were prepared using literature methods.[48] Dr. Susan Odom synthesized initiator **4** from **3** (Sigma-Aldrich) by reaction with 3-bromopyridine.[14] Initiator **5** was synthesized as previously described[16] by Dr. Jian-Yang Cho and **6** (Strem) was used as received. Polymerization of the R-COTs via the ROMP method was carried out in an argon-filled glove box. The ROMP reactions were performed by mixing an initiator

directly with neat, liquid-phase monomers, or by dissolving the initiator in a small amount of solvent (1 mg initator in ~25 μL solvent; dichloromethane for **3** and **4**, toluene for **5** and **6**) before mixing with the monomer. In the case of initiator **5**, weakly coordinating ligands that could compete with the R-COT for vacant coordination sites on the metal, HFB and THF, were added to control the overall polymerization rate and film-forming process. During polymerization, the color of the monomer-initiator mixture was observed to gradually change (over a period of seconds to minutes depending on the initiator used) from the highly transparent, bright yellow color of the monomer to an opaque burgundy color, ultimately taking the form of a reflective film with a gold luster (Figure 3.2, upper right). The extent of conversion of monomer to polymer was estimated by weighing polymerized films before and after washing with methanol and then with dichloromethane (to remove residual soluble low molecular weight species). Initiator **3** showed less than 30% conversion efficiency while the rest of the initiators exhibited > 60% conversion.

3.6.2 Film Fabrication and Characterization

Films of poly(R-COT)s were fabricated by transferring the polymerizing liquid mixture with a pipette to a glass substrate and then sandwiching it between another substrate, which was held at a fixed thickness using Teflon or copper spacers. Sandwiched films were hermetically sealed by using epoxy adhesive. Vis-NIR linear absorption spectra were acquired using a Cary 5E UV-Vis-NIR spectrometer. Resonance Raman spectra were acquired using a Bruker Equinox 55 Raman spectrometer with an excitation wavelength of 1064 nm. This wavelength permitted preferential resonant

excitation of predominately long chain polymers in the films since the band edge positions, influenced mainly by those long chain polymers, ranged from 750 - 950 nm. 50 mW of laser power was used for each scan. The scan resolution was 4 cm^{-1} and each spectrum was averaged over 64 scans from 3500 cm^{-1} to 0 cm^{-1}. Film thicknesses were determined using a Dektak 6M contact profilometer and by measurement and analysis of interference fringes[49] observed in the absorption spectra for films with small thicknesses. Refractive indices were determined using the same fringe analysis and verified by using a prism coupler (Metricon 2010). The morphology and surface quality of the polymers were characterized by scanning electron microscopy (Hitachi S-800) and optical profilometry (Veeco, Wyco NT3300).

The nonlinear optical properties of the polymer films in the NIR regime were determined using femtosecond pulsed excitation with two nonlinear characterization techniques: Z-scan and DFWM,[50, 51] both of which have been described in Chapter 2. The values of $|\chi^{(3)}(-\omega; \omega, -\omega, \omega)|$ determined by both techniques were in good agreement with one another. The instrumental accuracy associated with these measurements is estimated to be ±15%.

3.6.3 Image Correlation

Optical correlation measurements were performed using an ultrafast optical parametric amplifier (Newport, TOPAS) pumped by a Ti:Sapphire regenerative amplifier (Newport, Spitfire) that produced ~80 fs pulses at 1550 nm with a repetition rate of 1 kHz. These experiments were implemented in a compact joint-transform correlator geometry[41] that uses a diffractive optical element (DOE) beam-splitter to generate the

beams to encode the 2D images used as the impulse response $h(\mathbf{r})$, object $g(\mathbf{r})$ and reconstruction $g(\mathbf{r})$ functions. The DOE assures the spatial and temporal overlap of the fs pulses in the nonlinear medium. For a detailed description see Reference [52]. After the DOE, the diffracted beams are collimated into a forward-folded crossed-beam phase-matched (BOXCARS) geometry so that parallel-propagating beams pass through the 2D transmission binary masks. The masks were printed on overhead transparencies and located at the front focal plane of a 4-*f* imaging system. Typical average powers of ~ 40 mW/beam were measured directly before the sample. The 4-*f* imaging system consisted of two (*L1* and *L2*) two-inch diameter singlet plano-convex spherical lenses with 10 cm focal lengths. The input beams were focused by *L1* onto the 200 μm thick polyacetylene sample at an external angle of 5.7^{o} with respect to the optical axis. A maximum resolution of 14.3 lines/mm, limited by spherical aberration, was determined at 1550 nm using a standard USAF resolution target. The diffracted signal was then collimated using *L2*, spatially filtered with an iris and captured at the back focal plane with a VIDICON (MicronViewer 7290A) image sensor having a resolution of 700 TV lines and with a minimum detectable signal of 200 nW/cm^2.

3.6.4 Photonic Crystal (Opal) Fabrication and *in situ* Polymerization

Silica microspheres (5% by weight dispersed in de-ionized water) were purchased from Polysciences, Inc. and then diluted with de-ionized water to 1% before use. Opal films made of silica microspheres were fabricated through the microcapillary method. In this method, two clean glass slides spaced by a 25μm Teflon spacer were clamped together to form a capillary cell. Glass slides are first processed by acid Piranha solution

(H_2SO_4: H_2O_2= 3: 1) to clean the surface and make the surface hydrophilic. Capillary cells were then stood vertically in 3.5mL of 1% microsphere solution in 5mL plastic beakers. Beakers were covered by crystallizing dishes to reduce the fluctuation of solution evaporation rate throughout the film growth period.

For *in situ* polymerization, the monomer-to-initiator equivalent ratio for the *in situ* polymerization was ~450 : 1. Initiator **3** was first dissolved in spectral grade DCM with a concentration of 0.01 M and then mixed with liquid *n*-butyl-COT (100 μL of monomer and 100 μL of initiator solution). While low-weight molecules were still dominated and the solution mixture was still fluid, the mixture was infiltrated into the PC by capillary action force. The optical properties of a PC, such as the reflectance and transmittance, before and after polymer infiltration were determined using an UV-Vis-Near IR spectrometer (SHIMADZU UV-3100). The microstructures of the infiltrated PCs and the infiltration ratio were determined using a scanning electron microscope (SEM) by fracturing and subsequently coating the films with ~ 1nm gold particles.

REFERENCES

[1] Halvorson, C., Hays, A., Kraabel, B., Wu, R. L., Wudl, F. and Heeger, A. J., "A 160-femtosecond optical-image processor based on a conjugated polymer," *Science* **265**, 1215-1216 (1994).

[2] Bredas, J. L., Adant, C., Tackx, P., Persoons, A. and Pierce, B. M., "3rd-order nonlinear-optical response in organic materials - theoretical and experimental aspects," *Chemical Reviews* **94**, 243-278 (1994).

[3] Hales, J. M., Zheng, S. J., Barlow, S., Marder, S. R. and Perry, J. W., "Bisdioxaborine polymethines with large third-order nonlinearities for all-optical signal processing," *Journal of the American Chemical Society* **128**, 11362-11363 (2006).

[4] Hochberg, M., Baehr-Jones, T., Wang, G. X., Shearn, M., Harvard, K., Luo, J. D., Chen, B. Q., Shi, Z. W., Lawson, R., Sullivan, P., Jen, A. K. Y., Dalton, L. and Scherer, A., "Terahertz all-optical modulation in a silicon-polymer hybrid system," *Nature Materials* **5**, 703-709 (2006).

[5] Moon, Y. B., Rughooputh, S. D. D. V., Heeger, A. J., Patil, A. O. and Wudl, F., "X-ray-scattering study of the conversion of poly(*para*-phenylene vinylene) precursor to the conjugated polymer," *Synthetic Metals* **29**, E79-E84 (1989).

[6] Klavetter, F. L. and Grubbs, R. H., "Polycyclooctatetraene (polyacetylene) - synthesis and properties," *Journal of the American Chemical Society* **110**, 7807-7813 (1988).

[7] Halvorson, C., Moses, D., Hagler, T. W., Cao, Y. and Heeger, A. J., "Frequency-dependence of 3rd-harmonic generation in *cis*-polyacetylene and *trans*-polyacetylene - importance of the degenerate ground-state to nonlinear optical-response," *Synthetic Metals* **49**, 49-58 (1992).

[8] Fann, W. S., Benson, S., Madey, J. M. J., Etemad, S., Baker, G. L. and Kajzar, F., "Spectrum of $\chi^{(3)}(-3\omega; \omega, \omega, \omega)$ in polyacetylene - an application of the free-electron laser in nonlinear optical spectroscopy," *Physical Review Letters* **62**, 1492-1495 (1989).

[9] Halvorson, C., Hagler, T. W., Moses, D., Cao, Y. and Heeger, A. J., "Conjugated polymers with degenerate ground-state - the route to high-performance 3rd-order nonlinear optical-response," *Chemical Physics Letters* **200**, 364-368 (1992).

[10] Fincher, C. R., Chen, C. E., Heeger, A. J., Macdiarmid, A. G. and Hastings, J. B., "Structural determination of the symmetry-breaking parameter in trans-$(CH)_x$," *Physical Review Letters* **48**, 100-104 (1982).

[11] Grubbs, R. H., Gorman, C. B., Ginsburg, E. J., Perry, J. W. and Marder, S. R., eds. *Materials for nonlinear optics: Chemical perspectives* (American Chemical Societ, Washington, D. C., 1991).

[12] Bielawski, C. W. and Grubbs, R. H., "Living ring-opening metathesis polymerization," *Progress in Polymer Science* **32**, 1-29 (2007).

[13] Bielawski, C. W. and Grubbs, R. H., "Highly efficient ring-opening metathesis polymerization (romp) using new ruthenium catalysts containing N-heterocyclic carbene ligands," *Angewandte Chemie-International Edition* **39**, 2903-2906 (2000).

[14] Scholl, M., Trnka, T. M., Morgan, J. P. and Grubbs, R. H., "Increased ring closing metathesis activity of ruthenium-based olefin metathesis catalysts coordinated with imidazolin-2-ylidene ligands," *Tetrahedron Letters* **40**, 2247-2250 (1999).

[15] Love, J. A., Morgan, J. P., Trnka, T. M. and Grubbs, R. H., "A practical and highly active ruthenium-based catalyst that effects the cross metathesis of acrylonitrile," *Angewandte Chemie-International Edition* **41**, 4035-4037 (2002).

[16] Schaverien, C. J., Dewan, J. C. and Schrock, R. R., "A well-characterized, highly-active, Lewis acid free olefin metathesis catalyst," *Journal of the American Chemical Society* **108**, 2771-2773 (1986).

[17] Schrock, R. R., Murdzek, J. S., Bazan, G. C., Robbins, J., Dimare, M. and Oregan, M., "Synthesis of molybdenum imido alkylidene complexes and some reactions involving acyclic olefins," *Journal of the American Chemical Society* **112**, 3875-3886 (1990).

[18] Schrock, R. R. and Hoveyda, A. H., "Molybdenum and tungsten imido alkylidene complexes as efficient olefin-metathesis catalysts," *Angewandte Chemie-International Edition* **42**, 4592-4633 (2003).

[19] Gorman, C. B., Ginsburg, E. J., Sailor, M. J., Moore, J. S., Jozefiak, T. H., Lewis, N. S., Grubbs, R. H., Marder, S. R. and Perry, J. W., "Substituted polyacetylenes through the ring-opening metathesis polymerization (ROMP) of substituted cyclooctatetraenes - a route into soluble polyacetylene," *Synthetic Metals* **41**, 1033-1038 (1991).

[20] Herisson, J. L. and Chauvin, Y., "Transformation catalysis of olefins by tungsten complexes .2. Telomerization of cyclic olefins in presence of acyclic olefins," *Makromolekulare Chemie* **141**, 161-& (1971).

[21] Schrock, R. R., Feldman, J., Cannizzo, L. F. and Grubbs, R. H., "Ring-opening polymerization of norbornene by a living tungsten alkylidene complex," *Macromolecules* **20**, 1169-1172 (1987).

[22] Schrock, R. R., "Olefin metathesis by molybdenum imido alkylidene catalysts," *Tetrahedron* **55**, 8141-8153 (1999).

[23] Novak, B. M. and Grubbs, R. H., "The ring-opening metathesis polymerization of 7-oxabicyclo[2.2.1]hept-5-ene derivatives - a new acyclic polymeric ionophore," *Journal of the American Chemical Society* **110**, 960-961 (1988).

[24] Ritter, T., Hejl, A., Wenzel, A. G., Funk, T. W. and Grubbs, R. H., "A standard system of characterization for olefin metathesis catalysts," *Organometallics* **25**, 5740-5745 (2006).

[25] Hong, S. H., Wenzel, A. G., Salguero, T. T., Day, M. W. and Grubbs, R. H., "Decomposition of ruthenium olefin metathesis catalysts," *Journal of the American Chemical Society* **129**, 7961-7968 (2007).

[26] Gorman, C. B., *Highly conjugated, substituted polyacetylene via the ring-opening metathesis polymerization of monosubstituted cyclooctatetraenes* (California Institute of Technology, Pasadena, CA, 1992)

[27] Claverie, J., *Ring-opening metathesis polymerization with tungsten based catalyst: Kinetics, thermodynamics and mechanism* (California Institute of Technology, Pasadena, California, 1996)

[28] Klavetter, F. L., *Polyacetylene and novel conjugated derivatives through the metathesis polymerization of 1,3,5,7-cyclooctatetraenes* (California Institute of Technology, Pasadena, California, 1989)

[29] Schlund, R., Schrock, R. R. and Crowe, W. E., "Direct polymerization of acetylene to give living polyenes," *Journal of the American Chemical Society* **111**, 8004-8006 (1989).

[30] Schrock, R. R., "Living ring-opening metathesis polymerization catalyzed by well-characterized transition-metal alkylidene complexes," *Accounts of Chemical Research* **23**, 158-165 (1990).

[31] Schrock, R. R., Crowe, W. E., Bazan, G. C., Dimare, M., Oregan, M. B. and Schofield, M. H., "Monoadducts of imido alkylidene complexes, syn and anti rotamers, and alkylidene ligand rotation," *Organometallics* **10**, 1832-1843 (1991).

[32] Scherman, O. A. and Grubbs, R. H., "Polycyclooctatetraene (polyacetylene) produced with a ruthenium olefin metathesis catalyst," *Synthetic Metals* **124**, 431-434 (2001).

[33] Lauchlan, L., Chen, S. P., Etemad, S., Kletter, M., Heeger, A. J. and Macdiarmid, A. G., "Absolute Raman-scattering cross-sections of trans-$(CH)_x$," *Physical Review B* **27**, 2301-2307 (1983).

[34] Bredas, J. L., Silbey, R., Boudreaux, D. S. and Chance, R. R., "Chain-length dependence of electronic and electrochemical properties of conjugated systems - polyacetylene, polyphenylene, polythiophene, and polypyrrole," *Journal of the American Chemical Society* **105**, 6555-6559 (1983).

[35] Schaffer, H. E., Chance, R. R., Silbey, R. J., Knoll, K. and Schrock, R. R., "Conjugation length dependence of Raman-scattering in a series of linear polyenes - implications for polyacetylene," *Journal of Chemical Physics* **94**, 4161-4170 (1991).

[36] Lichtmann, L. S., Fitchen, D. B. and Temkin, H., "Resonant raman-spectroscopy of conducting organic polymers - $(CH)_x$, and an oriented analog," *Synthetic Metals* **1**, 139-149 (1980).

[37] Lefrant, S., Lichtmann, L. S., Temkin, H., Fitchen, D. B., Miller, D. C., Whitwell, G. E. and Burlitch, J. M., "Raman-scattering in $(CH)_x$ and $(CH)_x$ treated with bromine and iodine," *Solid State Communications* **29**, 191-196 (1979).

[38] Dinu, M., Quochi, F. and Garcia, H., "Third-order nonlinearities in silicon at telecom wavelengths," *Applied Physics Letters* **82**, 2954-2956 (2003).

[39] Pepper, D. M., Auyeung, J., Fekete, D. and Yariv, A., "Spatial convolution and correlation of optical fields via degenerate 4-wave mixing," *Optics Letters* **3**, 7-9 (1978).

[40] Volodin, B. L., Kippelen, B., Meerholz, K., Javidi, B. and Peyghambarian, N., "A polymeric optical pattern-recognition system for security verification," *Nature* **383**, 58-60 (1996).

[41] Tseng, S. Y., Fuentes-Hernandez, C. and Kippelen, B., "Compact and self-aligned all-optical image correlator based on third-harmonic generation," *Optics Letters* **32**, 2599-2601 (2007).

[42] Goodman, J. W., ed. *Introduction to Fourier Optics* (MacGraw-Hill, 1996).

[43] Prasad, P. N., *Nanophotonics* (John Wiley & Sons, Hoboken, NJ, 2004).

[44] Lopez, C., "Materials aspects of photonic crystals," *Advanced Materials* **15**, 1679-1704 (2003).

[45] Gates, B., Qin, D. and Xia, Y. N., "Assembly of nanoparticles into opaline structures over large areas," *Advanced Materials* **11**, 466-469 (1999).

[46] Park, S. H., Gates, B. and Xia, Y. N., "A three-dimensional photonic crystal operating in the visible region," *Advanced Materials* **11**, 462-466 (1999).

[47] Gates, B. and Xia, Y. N., "Fabrication and characterization of chirped 3D photonic crystals," *Advanced Materials* **12**, 1329-1332 (2000).

[48] Miller, J. T., Dekock, C. W. and Brault, M. A., "Synthesis of substituted cyclooctatetraenide dianions," *Journal of Organic Chemistry* **44**, 3508-3510 (1979).

[49] Manifacier, J. C., Gasiot, J. and Fillard, J. P., "Simple method for determination of optical-constants *n,k* and thickness of a weakly absorbing thin-film," *Journal of Physics E-Scientific Instruments* **9**, 1002-1004 (1976).

[50] Van Stryland, E. W. and Sheik-Bahae, M., eds. *Z-scan technique for nonlinear materials characterization* (Marcel Dekker, New York, NY, 1998).

[51] Kuebler, S. M., Denning, R. G. and Anderson, H. L., "Large third-order electronic polarizability of a conjugated porphyrin polymer," *Journal of the American Chemical Society* **122**, 339-347 (2000).

[52] Tseng, S. Y., Cao, W. L., Peng, Y. H., Hales, J. M., Chi, S. H., Perry, J. W., Marder, S. R., Lee, C. H., Herman, W. N. and Goldhar, J., "Measurement of complex $\chi^{(3)}$ using degenerate four-wave mixing with an imaged 2-D phase grating," *Optics Express* **14**, 8737-8744 (2006).

CHAPTER 4

POLY(PHENYLENE VIYNLENE)-FULLERENE BLEND WITH STRONG OPTICAL LIMITING IN THE NEAR-INFRARED

4.1 Abstract

Optical-quality, melt processable thick films of a conjugated polymer composite containing poly(methoxyethylhexylphenylene vinylene) (MEH-PPV), a C_{60} derivative (PCBM) and a plasticizer (di-octylphthalate) have been developed. Their nonlinear absorption, photophysical, and optical limiting properties have been investigated. These composite materials exhibited strong optical limiting characteristics in the near infrared region (750-900 nm), with broad temporal dynamic range spanning femtosecond to nanosecond pulse widths. Transient spectroscopic studies showed MEH-PPV has broad excited state absorption in the near IR ranging from 700-1600 nm with a lifetime of ~466 ps. Transient studies also revealed the formation of the MEH-PPV cation in the MEH-PPV:PCBM:DOP charge transfer composite with a long-lived lifetime up to ~3 ms. Femtosecond-pulsed optical limiting indicated two-photon absorption of MEH-PPV followed by excited state absorption was the dominate mechanism in the short pulsed regime. Nanosecond-pulsed optical limiting and the dispersion of figure-of-merit of the MEH-PPV:PCBM:DOP composite peaked near the wavelength of the MEH-PPV cation suggesting the important role of one-photon and two-photon induced charge transfer in the long pulsed nonlinear absorption response.

4.2 Introduction

Materials with strong nonlinear optical absorption properties have long been recognized as potential optical limiting (OL) materials for applications such as sensor protection [1-4], noise reduction [5], and pulse shaping [6] in various wavelength regions. With the development of mode-locked and amplified Ti:Sapphire lasers [7], the need for effective optical limiters in the 700-1000 nm spectral range has increased. The essential requirements for OL materials are high linear transmission (T_0), low turn-on threshold (F_{Th}, defined here as the fluence where $T(F) = T_0/2$), high damage threshold, and large pulse energy suppression (S,which is defined as the reciprocal of nonlinear transmittance, T_F, just before the damage threshold), which should be achieved over a wide spectral and temporal dynamic range. A figure-of-merit (FOM) for evaluating the pulse suppression performance of an optical limiter is defined here as $FOM = T_0S = T_0/T_F$.

Several organic materials systems utilizing different mechanisms for their nonlinear absorption (NLA) response have been reported previously [4, 5, 8-11]. Cha *et al.* reported on a blend of a conjugated polymer, poly(3-octyl thiophene) (P3OT), and a C_{60} fullerene derivative that was found to possess enhanced NLA and OL capability in the 700 – 950 nm range compared to the neat polymer or fullerene [8]. A nanosecond-pulse suppression of 9 dB (7.8X) was observed at 760 nm and was attributed to one-photon induced charge carrier absorption (CCA). The P3OT polymer functioned as a photoexcitable electron donor and the fullerene as an electron acceptor. The NLA was modeled and found to be enhanced due to CCA arising from fast and efficient charge transfer and charge separation, as well as relatively slow charge recombination [8, 12].

However, the P3OT:fullerene blend exhibited low linear transmission (~0.45) resulting in a modest OL-FOM = 3.5.

One route to improving the linear transmission is to make use of two-photon absorption (2PA) as an excitation route, with photon energies lying below the linear absorption band edge [5, 9-11]. However, because of the quadratic dependence of the excitation rate on intensity, purely 2PA-based systems are limited to use with relatively short pulse widths. With the contribution of subsequent absorption processes (e.g. excited state absorption, ESA, or CCA), the nonlinear attenuation can be dramatically increased [11] for longer (i.e. nanosecond) pulses, although the NLA response could diminish for yet longer pulses, depending on the timescale for relaxation of the excited state or charge recombination. While a recent report on a lead bis(ethynyl)porphyrin polymer material system exhibiting 2PA-induced ESA has shown promising broadband OL response at longer wavelengths (> 1050 nm) [10], 2PA-based systems in the current spectral region-of-interest (700-1000 nm) have resulted in OL-FOMs < 10 [9].

To develop an OL material in the near IR with improved linear transmittance and temporal dynamic range, a system with a combined contribution of 1PA- and 2PA-induced absorptions is of interest. In order to achieve such effective NLA, it is ideal to have spectral overlap of 1PA or 2PA with ESA or CCA in the spectral region-of-interest. If there is also spectral overlap of the 1PA and 2PA bands, both types of excitation can contribute to the induced absorption and can give rise to a nonlinear response over a wider temporal dynamic range. Furthermore, the states or species that contribute to the induced absorptions should be generated on a time scale much shorter than the pulse duration and the resulting excited states or carriers should have lifetimes comparable to

or longer than the excitation pulse width. This is generally a difficult task to achieve in a single-component OL material.

In this chapter, a ternary blend of MEH-PPV, PCBM, and DOP was investigated as a promising candidate OL system in the near IR (700-900 nm) region. The choice was based on the fact that MEH-PPV/fullerene blends are well known to show efficient one-photon induced charge carrier generation and have been studied extensively as solar cell materials [13]. Furthermore, the 2PA spectrum of MEH-PPV was recognized to have good spectral overlap with the MEH-PPV radical cation absorption, such that CCA should be induced and lead to strong NLA. The plasticizer DOP was utilized to overcome poor optical quality and reduce optical scattering in films of MEH-PPV and PCBM. The ternary mixture comprising MEH-PPV, PCBM and DOP was melt-processable. Optical quality, thick films (25 μm) of this mixture were successfully produced. Studies of its nonlinear optical, photophysical and OL responses are reported below.

4.3 Background

MEH-PPV:PCBM blends are interesting as potential nonlinear absorbing optical elements because of the linear and nonlinear absorption properties of MEH-PPV as well as the excited state and charge carrier absorption characteristics of both MEH-PPV and PCBM. Relative to P3OT, MEH-PPV has a larger bandgap (E_g) providing improved linear transmission in the near IR region. It has been shown that one-photon induced charge transfer can occur between MEH-PPV (electron donor) and PCBM (electron acceptor) leading to strongly absorbing charge carriers; the MEH-PPV cation shows a

broad absorption band from 600 to 1100 nm and the PCBM anion shows absorption bands ranging from 850 to 1070 nm [12, 14-17]. MEH-PPV has 2PA bands ranging from 750 to 900 nm [18, 19] and ESA also in the near IR peaking at 1300 nm [20, 21]. Furthermore, blends of MEH-PPV and PCBM have been shown to form ground-state charge transfer complexes (CTCs) that exhibit weak 1PA extending to wavelengths above the 1PA band edge of MEH-PPV [22]. Therefore, one-photon or two-photon excitation of the MEH-PPV:PCBM blend in the 700-900 nm range should lead to the generation of charge carriers [14, 16, 17] and/or excited states [20, 21, 23] that are strongly absorbing in the same wavelength range, as needed for effective NLA (see **Scheme 4.1**). The photoinduced charge transfer and separation are known to occur within 1 ps following excitation [24] in MEH-PPV:PCBM films, while the recombination of MEH-PPV cations and fullerene anions is slow (300 ns – 10 ms) [25]. For MEH-PPV, the singlet ESA lifetime is ~600 ps [20, 21], which allows for efficient electron transfer quenching by PCBM. Thus, the combination of MEH-PPV and PCBM was investigated as a candidate OL material that could have 2PA- and 1PA-induced ESA or CCA working together to contribute to effective OL in the same spectral range for various pulse durations.

4.4 Results and Discussion

4.4.1 Formulation and Processing of Thick Film Conjugated Polymer Composites

The NLA of a blend material scales with the sample pathlength and the concentration of optically active chromophores within the sample. Moreover, charge transfer efficiency depends on the distance between donors and acceptors in a blended

solid film. Thus, considering these factors, the primary task in this study was to fabricate thick (> 15 μm) solid films of MEH-PPV and PCBM with high volume loading of the constituents, while maintaining optical transparency in the near IR. However, obtaining good optical quality, thick blended films involving conjugated polymers is rather challenging due to potential phase separation of components and degradation caused by high processing temperatures. These factors can lead to increased scattering and reduced linear transmittance in the films. Melt processing is often a viable route to the formation of optical quality glasses of polymers via rapid quenching of the melt. However, MEH-PPV has a high melting temperature (250-300 °C) [26, 27] due to interchain interactions as is the case for many long-chain conjugated polymers, and was found to decompose before melting sufficiently for film processing. The addition of a plasticizer, such as DOP, dissolves and dilutes the polymer chains, and induces additional free volume in the blend which leads to a number of favorable characteristics: reduced melting and blend processing temperatures, improved processability and miscibility of the two component systems, and reduced crystallinity in the resulting films. Various ratios of DOP were investigated. Upon the addition of 50% DOP, the ternary DOP-containing blends could be processed at temperatures around 200-230°C. This permitted fabrication of optical quality films with thicknesses ranging from 15 – 200 μm and excellent transparency from 700 to 900 nm, while maintaining a high concentration of the polymer and fullerene (see **Figure 4.1** and **Table 4.1**)

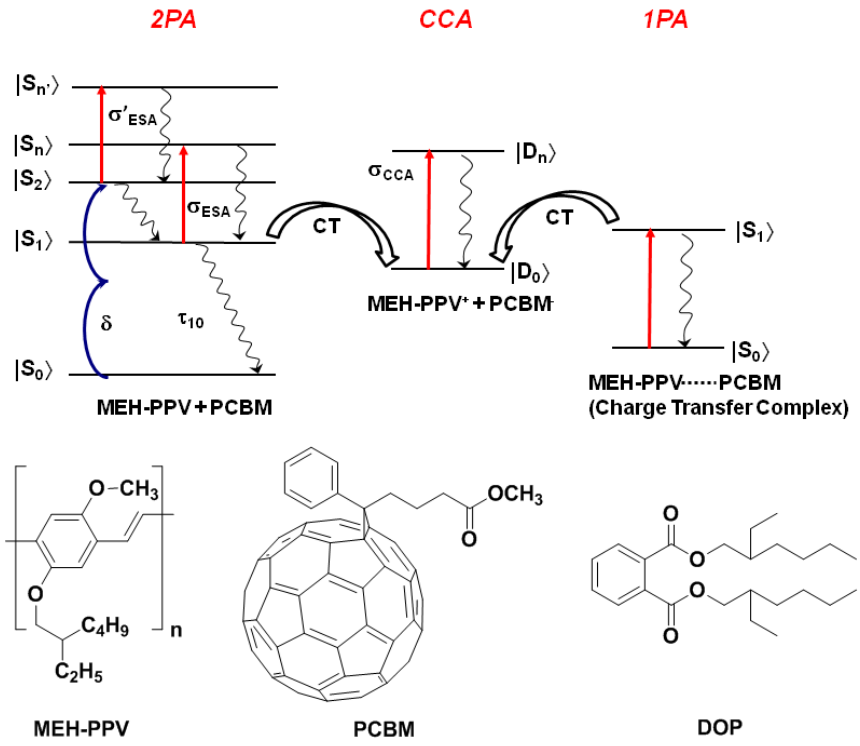

Scheme 4.1. Illustration of one- and two-photon induced excited state and charge carrier absorption in MEH-PPV:PCBM:DOP blends and the chemical structures of constituent compounds. The states illustrated represent only the MEH-PPV related electronic states in the system. The S symbols represent singlet states of MEH-PPV and MEH-PPV--PCBM charge transfer complex and the D symbols represent doublet states of the MEH-PPV radical cation.

4.4.2 Linear and Nonlinear Absorption of MEH-PPV:DOP and MEH-PPV:PCBM:DOP

Figure 4.1 shows the linear absorption of thin and thick films of MEH-PPV:DOP, MEH-PPV:PCBM:DOP, and PMMA:PCBM:DOP. Spin-casted thin films of MEH-PPV:DOP and MEH-PPV:PCBM:DOP show the electronic absorption peaks of MEH-PPV at 505 and 512 nm. The PMMA:PCBM:DOP thin film shows the expected electronic absorption bands for PCBM in the range of 400 to 750 nm, including a distinct

weak band at 700 nm [28]. For the melt-processed thick films, the MEH-PPV:DOP film shows a sharp band edge at 625 nm. The film of the MEH-PPV:PCBM:DOP blend shows a weak absorption at ~700 nm, that we attribute to the PCBM, on top of an extended absorption tail that lies below the band edge of MEH-PPV (out to ~870 nm) and likely results from the formation of a ground-state CTC [22, 29, 30]. Minor inhomogeneities were observed in optical microscopy, which might also contribute to some of the optical loss tail in the near IR. Such inhomogeneities may result from a small amount of crystallization of PCBM, as evidence by the low density of very small crystallites in Figure 1c.

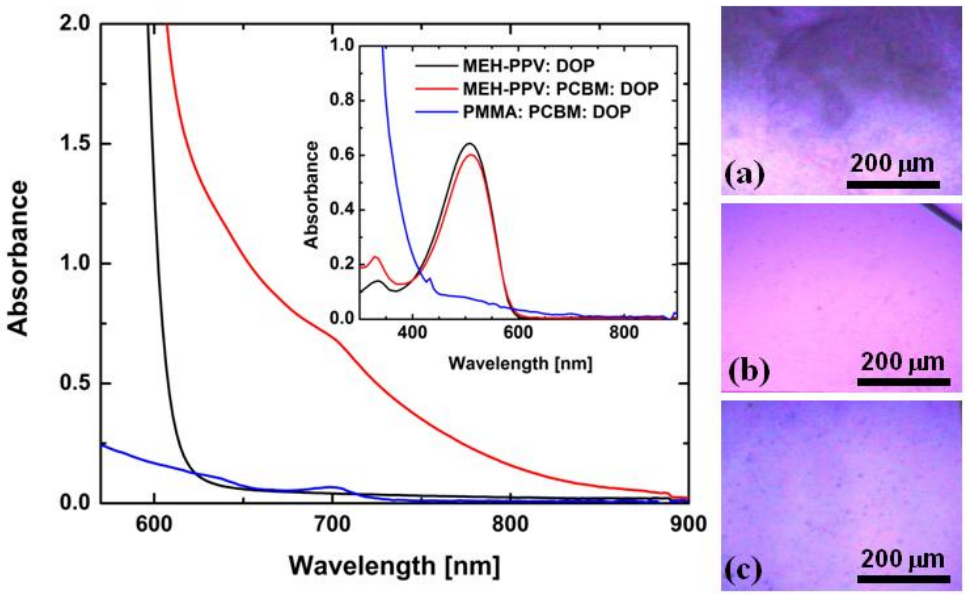

Figure 4.1. (Left) Linear absorption spectra of melt-processed 25-μm thick MEH-PPV:DOP film (black) and MEH-PPV:PCBM:DOP (red) film and drop-cast 10 μm thick PMMA:PCBM:DOP (blue). Inset: Linear absorption spectra of spin-coated thin films of MEH-PPV:DOP (black, 100 nm), MEH-PPV:PCBM:DOP (red, 100 nm), and PMMA:PCBM:DOP (blue, 1.7 μm). (Right) Transmission optical microscopic images at 40X magnification of 25-μm thick melt-processed films of (a) neat MEH-PPV, (b) MEH-PPV:DOP, and (c) MEH-PPV:PCBM:DOP.

Femtosecond-pulsed open-aperture Z-scan measurements (Table 4.1) yielded β values for MEH-PPV:DOP films which were found to be about half the reported value (80 cm/GW at 800 nm) of neat MEH-PPV [19, 31], which is consistent with the ~50% dilution of MEH-PPV in the blend film. These 2PA coefficients are nearly an order-of-magnitude larger than ZnSe, a wide bandgap semiconductor that has been used previously for OL in this spectral region [32]. Also, the values of β showed negligible intensity dependency in the irradiance range used, i.e. 1 – 12 GW/cm^2. While this result suggested that the dominant mechanism for NLA in MEH-PPV was 2PA, as might be expected in the femtosecond region, it does not preclude subsequent ESA of MEH-PPV at higher intensities. At 870 nm, the magnitudes of β were not significantly different for the MEH-PPV:DOP and MEH-PPV:PCBM:DOP films. At 730 nm, on the other hand, the value of β for MEH-PPV:PCBM:DOP showed a marked difference relative to MEH-PPV:DOP, possibly indicating an additional pathway for NLA which could be due to the presence of CTCs leading to 1PA-induced ESA.

Table 4.1. Linear and nonlinear optical properties as well as optical limiting characteristics of blends examined.

Sample	T_0[a]	β [cm/GW]		ns-OL[b]		fs-OL[c]	
	800 nm	730 nm	870 nm	F_{Th} [J/cm^2]	FOM	F_{Th} [J/cm^2]	FOM
MEH-PPV:PCBM:DOP	0.76 ± 0.056	57	37	0.15	21	0.0019	9.7
MEH-PPV:DOP	0.90 ± 0.065	40 (955)[d]	33 (660)[d]	2.3	2.7	0.0021	8.2 (2.8)[e]
PMMA:PCBM:DOP	0.31 ± 0.084	-	-	4.3	2.4	0.03	1.1

[a] These are average values based on linear spectroscopic measurements on different spots for several films.

[b] Nanosecond OL with 4 ns, 830 nm pulses. The measurement uncertainty is ~ ±15%.

[c] Femtosecond OL with 75 fs, 810 nm pulses. The measurement uncertainty is ~ ±15%.

[d] The numbers in the parentheses are extracted 2PA cross-sections (δ). The conversion from 2PA coefficient (β) to δ is given as $\delta = \beta E_{ph}/N$, where N is the number density of MEH-PPV per repeat unit and E_{ph} is the photon energy of the excitation. The units of δ are 10^{-58} m^4·s·photon^{-1} (or GM).

[e] MEH-PPV:DOP showed minor, non-catastrophic damage at 4×10^{-3} J/cm^2 giving a FOM of ~2.8. However, the suppression capability of MEH-PPV:DOP continued until ~2×10^{-2} J/cm^2 giving a FOM of ~8.2.

4.4.3 Transient Dynamics of Charge-Transfer Composites

Both femtosecond- and nanosecond-pulsed transient-absorption studies were performed to investigate the excited state characteristics of these DOP-containing composites. For the MEH-PPV:DOP film, transient absorption spectra obtained with pump pulses at 700 nm and 790 nm showed strong and broad ESA in the near IR that peaked ~1300 nm. (Figure 4.2 and **Figure 4.3**) The decay kinetic of MEH-PPV ESA at 1300 nm can be globally-fitted by the equation of $\Delta OD = y_0 + A_1 e^{-(t-t_0)/\tau_1} + A_2 e^{-(t-t_0)/\tau_2}$ indicating at least 3 relaxation processes contributed to the ESA band at 1300 nm. (**Figure 4.4**) The result of global fitting showed τ_1 ~ 6.7 ps and τ_2 ~ 466 ps and both are close to the literature reported values [20, 33]. These two decays likely correspond to S_2-S_1 and S_1-S_0 relaxation processes. The offset y_0, which might be a long-lived species on the femtosecond time scale, was relatively small. With 790 nm excitation, intensity-dependent measurements showed the amplitude of the τ_1 (6.7 ps) component was quadratically dependent on the input energy confirming the S_2 state was populated by 2PA. The amplitude of the τ_2 (466 ps) component did not have a quadratic dependence on the input intensity but did show a superlinear dependence on the order of 1.45. This suggested the population of S_2 did not fully relax to the S_1 state. The proposed excitation transitions are shown in the inset of figure 4.4. Transient absorption spectra of PMMA:PCBM:DOP showed very weak but long-lived triplet excited state absorption from 700 to 1100 nm upon one-photon excitation at 700 nm. (Figure 4.2) Such weak signal is due to the relatively low concentration compared to MEH-PPV and the small absorption cross section at 700 nm. When PCBM was excited off one-photon resonance (i.e. at 790 nm), the signal of triplet excited state absorption was diminished

significantly suggesting there is minimal direct excitation of PCBM which helps explain the result of the poor nanosecond optical pulse suppression at 800 nm (see below).

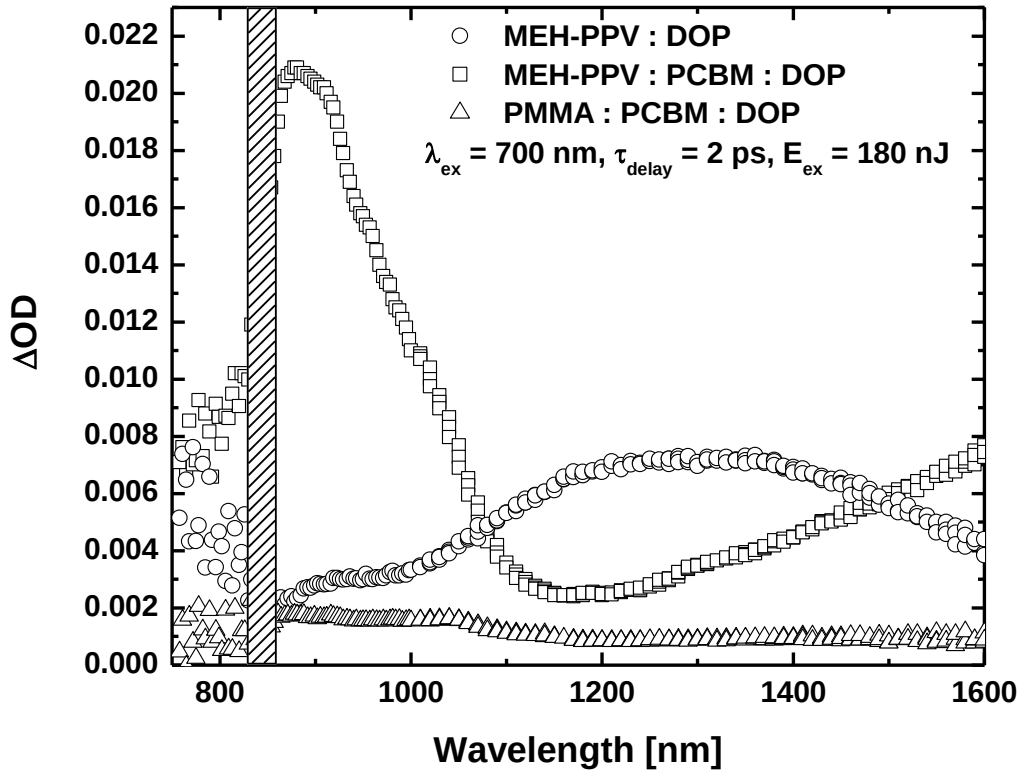

Figure 4.2. Femtosecond transient absorption spectra of MEH-PPV:DOP, MEH-PPV:PCBM:DOP, and PMMA:PCBM:DOP with excitation pulses at 700 nm and a time delay of 2ps.

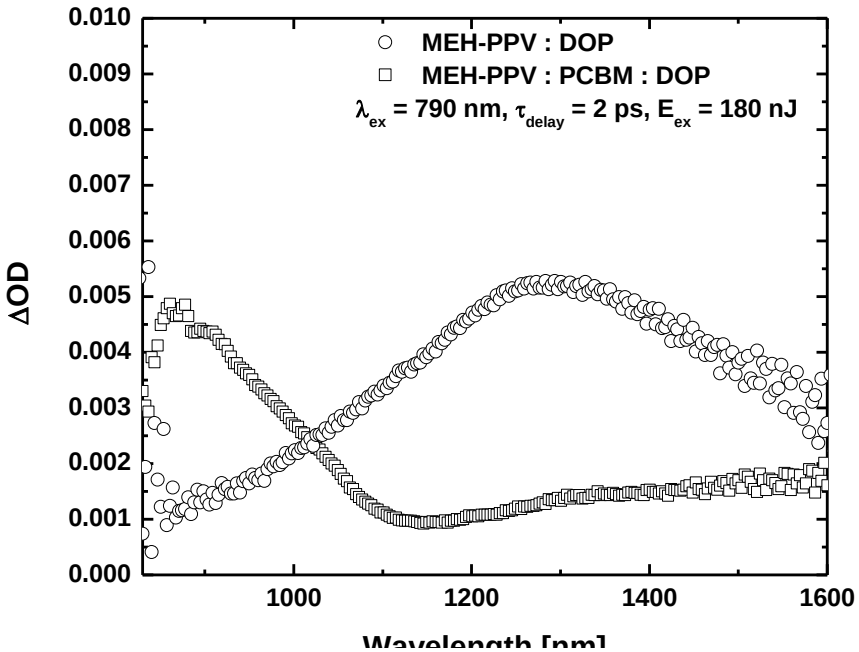

Figure 4.3. Femtosecond transient absorption spectra of MEH-PPV:DOP and MEH-PPV:PCBM:DOP with excitation pulses at 790 nm and a time delay of 2ps.

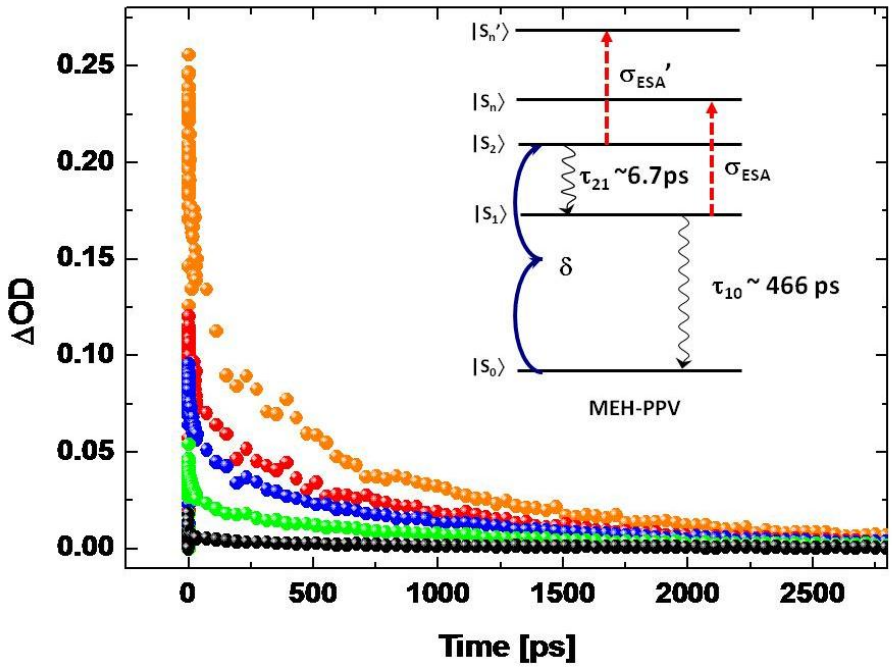

Figure 4.4. Decay kinetics of ESA at1300 nm of MEH-PPV:DOP with femtosecond-pulsed excitation at 790 nm and various pumping energies: 180 nJ (black), 470 nJ (green), 750 nJ (blue), 1000 nJ (red), and 1950 nJ (orange). Inset: Scheme of proposed MEH-PPV excited state transitions.

As shown in Figures 4.2 and 4.3, femtosecond pulsed transient absorption spectra of films of MEH-PPV:DOP and PMMA:PCBM:DOP showed dramatically different transient absorption bands compared to the composite MEH-PPV:PCBM:DOP with both pumping wavelengths of 700 and 790 nm. The MEH-PPV:PCBM:DOP composite showed significant quenching of the singlet-singlet ESA of MEH-PPV at ~1300 nm and the generation of a distinct transient species that showed long-lived, strong absorption over the range of 700 to 1100 nm, with a peak wavelength of ~860 nm. This is consistent with charge transfer from the MEH-PPV singlet state to PCBM. The location of the transient absorption band of the composite film is quite similar to that of the MEH-PPV cation CCA, i.e. ~810 nm; for the film, the red-shifted absorption peak (860 nm) may be due to the presence of DOP, which increases the polarity of the surrounding medium. The decay kinetics of CCA are shown in **Figure 4.5**. With 790 nm excitation and a low input energy of 180 nJ, a fast growth (~ 1 ps) was observed (shown in the inset of figure 4.5). This fast growth was assigned to the ultrafast generation of charge carriers. As the input energy was increased, the 2PA signal became prominent and the growth curves in the decay kinetics were obscured by the 2PA signal and were no longer resolvable. Through global fitting with a bi-exponential decay function, a transient species with lifetime ~430 ps was observed and this component was assigned to the residual MEH-PPV ESA. However, global fitting also showed the existence of a large offset (y_0). The offset was later evidenced to be the long lived CCA by nanosecond transient absorption measurements. The yield of CCA was estimated to be ~ 20%. Furthermore, the intensity-dependence of the kinetics showed the generation of the CCA was not quadratically but linearly dependent on the input intensity with an order of 1.06. This

suggested that 2PA might not be the only pathway contributing to the generation of CCA and a contribution from 1PA might also be possible.

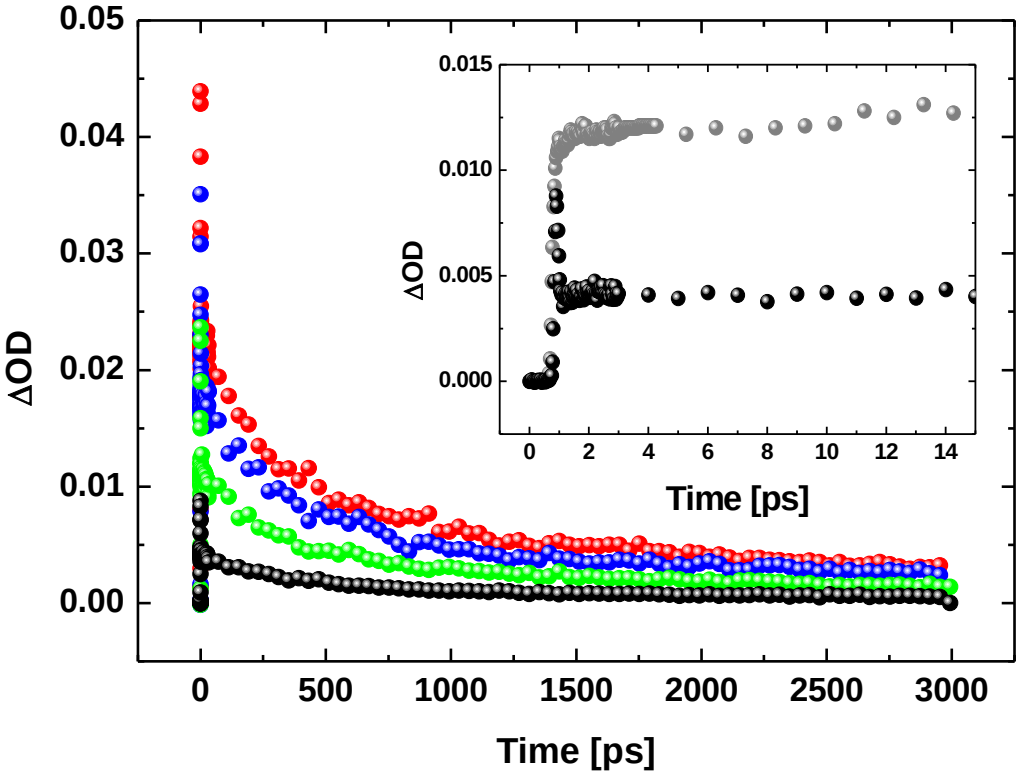

Figure 4.5. Decay kinetics of CCA at900 nm of MEH-PPV:PCBM:DOP with femtosecond-pulsed excitation at 790 nm and various pumping energy: 180 nJ (black), 470 nJ (green), 750 nJ (blue), and 1000 nJ (red). Inset: the growth kinetics of CCA with pumping energy of 180 nJ at 900 nm with excitation wavelengths 700 nm (grey) and 790 nm (black).

To further confirm the mechanism observed, nanosecond transient studies were carried out on the same set of films containing 50%$_{wt}$ DOP. Similar to the femtosecond transient studies, the film of MEH-PPV:PCBM:DOP showed distinctive transient spectra compared to both MEH-PPV:DOP and PMMA:PCBM:DOP films. Both the 580 nm and

800 nm pumped nanosecond transient spectra of MEH-PPV:PCBM:DOP film resembled the spectral feature of the MEH-PPV cation absorption observed in the femtosecond transient absorption measurements (**Figure 4.6**) and the decay of the cations were as slow as 0.5-3.7 ms (**Figure 4.7**). The 580 nm pumped nanosecond transient absorption spectra of PMMA:PCBM:DOP also reproduced the feature of the long-lived, weak triplet excited state absorption detected in femtosecond transient measurements and, similarly, off-resonant excitation at 800 nm again showed negligible contribution of nonlinear absorption from PCBM. The singlet ESA of MEH-PPV was not observable on this nanosecond scale, due to its fast decay after excitation.

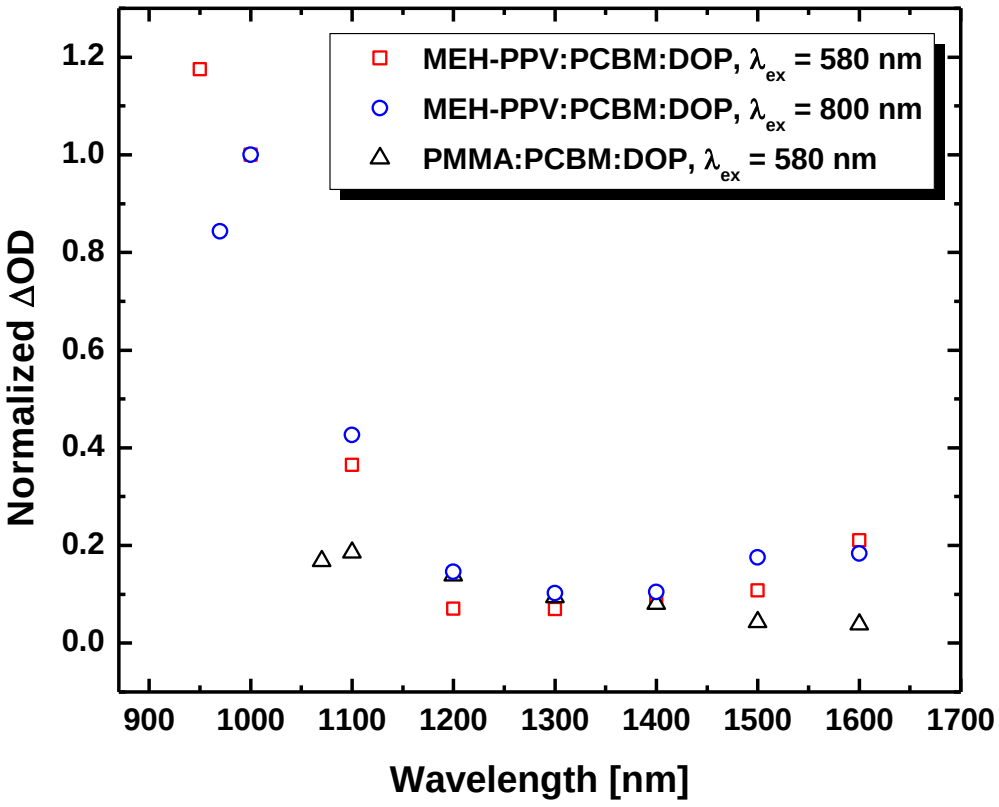

Figure 4.6. Nanosecond transient absorption spectra of MEH-PPV:PCBM:DOP and PMMA:PCBM:DOP.

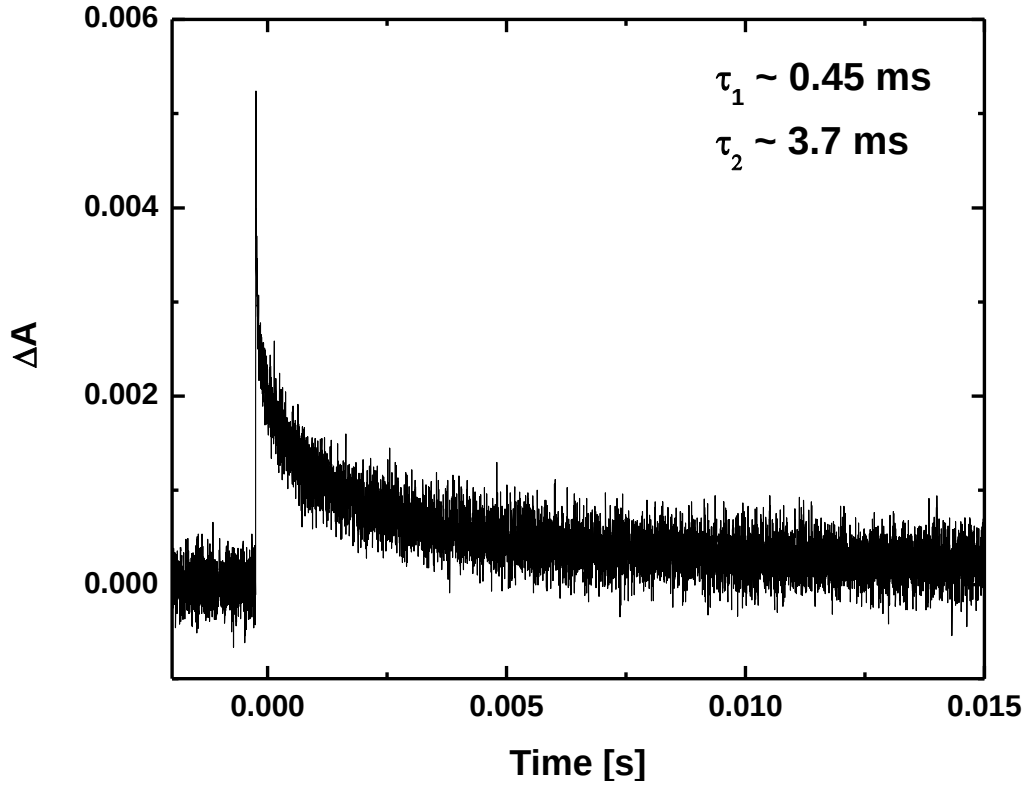

Figure 4.7. Decay kinetics of MEH-PPV cation at 970 nm with 800 nm, 400μJ, 4ns-pulsed excitation.

4.4.4 Optical Limiting Applications of Charge-Transfer Composites

Given the successful fabrication of thick, optical quality films of MEH-PPV based blends with strong NLA properties, femtosecond- and nanosecond-pulsed OL studies were undertaken to determine the pulse suppression efficacy of the films. As indicated in Table 4.1 and **Figure 4.8**, MEH-PPV:DOP and MEH-PPV:PCBM:DOP showed significant differences in nanosecond-pulsed OL performance while the suppression behavior is similar when using femtosecond pulses. With femtosecond-pulsed excitation, MEH-PPV:DOP and MEH-PPV:PCBM:DOP both showed a similar turn-on threshold and pre-damage suppression, i.e. 10 dB (9X). It should be noted that damage occurred at

~0.01 J/cm^2 for both MEH-PPV:DOP and MEH-PPV:PCBM:DOP, although MEH-PPV:DOP showed signs of minor, non-catastrophic damage at lower input fluences (see Table 1 and Figure 4.8). With nanosecond-pulsed excitation, MEH-PPV:DOP showed limited pulse suppression, 5 dB (3X), and a high turn-on threshold (F_{th} ~ 2.3 J/cm^2), while MEH-PPV:PCBM:DOP exhibited a threshold fluence 100 times lower than MEH-PPV:DOP and a suppression that was 10 times higher (15 dB, 30X). Such a large suppression by MEH-PPV:PCBM:DOP exceeds the reported value achieved previously with a P3OT:fullerene blend [8]. Furthermore, by virtue of the improved linear transmittance of the MEH-PPV:PCBM:DOP blend, the peak OL-FOM (at 800 nm) shows nearly a 7-fold enhancement over the P3OT:fullerene blend [8].

The differences in OL behavior between the femtosecond and nanosecond pulsed excitation for MEH-PPV:DOP and MEH-PPV:PCBM:DOP indicates that the NLA mechanisms contributing to the suppression are likely different in these two temporal regimes. For the MEH-PPV:DOP film, since MEH-PPV is the only active nonlinear absorbing chromophore, the dominant mechanisms for NLA are primarily 2PA and ESA in both femtosecond and nanosecond regimes. For MEH-PPV:PCBM:DOP however, charge carrier generation and absorption could contribute to the NLA mechanism, especially for nanosecond pulse durations. As evidenced by the poor OL suppression of the PMMA:PCBM:DOP control film in both temporal regimes, direct excitation of PCBM by either 1- or 2PA likely provides a negligible contribution, by itself, to the NLA of the blend. For femtosecond-pulsed excitation, the timescale for charge transfer and separation of charge carriers (~1 ps for MEH-PPV:PCBM [24]) is longer than the duration of the pulse width, therefore it is likely that ESA following excitation of MEH-

PPV is still the primary route for NLA. This is consistent with the similar OL suppression observed for MEH-PPV:PCBM:DOP and MEH-PPV:DOP. On the other hand in the nanosecond regime, charge transfer occurs essentially instantaneously with respect to the pulse width which, coupled with the lifetime of the charge carriers (i.e. up to 3 ms [25]), suggests that CCA would be the dominant NLA mechanism. Furthermore, the turn-on threshold for MEH-PPV:PCBM:DOP is much lower (Figure 4.8d) than that of MEH-PPV:DOP. Such a low threshold indicates an additional excitation pathway different from 2PA may provide a significant contribution. Since PMMA:PCBM:DOP showed negligible suppression, this additional pathway could be attributed to CTC absorption and, given its spectral overlap with MEH-PPV 2PA, it is likely that the large OL suppression of MEH-PPV:PCBM:DOP benefits from a combination of 1PA and 2PA excitation processes (Scheme 4.1). In order to understand and distinguish the contributions of 2PA (MEH-PPV) and 1PA (CTC) in the NLA response of MEH-PPV:PCBM:DOP, wavelength-dependent OL studies and numerical simulations of the OL data were carried out and are discussed below.

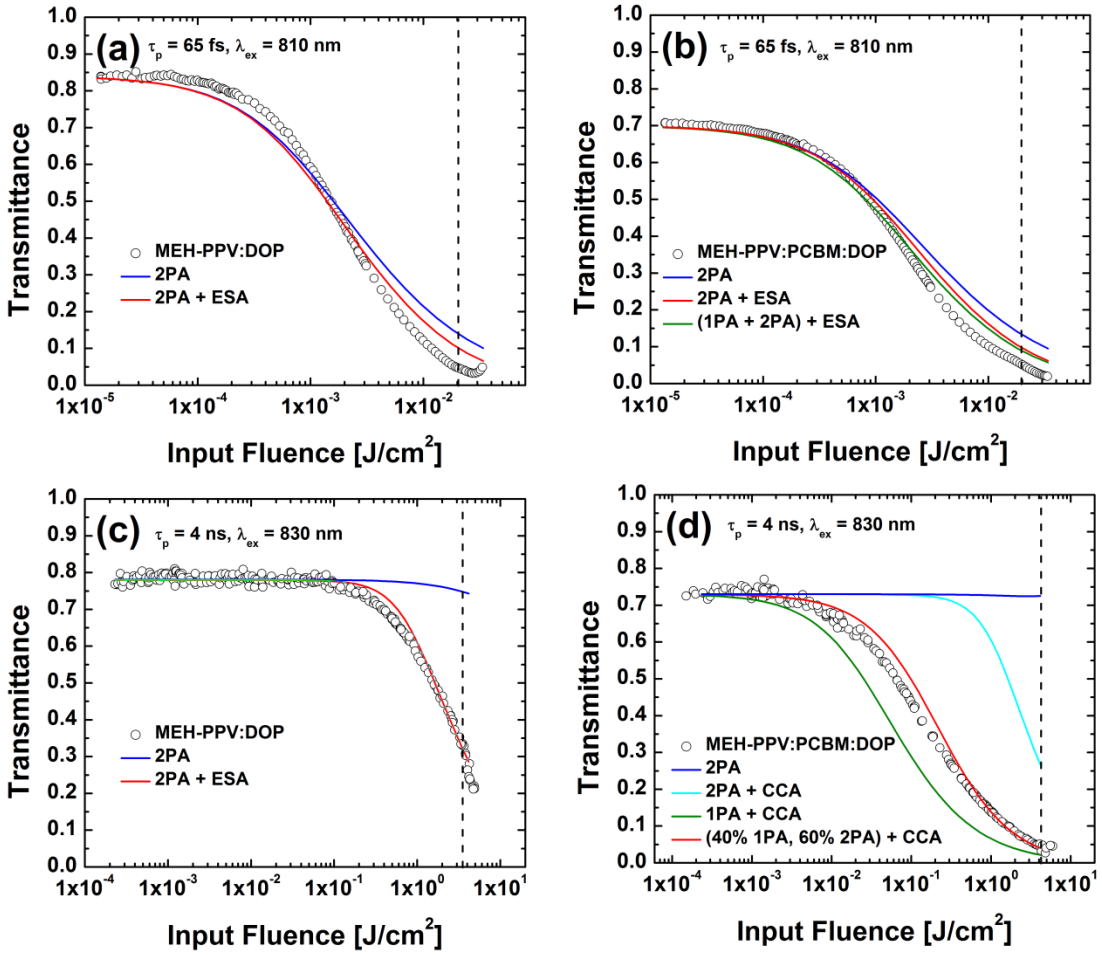

Figure 4.8. Optical limiting and numerical simulations of the 25-μm thick MEH-PPV:DOP and MEH-PPV:PCBM:DOP films. Femtosecond-pulsed (HW1/e ~ 65 fs) OL on MEH-PPV:DOP (a) and MEH-PPV:PCBM:DOP (b) at 810 nm. Nanosecond-pulsed (HW1/e ~ 4ns) OL on MEH-PPV:DOP. (c) and MEH-PPV:PCBM:DOP (d) at 830 nm. Parameters for numerical simulations were described in the text. Dashed lines mark the damage points of samples.

4.4.4.1 Dispersion of Optical Limiting

Wavelength-dependent OL studies of the MEH-PPV:DOP and MEH-PPV:PCBM:DOP blends were performed with nanosecond pulses in the 750 – 900 nm region. As shown in **Figure 4.9**, MEH-PPV:PCBM:DOP has considerably larger OL-

FOM than MEH-PPV:DOP, particularly at shorter wavelengths. The dispersion of the OL-FOM for MEH-PPV:PCBM:DOP shows a peak at ~800 nm and monotonically decreases going towards 900 nm. The large suppression at shorter wavelengths again suggests a contribution from CTC absorption. At longer wavelengths, where CTC absorption is diminished, the 1PA contribution vanishes and only 2PA-induced CCA remains. Therefore, at shorter excitation wavelengths, the suppression mechanism in MEH-PPV:PCBM:DOP is likely due to both 1PA- and 2PA-induced CCA. While MEH-PPV:PCBM:DOP showed similar suppressions from 750-830 nm, the FOMs were found to be optimal at 800 nm (FOM ~ 23) and 830 nm (FOM ~ 21) as a result of the compromise between linear transmission loss and pulse suppression.

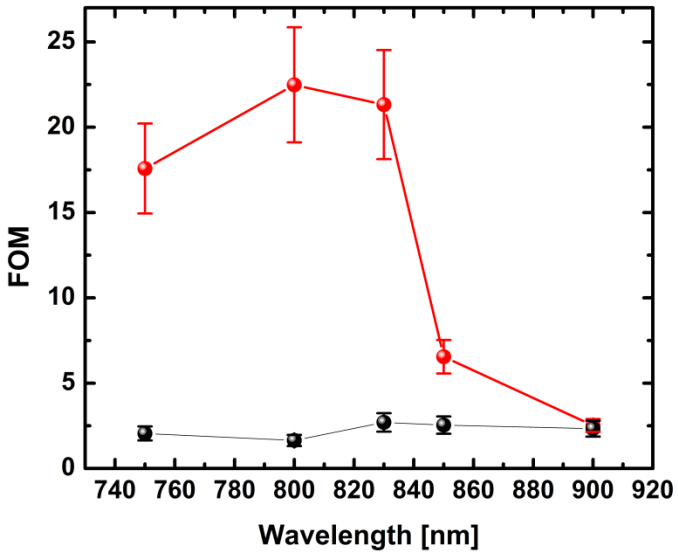

Figure 4.9. FOM of wavelength-dependent nanosecond-pulse suppression of 25 μm thick MEH-PPV:DOP (black) and MEH-PPV:PCBM:DOP (red) films.

4.4.4.2 Numerical Simulation of Optical Limiting

A method for nonlinear beam propagation (see ref. [10] for details) was employed to simulate the OL data in both femtosecond and nanosecond regimes in order to better understand the potential mechanisms contributing to the pulse suppression. Figure 4.8 shows these simulations alongside the experimental data for MEH-PPV:DOP and MEH-PPV:PCBM:DOP. Experimentally-determined beam profile and pulse shape parameters were used in the simulations as were sample-specific parameters (e.g. film thickness, concentration, linear transmittance, etc.). Parameters such as ESA and CCA lifetimes and charge transfer rates were adopted from the adopted from the result of transient absorption measurements. The 2PA cross-section was estimated to be ~780 GM in the 810-830 nm range based on the femtosecond Z-scan results (see Table 4.1). Consequently, the MEH-PPV ESA cross section became the only free fitting parameter when simulating the nanosecond-pulsed OL of the MEH-PPV:DOP film at 830 nm. The extracted value for the cross section was found to be $\sigma_{ESA} = 1.1 \times 10^{-20}$ m^2 at 830 nm, which is very similar to the value at 775 nm reported in the literature [20]. It should be noted that the MEH-PPV ESA was modeled as a single effective excited state absorption, although $S_2 \rightarrow S_{n'}$ and $S_1 \rightarrow S_n$ absorption processes could contribute on short timescales. Figure 4.8c shows that 2PA itself has a negligible contribution to the nanosecond OL without including the subsequent ESA. This simulation as well as the absence of any appreciable 1PA for MEH-PPV:DOP in this spectral region validates the use of the 2PA-induced ESA process. The same NLA mechanism was used to simulate the femtosecond OL data in Figure 4.8a. The simulations closely follow the experimental data, although it

is clear that 2PA itself plays the predominant role in the pulse suppression for this temporal regime.

As discussed above, the same NLA mechanism responsible for the femtosecond OL response in MEH-PPV:DOP should also be responsible for the pulse suppression in MEH-PPV:PCBM:DOP. This is confirmed in Figure 4.8b where 2PA is shown to be prominent in the nonlinear response of the blend. Not surprisingly, including 1PA as an additional excitation process (due to CTC absorption) showed only moderate improvement in the femtosecond OL response. For the nanosecond OL simulations of MEH-PPV:PCBM:DOP, the CCA cross section was extracted from the data taken at 900 nm. Since the contribution from CTC absorption is negligible at this wavelength, a 2PA-induced CCA model could be employed. The extracted cross section value was $\sigma_{CCA} = 1.3 \times 10^{-21}$ m^2 which is quite similar to the value found previously for the MEH-PPV cation [17]. This is consistent with transient absorption data taken on MEH-PPV:PCBM blends [24], which show the MEH-PPV cation plays a dominant role in the CCA following excitation. Furthermore, the dispersion of the OL-FOM shown in Figure 4.9 is also reminiscent of the MEH-PPV cation spectrum. With the value of σ_{CCA} (scaled according to the cation spectrum at the appropriate wavelength), nanosecond-pulsed OL could be simulated for the 830 nm data. It is clear from Figure 4.8d that the mechanism of 2PA-induced CCA does not achieve the observed pulse suppression. However, 1PA-induced CCA (via the ground-state CTC) overestimates the suppression. Only by assuming a fractional contribution from both the CTC absorption and MEH-PPV 2PA (40% 1PA-CCA and 60% 2PA-CCA) could the data be reliably simulated. This is entirely consistent with the notion that only a fraction of the MEH-PPV units form CTCs

while the remaining population exists as uncomplexed sub-units. Consequently, the OL response of MEH-PPV:PCBM:DOP results from a combination of both 1PA- and 2PA-induced CCA which is consistent with the results from the OL-FOM dispersion studies as well as the intensity-dependent transient absorption measurements.

4.5 Summary

In summary, a ternary mixture including a conjugated polymer electron donor, a fullerene electron acceptor and a plasticizer allowed for the fabrication of an optical quality, thick film of a MEH-PPV:PCBM:DOP blend for optical limiting. In the femtosecond regime, two-photon absorption induced excited state absorption of MEH-PPV dominated the suppression and ~10 dB of suppression was observed for both MEH-PPV:DOP and MEH-PPV:PCBM:DOP blends. In the nanosecond regime, the suppression was enhanced by the accumulation of absorbing charge carriers over the long pulse duration and a contribution of one-photon absorption to the carrier generation due to a ground-state charge-transfer complex of MEH-PPV and PCBM, especially at the shorter wavelengths studied. MEH-PPV:PCBM:DOP showed a significantly reduced turn-on threshold and increased suppression of 15 dB, relative to MEH-PPV:DOP. The MEH-PPV:PCBM:DOP blend shows stronger suppression than what has been reported to date for organic optical limiters in the 750-900 nm range [5, 8, 9, 11] and thus has potential as an efficient optical limiting material in the femtosecond to nanosecond temporal range for near IR wavelengths.

4.6 Experimental Details

4.6.1 Sample Preparation

MEH-PPV (M_n = 40,000-70,000, Sigma-Aldrich), poly(methyl methacrylate) (PMMA, M_n = 15,000, Sigma-Aldrich), PCBM (Sigma-Aldrich), and DOP (Sigma-Aldrich) were used as received. 25 μm thick films of three different compositions were fabricated for OL measurements and nonlinear spectroscopic characterization: (1) MEH-PPV:DOP (50%:50%, by weight) (2) MEH-PPV:PCBM:DOP (40%:10%:50%, by weight), and (3) PMMA:PCBM:DOP (35%:15%:50%, by weight). Each component was dissolved in spectroscopic-grade dichloromethane separately, and then the solutions were mixed to obtain the appropriate composition ratio by weight. Solvent was then removed under vacuum to obtain a homogenous mixture of the selected components. The dried mixtures were then transferred into an Ar-filled glove box and melted into films under inert atmosphere to avoid potential degradation at high temperature. To process the blend films, a hot plate was first preheated to the processing temperature (190-250℃). Then, the blend was transferred onto a thoroughly cleaned microscope glass slide and sandwiched between another slide. 25 μm thick PTFE spacers were used to control the film thickness. Next, the sandwiched sample was then placed on the preheated hot plate and a static compressive force was applied evenly to distribute the mixture. As soon as the sample had melted and flowed, the sandwiched film was immediately transferred onto a cold metal block (chilled in a -40℃ freezer) and rapidly quenched. The fabricated blend films were then hermetically sealed with epoxy glue to avoid oxidation under ambient conditions.

Spin-coated films of MEH-PPV:DOP (100 nm thickness), MEH-PPV:PCBM:DOP (100 nm) and PMMA:PCBM:DOP (1.6 μm) were also prepared for linear spectroscopic measurements in order to observe distinct spectral features of the individual components. A 10-μm thick PMMA:PCBM:DOP was also prepared by drop-casting for observation of the weak absorption of PCBM in the 600 – 750 nm range. Film thicknesses were determined using a Dektak 6M contact profilometer.

4.6.2 Linear and Nonlinear Spectroscopic Measurements

Linear transmission properties of blend films were determined by Vis-NIR linear absorption spectroscopy using a Shimadzu UV3100 UV-Vis-NIR spectrometer. The 2PA coefficients (β) of the blends were determined at 730 nm and 870 nm using the femtosecond-pulsed open-aperture Z-scan technique which has been described in detail elsewhere [10]. The instrumental accuracy associated with these measurements is estimated to be ±15%.

4.6.3 Transient Absorption Spectroscopy

Transient measurements were carried out with both femtosecond and nanosecond pulses. The detailed experimental setups were described in chapter 2. For femtosecond measurements, the excitation wavelengths were 700 and 790 nm and the excitation energies ranged from 180 to 1950 nJ. The pump beam waist ($HW1/e^2$) for 700 nm was 510 μm and for 790 nm was 212 μm. The probe beam waists ($HW1/e^2$) were 170 and 240 μm for the visible and near IR regions. For nanosecond measurements, the excitation

wavelengths were 580 and 800 nm and the excitation energy was ~500 μJ. Again, all samples were hermetically sealed to exclude effects due to the presence of oxygen.

4.6.4 Optical Limiting

Optical limiting measurements were carried out with both femtosecond and nanosecond pulses to determine the power suppression capability of blends in the near IR region. The detailed experimental setup has been discussed in a previous publication [10], however a brief description will be given here. The nanosecond-pulsed OL measurements were set up using a flat top beam focused with an f/5 lens. The measurements were performed in the wavelength region from 750 – 900 nm with beam radii ($HW1/e^2$) measuring 30-40 μm at the sample position and pulse energies ranging from 5 nJ to 400 μJ. The femtosecond-pulsed OL measurements were performed using a Gaussian beam with radius of ~35 μm ($HW1/e^2$) at the sample position. The excitation wavelength of 810 nm was used with excitation energies from 0.5 to 1000 nJ.

REFERENCES

[1] Geusic, J. E., Singh, S., Tipping, D. W. and Rich, T. C., "3-photon stepwise optical limiting in silicon," *Physical Review Letters* **19**, 1126-1128 (1967).

[2] Perry, J. W., Mansour, K., Lee, I. Y. S., Wu, X. L., Bedworth, P. V., Chen, C. T., Ng, D., Marder, S. R., Miles, P., Wada, T., Tian, M. and Sasabe, H., "Organic optical limiter with a strong nonlinear absorptive response," *Science* **273**, 1533-1536 (1996).

[3] Tutt, L. W. and Kost, A., "Optical limiting performance of C_{60} and C_{70} solutions," *Nature* **356**, 225-226 (1992).

[4] Perry, J. W., *Organic and metal-containing reverse saturable absorbers for optical limiters* (CRC Press INC, Boca Raton, FL, 1997).

[5] He, G. S., Weder, C., Smith, P. and Prasad, P. N., "Optical power limiting and stabilization based on a novel polymer compound," *IEEE Journal of Quantum Electronics* **34**, 2279-2285 (1998).

[6] He, G. S., Yuan, L. X., Bhawalkar, J. D. and Prasad, P. N., "Optical limiting, pulse reshaping, and stabilization with a nonlinear absorptive fiber system," *Applied Optics* **36**, 3387-3392 (1997).

[7] Moulton, P. F., "Spectroscopic and laser characteristics of $TiAl_2O_3$," *Journal of the Optical Society of America B-Optical Physics* **3**, 125-133 (1986).

[8] Cha, M., Saricftci, N. S., Heeger, A. J., Hummelen, J. C. and Wudl, F., "Enhanced nonlinear absorption and optical limiting in semiconducting polymer/methanofullerene charge transfer films," *Applied Physics Letter* **67**, 3850-3852 (1995).

[9] Ehrlich, J. E., Wu, X. L., Lee, I. Y. S., Hu, Z. Y., Rockel, H., Marder, S. R. and Perry, J. W., "Two-photon absorption and broadband optical limiting with bis-donor stilbenes," *Optics Letters* **22**, 1843-1845 (1997).

[10] Hales, J. M., Cozzuol, M., Screen, T. E. O., Anderson, H. L. and Perry, J. W., "Metalloporphyrin polymer with temporally agile, broadband nonlinear absorption for optical pulse suppression in the near infrared," *Optics Express* **17**, 18478-18488 (2009).

[11] Perry, J. W., Barlow, S., Ehrlich, J. E., Heikal, A. A., Hu, Z. Y., Lee, I. Y. S., Mansour, K., Marder, S. R., Rockel, H., Rumi, M., Thayumanavan, S. and Wu, X. L., "Two-photon and higher-order absorptions and optical limiting properties of bis-donor substituted conjugated organic chromophores," *Nonlinear Optics* **21**, 225-243 (1999).

[12] Kraabel, B., McBranch, D., Sariciftci, N. S., Moses, D. and Heeger, A. J., "Ultrafast spectroscopic studies of photoinduced electron transfer from semiconducting polymers to C_{60}," *Physical Review B* **50**, 18543-18552 (1994).

[13] Brabec, C. J., Sariciftci, N. S. and Hummelen, J. C., "Plastic solar cells," *Advanced Functional Materials* **11**, 15-26 (2001).

[14] Sariciftci, N. S., Smilowitz, L., Heeger, A. J. and Wudl, F., "Photoinduced electron transfer from a conducting polymer to buckminsterfullerene " *Science* **258**, 1474-1476 (1992).

[15] Moses, D., Dogariu, A. and Heeger, A. J., "Mechanism of carrier generation and recombination in conjugated polymers," *Synthetic Metals* **116**, 19-22 (2001).

[16] Kato, T., Kodama, T. and Shida, T., "Electronic absorption spectra of the radical anions and cations of fullerenes: C_{60} and C_{70}," *Chemical Physics Letters* **180**, 446-450 (1991).

[17] van Hal, P. A., Christiaans, M. P. T., Wienk, M. M., Kroon, J. M. and Janssen, R. A. J., "Photoinduced electron transfer from conjugated polymers to TiO," *Journal of Physical Chemistry B* **103**, 4352-4359 (1999).

[18] Chung, S.-J., Maciel, G. S., Pudavar, H. E., Lin, T.-C., He, G. S., Swiatkiewicz, J., Prasad, P. N., Lee, D. W. and Jin, J.-I., "Two-photon properties and excitation dynamics of poly(*p*-phenylenevinylene) derivatives carrying phenylanthracene and branched alkoxy pendents," *Journal of Physical Chemistry A* **106**, 7512-7520 (2002).

[19] Samoc, A., Samoc, M., Woodruff, M. and Lutherdavies, B., "Tuning the properties of poly(*p*-phenylenevinylene) for use in all-optical switching," *Optics Letters* **20**, 1241-1243 (1995).

[20] Dogariu, A., Vacar, D. and Heeger, A. J., "Picosecond time-resolved spectroscopy of the excited state in a soluble derivative of poly(phenylene vinylene): Origin of the bimolecular decay," *Physical Review B* **58**, 10218-10224 (1998).

[21] Smilowitz, L. and Heeger, A. J., "Photoinduced absorption from triplet excitations in poly(2-methoxy-5-(2'-ethyl-hexyloxy)-*p*-phenylene vinylene) oriented by gel-processing in polyethylene," *Synthetic Metals* **48**, 193-202 (1992).

[22] Vandewal, K., Gadisa, A., Oosterbaan, W. D., Bertho, S., Banishoeib, F., Van Severen, I., Lutsen, L., Cleij, T. J., Vanderzande, D. and Manca, J. V., "The relation between open-circuit voltage and the onset of photocurrent generation by charge-transfer absorption in polymer: Fullerene bulk heterojunction solar cells," *Advanced Functional Materials* **18**, 2064-2070 (2008).

[23] Ebbesen, T. W., Tanigaki, K. and Kuroshima, S., "Excited-state properties of C_{60}," *Chemical Physics Letters* **181**, 501-504 (1991).

[24] Drori, T., Sheng, C. X., Ndobe, A., Singh, S., Holt, J. and Vardeny, Z. V., "Below-gap excitation of π-conjugated polymer-fullerene blends: Implications for bulk organic heterojunction solar cells," *Physical Review Letters* **101**, - (2008).

[25] Nelson, J., "Diffusion-limited recombination in polymer-fullerene blends and its influence on photocurrent collection," *Physical Review B* **67**, - (2003).

[26] Holzer, W., Penzkofer, A., Tillmann, H. and Hörhold, H.-H., "Spectroscopic and travelling-wave lasing characterisation of gilch-type and horner-type MEH-PPV," *Synthetic Metals* **140**, 155-170 (2004).

[27] Chou, H. L., Lin, K. F. and Wang, D. C., "Miscibility and luminescence properties of MEH-PPV/DPO-PPV polyblends," *Journal of Polymer Research* **13**, 79-84 (2006).

[28] Shinar, J., Vardeny, Z. V. and Kafafi, Z. H., eds. *Optical and electronic properties of fullerenes and fullerene-based materials* (Marcel Dekker, Inc., New York, NY, 2000).

[29] Bakulin, A. A., Martyanov, D. S., Paraschuk, D. Y., Pshenichnikov, M. S. and van Loosdrecht, P. H. M., "Ultrafast charge photogeneration dynamics in ground-state charge-transfer complexes based on conjugated polymers," *Journal of Physical Chemistry B* **112**, 13730-13737 (2008).

[30] Goris, L., Poruba, A., Hod'akova, L., Vanecek, M., Haenen, K., Nesladek, M., Wagner, P., Vanderzande, D., De Schepper, L. and Manca, J. V., "Observation of the subgap optical absorption in polymer-fullerene blend solar cells," *Applied Physics Letters* **88**, - (2006).

[31] Lin, Y., Zhang, J., Brzozowski, L., Sargent, E. H. and Kumacheva, E., "Nonlinear optical figures of merit of processible composite of poly(2-methoxy,5-(2 '-(ethyl)hexyloxy)-*p*-phenylene vinylene) and poly(methyl methacrylate)," *Journal of Applied Physics* **91**, 522-524 (2002).

[32] Van Stryland, E. W., Wu, Y. Y., Hagan, D. J., Soileau, M. J. and Mansour, K., "Optical limiting with semiconductors," *Journal of the Optical Society of America B-Optical Physics* **5**, 1980-1989 (1988).

[33] Samuel, I. D. W., Rumbles, G., Collison, C. J., Friend, R. H., Moratti, S. C. and Holmes, A. B., "Picosecond time-resolved photoluminescence of PPV derivatives," *Synthetic Metals* **84**, 497-500 (1997).

CHAPTER 5

NONLINEAR ABSORPTION AND TRANSIENT SPECTROSCOPY OF DITHIENOPYRROLE-BASED DONOR-ACCEPTOR CONJUGATED COPOLYMERS

5.1 Abstract

This chapter reports a study of photophysical and nonlinear optical properties of a set of low band gap, dithienopyrrole (DTP) –based donor-acceptor conjugated copolymers and their potential for optical limiting applications in the near infrared (near-IR) spectrum. Transient absorption measurements with both femtosecond and nanosecond pulses were performed and evidenced the existence of broad and strong excited state absorptions throughout the range of telecommunications wavelengths. Solvent-dependent and intensity-dependent photophysical responses were studied. Femtosecond-pulse open-aperture Z-scan showed large effective two-photon absorption cross sections in these conjugated polymers in the near-IR region. Large, nanosecond-pulse energy suppression was achieved at 1064 nm, suggesting these DTP-based low band gap materials could be promising candidates for optical limiting applications in the near-IR.

5.2 Introduction

With the growth of laser tracking and all-optical signal processing (AOSP) technologies, the need for effective optical limiters to perform sensor protection is

increasing. In the past two decades, organic materials have shown potential as efficient optical limiters [1-7] through different nonlinear absorption processes such as reverse saturable absorption (RSA) [1, 6] and photo-induced charge transfer (PICT) absorption [2, 7, 8]. In the region of 1064-1550 nm (telecommunication bands), reverse saturable absorbers like porphyrin polymers have shown excellent optical limiting capability [1].

Recently, the low bandgap conjugated polymers (LBPs) have been developed that show absorption band edges that extend to wavelengths approaching 1.5 μm, and have opened the prospect of applying LBPs to photonic telecommunication applications [9]. LBPs such as DTP-based polymers have been shown to possess a relative large charge mobility (0.2 $cm^2/V\ s$) in organic field effect transistors [10]. The DTP based LBPs would be expected to exhibit large third-order optical nonlinearity, such as two-photon absorption and nonlinear refraction, as a result a result of the low bandgaps and the strong electronic absorption strength.

In DTP donor (D) –acceptor (A) copolymers, the alternating donor and acceptor moieties in the conjugated backbone are electronically coupled and lead to significant intramolecular charge transfer (ICT) interactions. Various electronic and optical properties can be affected by changes in the electronic coupling between the donors and acceptors in conjugated systems. Previous research has shown that the optical nonlinearity of such donor-acceptor type conjugated systems is largely determined by the relative energy of the resonance structures of neutral and charge separated forms (that is, aromatic ground state and quinoid charge separated state) [11-15]. The factors affecting the energy difference between these two forms (or the stabilization of charge separated form) include the donor and the acceptor strength, the difference in the bridge π-

electronic energy in the resonance structures, and the solvent-mediated polarization [11, 13]. It has been shown that increasing the aromaticity of ground state structure will result in decreased coupling strength between donor and acceptor moieties giving reduced electronic polarization [11]. On the other hand, due to the aromatic stabilization, increasing the aromaticity of the charge separated state would stabilize the charge separated state and thus assist electronic polarization in an applied field [15]. Such structural-property relationship implies the photophysical and nonlinear optical properties of a given donor-acceptor conjugated system could be molecular engineered to meet the needs of a specific application. The DTP polymers studied here have donor-acceptor type repeat units in the polymer backbone. However, there is conjugation between the acceptor and donor groups of adjacent repeat units. Thus, DTP-based polymers may be viewed as resulting from more extended segments in the backbone such as D-π-A-π-D or A-π-D-π-A or longer segments of the backbone. Even in these cases, it is expected that the coupling of the donor and acceptor groups and the energetics of the neutral and charge-transferred forms of the system play an important role in the linear and nonlinear optical properties. [16-18] As described in chapter 4, well-overlapped nonlinear absorption (i.e. two-photon absorption) and subsequent excited-state absorption (i.e. reverse saturable absorption or charge carrier absorption) spectra are critical for optical limiting applications.

In this chapter, a set of dithienopyrrole (DTP) -based donor-acceptor conjugated polymers with different connecting aromatic and heteroaromatic π-bridges is studied. (**Scheme 5.1**) The focus of this study is to understand the structure-nonlinear optical property relationship of these polymers and provide feedback and guidance to the

development of new high performance DTP-based conjugated polymers. The goal of this study is to manipulate the nonlinear absorption and excited state absorption spectra and thus, achieve an improved performance for optical limiting at 1064 nm. In this set of polymers, the connecting bridges varied from thiophene, hexylthiophene, to phenylene. The choices of these connecting bridges include two strategies to alter the electronic interaction between donor and acceptor moieties. One approach involves introducing steric hindrance which forces torsion in the backbone and reduces planarity of the ground state structure (thiophene vs. hexylthiophene bridges) and the other one is increasing the aromaticity of neutral ground state form giving reduced neutral-charge transfer state mixing (thiophene vs. phenylene bridges). It is known that phenylene has relative larger aromatic stabilization in the ground state compared to thiophene resulting in a larger energy difference between aromatic and quinoid resonance structures [19]. Thus, replacing the thiophene bridge with benzene bridge will result in increased aromaticity in the ground state and a lower neutral form energy leading to reduced neutral-charge transfer state mixing. Additionally, it has been shown that thiophene conjugated oligomers have better charge transfer efficiency, and a larger third-order nonlinearity than phenylene conjugated oligomers [20, 21]. Again, this was attributed to the energy difference between the benzenoid-like ground state and quinoid-like excited state for the benzene compared to the thiophene linker.

In the following section, the investigation of photophysical and nonlinear optical properties of these DTP-based donor-acceptor conjugated polymers is presented. Femtosecond and nanosecond transient absorption sepectra and kinetics were measured to characterize the excited state properties of these polymers. Solvent-dependent

experiments were carried out to assist in the understanding of structure-dependent photophysical properties. Femtosecond, open-aperture Z-scan was performed to obtain the two photon absorption cross sections of these polymers in the near infrared. All three polymers showed strong excited state absorption and two-photon absorption in the near infrared suggesting the potential of these polymers for photonic applications. Thus, nanosecond-pulsed optical limiting was used to test the performance of these polymers and showed that these polymers do function as optical limiting materials at 1064 nm.

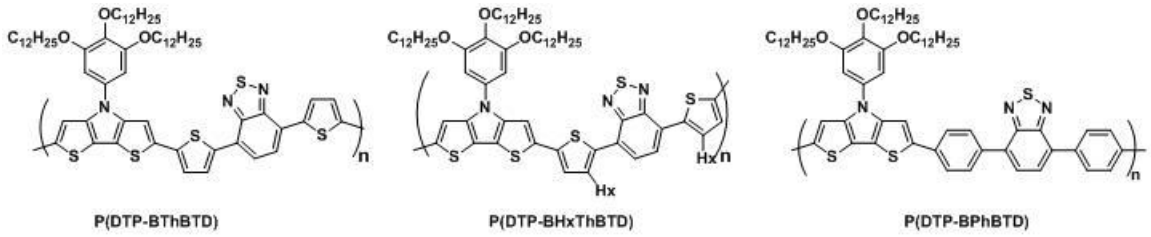

Scheme 5.1. Chemical structures of dithienopyrrole-based conjugated copolymers.

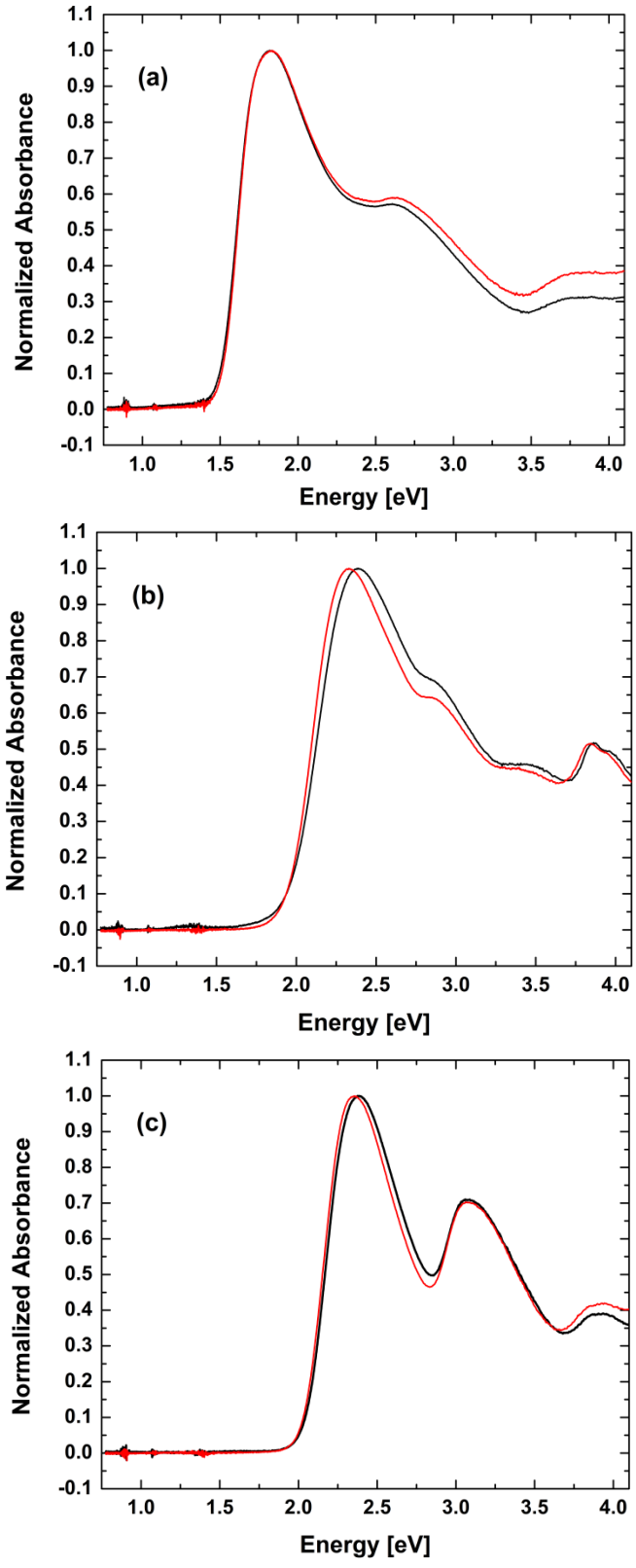

Figure 5.1. Normalized absorption spectra of ~ 15 μM (a) P(DTP-BThBTD), (b) P(DTP-BHxThBTD), and (c) P(DTP-BPhBTD) in toluene (red) and DCM (black).

Table 5.1. Ground state, excited state and nonlinear absorption properties of DTP-based polymers.

Polymer	**Solvent**	ΔE_{max} **[eV]**	σ_{max} **[$\times 10^{-20}$ m^2]**	σ_{ESA}[a] **[$\times 10^{-20}$ m^2]**			δ[b] **[GM]**		
				1150nm	**1300nm**	**1550 nm**	**1150 nm**	**1300 nm**	**1550 nm**
P(DTP-BThBTD)	Toluene	1.83	1.74	3.71	4.62	4.20	3000	1889	337
	DCM	1.82	1.34	3.85	4.99	4.76	-	-	-
P(DTP-BHxThBTD)	Toluene	2.33	1.58	3.65	3.00	2.03	373	217	136
	DCM	2.38	1.56	1.42	1.21	1.08	-	-	-
P(DTP-BPhBTD)	Toluene	2.36	1.46	0.949	0.759	0.721	237	233	167
	DCM	2.38	1.59	0.639	0.536	0.536	-	-	-

[a] The excited-state cross section (σ_{ESA}) was extracted from the transient absorption measurement by comparing the ratio of ΔOD of ground state bleaching (saturable absorption) and that of excited state absorption: $\sigma_{ESA} = - \sigma_g \times \Delta OD_{ESA} / \Delta OD_{GSA}$.
[b] The two-photon absorption cross section (δ) was extracted from a numerical fitting of open-aperture Z-scan measurements by assuming a mechanism of two-photon absorption followed by excited state absorption.

Table 5.2. Ground-state recovery kinetics of DTP-based polymers.[a]

Polymer	Solvent	τ_1 [ps]	A^N_1[b]	τ_2 [ps]	A^N_2	τ_3 [ps]	A^N_3	A^N_{y0}	$\tau_{triplet}$ [μs][c]
P(DTP-BThBTD)	Toluene	1.3 ± 0.1	0.47	22 ± 3	0.28	430 ± 50	0.21	0.05	2.1 ± 0.1 (0.33 ± 0.01)
	DCM	0.34 ± 0.01	0.09	3.8 ± 0.1	0.55	150 ± 10	0.30	0.06	0.43 ± 0.03 (0.38 ± 0.03)
P(DTP-BHxThBTD)	Toluene	0.47 ± 0.01	0.36	14 ± 1	0.03	900 ± 10	0.25	0.36	6.6 ±0.1 (0.20 ±0.01)
	DCM	0.31 ± 0.01	0.41	74 ± 20 (1.8 ± 0.4)[d]	0.27	440 ± 10	0.25	0.08	5.4 ±0.1 (0.32 ±0.02)
P(DTP-BPhBTD)	Toluene	0.93 ± 0.01	0.44	26 ± 1	0.18	870 ± 10	0.24	0.14	19 ± 1 (0.69 ± 0.01)
	DCM	1.0 ± 0.1	0.28	31 ± 1	0.22	960 ± 20	0.29	0.21	1.9 ±0.2 (0.15 ±0.01)

[a] The kinetic fitting was performed via a global fitting with a three-exponential decay function: $\Delta OD(t) = A_1 e^{-t/\tau 1} + A_2 e^{-t/\tau 2} + A_3 e^{-t/\tau 3} + y_0$; here τ is the time constant of transient species and y_0 is a constant background offset.

[b] The amplitudes reported in the table were normalized as follows: $A^N_i = A_n / (A_1 + A_2 + A_3 + y_0)$, i = 1, 2, or 3.

[c] The decay kinetic of triplet species was acquired via nanosecond transient absorption and fitted with a bi-exponential decay function: $\Delta OD(t) = A_1 e^{-t/\tau 1} + A_2 e^{-t/\tau 2} + y_0$. The numbers in parenthesis indicate the lifetime of oxygen-quenched triplet species.

[d] This is the growth time of species 2, as shown in the inset of **Figure 5.8**.

5.3 Results and Discussion

5.3.1 Linear Absorption

Representative absorption spectra of DTP-based polymers are shown in **Figure 5.1**. The locations of the first electronic transition (λ_{max}) and the corresponding cross section (σ_{max} in m^2) in toluene and dichloromethane are listed in **Table 5.1**. All three polymers have similar first electronic transition absorption cross-sections. P(DTP-BThBTD) showed the lowest energy absorption maximum (ΔE_{max} ~1.8 eV, λ_{max} = 675 nm) among all three polymers. P(DTP-BHxThBTD) showed broadest, less resolved absorption bands compared to P(DTP-BThBTD) and P(DTP-BPhBTD), suggesting that hexyl group induced torsion may be leading to greater torsional fluctuations in solution. Furthermore, the electronic absorption band of P(DTP-BHxThBTD) and to a lesser extent of P(DPT-BPhBTD) were broadened in DCM as compared with toluene, while the absorption band width of P(DTP-BThBTD) showed negligible changes between these solvents.

5.3.2 Transient Spectroscopy

Transient absorption measurements with femtosecond and nanosecond pulsed excitation were used to characterize the excited state absorptions and decay kinetics of DTP-based polymers. The excitation wavelengths were chosen at the long-wavelength edge of first electronic transition band to ensure only the first excited singlet state was populated.

5.3.2.1 Comparison of Spectral and Kinetic Characteristics of Thiophenyl and Phenyl Bridge

Figure 5.2, **5.3**, and **5.4** show the femtosecond transient spectra at different time delays, global fitting results of femtosecond transient kinetics, and nanosecond transient kinetics of P(DTP-BThBTD), P(DTP-BHxThBTD), and P(DTP-BPhBTD) in toluene, respectively. As seen in the transient spectra (Figure 5.2a, 5.3a, and 5.4a), all three polymers have broad excited state absorptions throughout the entire near IR region. The transient absorption spectra of the initially excited singlet state where the electron is shown after a short time delay of 400 fs. The peaks of the first excited state absorptions can be identified at 1050 nm and 1350 nm for P(DTP-BThBTD), 900 nm and 1200 nm for P(DTP-BHxThBTD), and 650 nm and 950 nm for P(DTP-BPhBTD). The first excited state absorptions of P(DTP-BHxThBTD) blue shift as the twisting of backbone increases and leads to reduced conjugation which would be expected to give an increased transition energy. On the other hand, the first excited-state absorption of P(DTP-BPhBTD) also blue shifts as the result of aromatic stabilization, which would also be expected to give a higher transition energy.

Ground-state saturable absorption was also observed in all three polymers. The absorption saturation can be used to determine the initial number density of excited states and the yield of transient species. In addition, time dependent measurements of the absorption saturation give information on the kinetics of the relaxation processes that repopulate the ground state. The peak wavelengths of the saturable absorptions are 702 and 468 nm for P(DTP-BThBTD), 540 nm for P(DTP-BHxThBTD), and 530 nm for P(DTP-BPhBTD). For P(DTP-BThBTD) and P(DTP-BHxThBTD). These peak

positions are somewhat different from the ground state absorption peak due to distortions of the band shapes arising from stimulated emission at early time delay. For P(DTP-BHxThBTD) and P(DTP-BPhBTD), the excited state absorption spectra exhibit a plateau between 600-800 nm. This suggests that stimulated emission also overlaps spectrally with short wavelength excited state absorptions, resulting in a distortion or reduction of the transient absorption spectral signal. The peak absorption cross sections of the excited state absorption bands of the three polymers, well away from the stimulated emission, were obtained using the following equation:

$$\sigma_{ESA} = - \sigma_g \times \Delta OD_{ESA} / \Delta OD_{GSA} \qquad \text{(Eq. 5.1)}$$

and the values are listed in Table 5.1. The ground-state absorption saturation, ΔOD_{GSA}, of P(DTP-BThBTD), P(DTP-BHxThBTD), and P(DTP-BPhBTD) was probed on the short wavelength side of the absorption band at 650nm, 500 nm, and 530 nm, to avoid contributions from stimulated emission. The ground-state absorption cross sections (σ_g) at these probe wavelengths were calculated from the linear absorption spectra of the solutions. The excited state absorption cross sections decrease in the order P(DTP-BThBTD) > P(DTP-BHxThBTD) > P(DTP-BPhBTD).

The results of a global fitting analysis of the femtosecond transient absorption decays of all three polymers in toluene are shown in Figures 5.2b, 5.3b, and 5.4b. The analysis included the global fitting of both ground state recovery and excited state decay transients. To obtain the time constants the ground state recovery transients were fit over a spectra range that avoided the stimulated emission. The time constants obtained from this analysis were then used a initial values for the global analysis of the transient spectra in the induced absorption region of the spectrum. The time constants obtained from the

transient absorption fitting were in good agreement (within ~10%) with those of from the fitting of the ground state recovery. The fitting results of transient kinetics are listed in **Table 5.2**. Global fitting analyses on all three polymers in toluene and DCM showed the presence of at least four components in the decay kinetics to the ground state. For all three polymers, two routes were fast, and the decay times of the first component (species 1) were in the range of several hundred femtoseconds to a few (< 2) picoseconds and several tens picoseconds (species 2). The another component was relatively slow with a decay time that was subnanosecond (species 3) and a fourth component had a decay time too long to be determined with the femtosecond transient absorption system (species 4) and was accounted for using a normalized constant offset ($A(y_0)$).

Nanosecond transient absorption was utilized to resolve the lifetime of species 4, which was found to range from 2 to 19 μs for the different polymers. This component was assigned to the triplet state in these polymers, based on oxygen quenching of this component. As can be determined from the data in Table 5.2, the total yield of long-lived components (based on the sum of amplitudes for species 3 and 4) are significantly higher in P(DTP-BHxThBTD) (61%) and P(DTP-BPhBTD) (38%) than in P(DTP-BThBTD) (26%). It must be noted that the yields of species 3 in all three polymers are relatively close ranging from 21-26%. However, the species 4 in both P(DTP-BHxThBTD) and P(DTP-BPhBTD) showed significantly increased yields compared to P(DTP-BThBTD). The increased triplet yields of P(DTP-BHxThBTD) and P(DTP-BPhBTD) may be as a result of a smaller S_1-T_1 energy splitting and larger intersystem crossing rate, due to the energy gap law [22], for the polymers with the hexylthiophene and benzene linkers as

compared with the thiophene linker, which is consistent with a lower degree of charge transfer in the ground state for case of the hexylthiophene and benzene linkers.

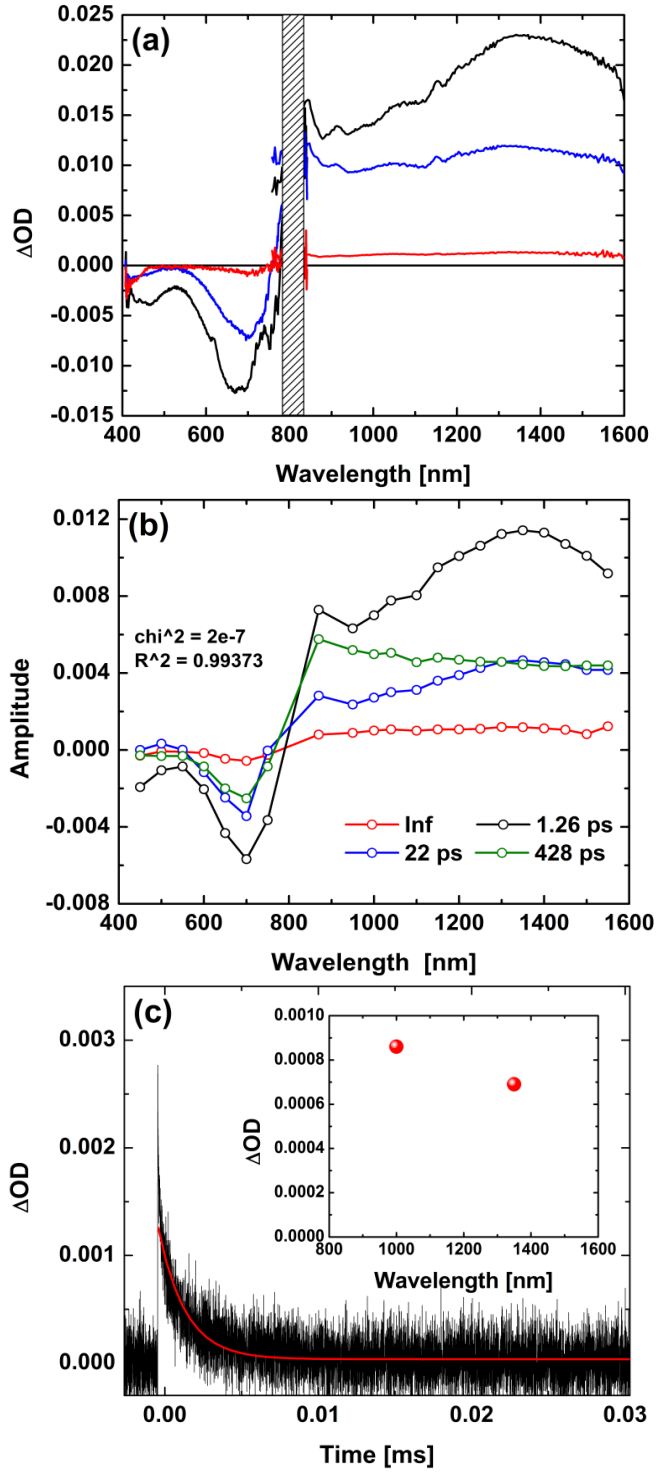

Figure 5.2. Transient absorption measurements of P(DTP-BThBTD) with (a and b) femtosecond and (c) nanosecond pulses in toluene: (a) Transient spectra at time delays of 400 fs (black), 2 ps (blue), and 2 ns (red), (b) global fitting of decay kinetics at various wavelengths, and (c) decay kinetics of the triplet state obtained in deoxygenated solution. The inset shows two points on the ns TA spectrum. (λ_{ex} = 780 nm, E_{ex} = 420 nJ)

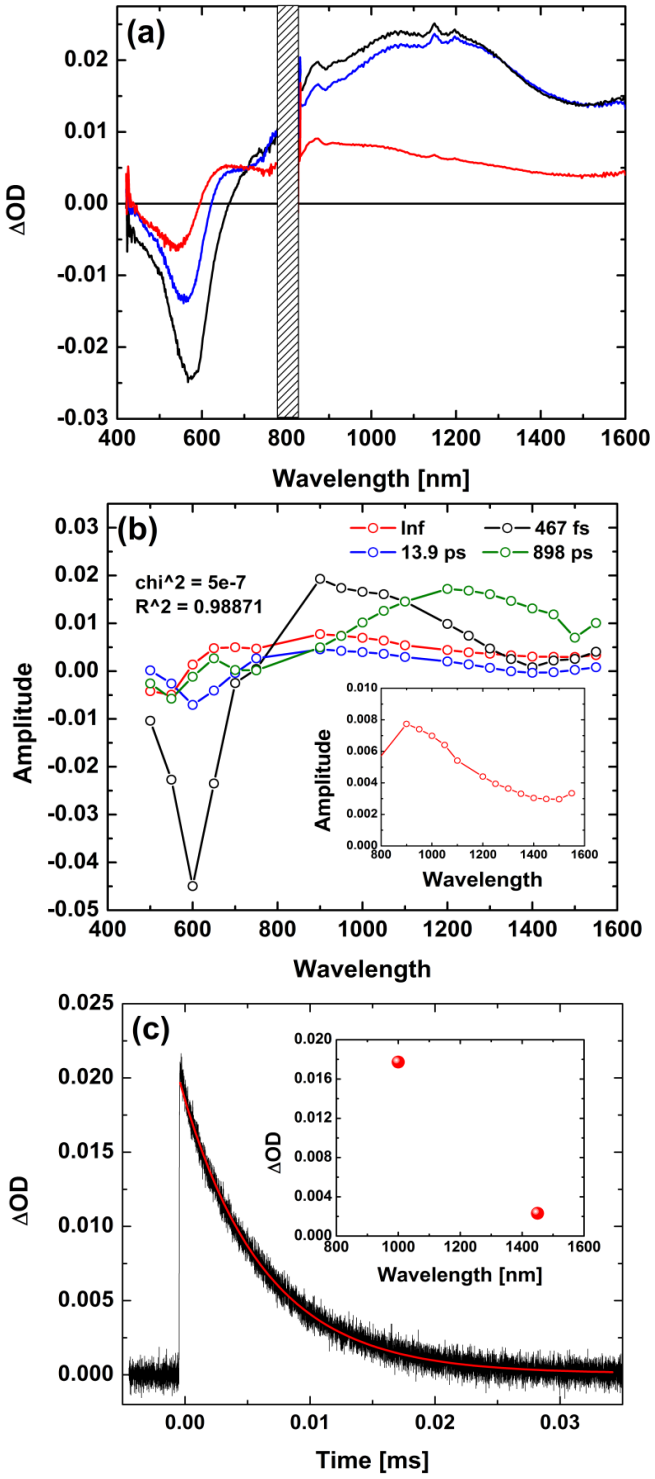

Figure 5.3. Transient absorption measurements of P(DTP-BHxThBTD) with (a and b) femtosecond and (c) nanosecond pulses in toluene: (a) Transient spectra at time delays of 400 fs (black), 2 ps (blue), and 2 ns (red), (b) global fitting of decay kinetics at various wavelengths, and (c) decay kinetics of the triplet state obtained in deoxygenated solution. The inset shows two points on the ns TA spectrum. (λ_{ex} = 610 nm, E_{ex} = 430 nJ)

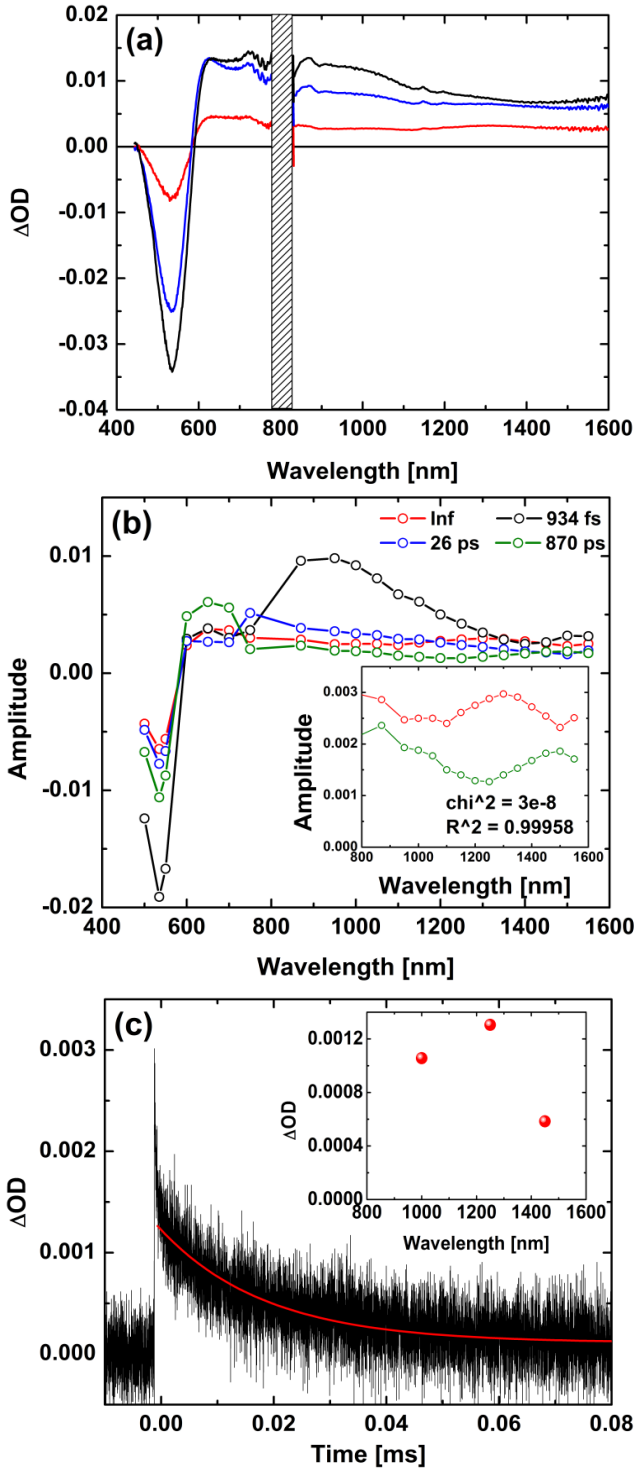

Figure 5.4. Transient absorption measurements of P(DTP-BPhBTD) with (a and b) femtosecond and (c) nanosecond pulses in toluene: (a) Transient spectra at time delays of 400 fs (black), 2 ps (blue), and 2 ns (red), (b) global fitting of decay kinetics at various wavelengths, and (c) decay kinetics of the triplet state obtained in deoxygenated solution. The inset shows three points on the ns TA spectrum. (λ_{ex} = 585 nm, E_{ex} = 440 nJ)

5.3.2.2 Solvent-Dependent Photophysical Properties of DTP-based Polymers

Solvent-dependent photophysical properties were observed in DTP-based polymers. Comparative transient absorption measurements were carried out on DTP-based polymer solutions in toluene and dichloromethane. In both sets of solution measurements, the concentration of DTP-based polymers was kept between 6 – 8.3 μM, and the transmittance of each solution at each excitation wavelength was kept between 60-70%.

Both P(DTP-BThBTD) and P(DTP-BHxThBTD) showed significant solvent-dependent photophysical properties, as evidenced by changes in transient spectra (**Figure 5.5** and **Figure 5.7**), as well as in ground state recovery kinetics (**Figure 5.6** and **Figure 5.8**). On the other hand, P(DTP-BPhBTD) showed minor changes between the two solvents as shown in the transient spectra (**Figure 5.9**) and the recovery kinetics (**Figure 5.10**). Detailed kinetic fitting results are listed in Table 5.2.

The transient spectra of P(DTP-BThBTD) and P(DTP-BHxThBTD) both showed blue-shifted excited state absorption peaks and a lower yield of long-lived components (species 3 and 4). The blue-shifted excited state absorptions indicate the stabilization of charge transfer excited state in the more polar solvent. The yield of the long-lived components (3 and 4) of P(DTP-BThBTD) increased from 26% to 36% (Figure 5.6). For P(DTP-BThBTD), the yield of species 3 went from 20% to 30% and its lifetime dropped from 430 ps to 150 ps on going from toluene to DCM. Furthermore, the lifetime of the triplet state (species 4) also dropped from 2.1 μs (in toluene) to 0.43 μs (in dichloromethane) but the yield remained the same. The polymer with larger steric hindrance (P(DTP-BHxThBTD)), and likely a greater degree of torsional distortion in the

ground state, showed a strong solvent-dependence of the excited state dynamics. The yield of the rapid relaxing species (1 and 2) increased from 39 to 68%. Also the lifetime of species 3 decreased from 900 to 440 ps on going from toluene to DCM. It is likely that backbone torsional motions plays an important role in the yield of long-lived transient components, as the torsionally induced relaxation of the excited state could well depend on solvent polarity. In polar solvent like DCM, the yield of long-lived components in P(DTP-BHxThBTD) is significantly reduced and this suggests that the torsional motion favors fast nonradiative decay to the ground state. The may be due to a stabilization of the fully twisted charge transfer state and lowering of the potential barrier to twisting, as is the case for other charge transfer molecules [17] and the classic case of cis-stilbene [23]. The yield of the long-lived components of P(DTP-BHxThBTD) dropped from 61% to 33% as the solvent changed from toluene to dichloromethane (Figure 5.8), consistent with the more rapid initial decay. The lifetime of the triplet state (species 4) of P(DTP-BHxThBTD) did not show notable reduction like that of P(DTP-BThBTD) in DCM. It should be noted that, as indicated by the inset of Figure 5.8, a growth of species 2 was observed in dichloromethane. The origin of this apparent growth in the ground state bleaching is currently under study.

Comparing P(DTP-BThBTD) and P(DTP-BPhBTD), the planarity of conjugated backbones should be fairly similar but the aromatic phenyl bridge should stabilize the neutral form energy relative to that for the heteroaromatic thiophenyl bridge. The polymer with larger aromatic stabilization, P(DTP-BPhBTD), showed least solvent-dependency in transient absorption measurements. P(DTP-BPhBTD) shows a different change relative to P(DTP-BThBTD) in recovery kinetics upon changing the solvent from

toluene to dichloromethane, while the transient spectra of excited state absorptions are identical in both solvents. This is consistent with a smaller degree of charge transfer upon excitation for the phenyl linker. In dichloromethane, the yield of species 3 and 4 was 50% compared to 38% in toluene. The lifetime of species 3 showed slightly increase from 870 ps in toluene to 960 ps in dichloromethane. The lifetime of the triplet state, however, decreased from 19 μs to 1.9 μs.

5.3.2.3 Intensity-Dependent Transient Kinetics

Intensity-dependent transient measurements were carried out on the same set of solutions of all three polymers in both toluene and dichloromethane, as mentioned previously. The excitation energy was varied from 200 nJ to > 2400 nJ. As shown in **Figure 5.12**, P(DTP-BHxThBTD) showed negligible intensity-dependent ground state recovery kinetics in both toluene and dichloromethane. This might be due to the existence of highly twisted backbone structures preventing exciton or charge transport and exciton-exciton annihilation or possibly charge recombination. P(DTP-BThBTD) showed intensity-dependent kinetics in toluene but not in dichloromethane (**Figure 5.11)**. The transient kinetics in dichloromethane is similar to that in toluene at high excitation energy. This suggests that, in dichloromethane, P(DTP-BThBTD) may be in a more planar backbone geometry and promote the exiton-exiton annihilation or charge recombination. P(DTP-BPhBTD) showed significant intensity-dependent kinetics in both polar and nonpolar solvent which suggests that torsional fluctuations may be minimal for this polymer (**Figure 5.13)**. The yield of long-lived components dropped to 20% as the energy increased to 2400 nJ

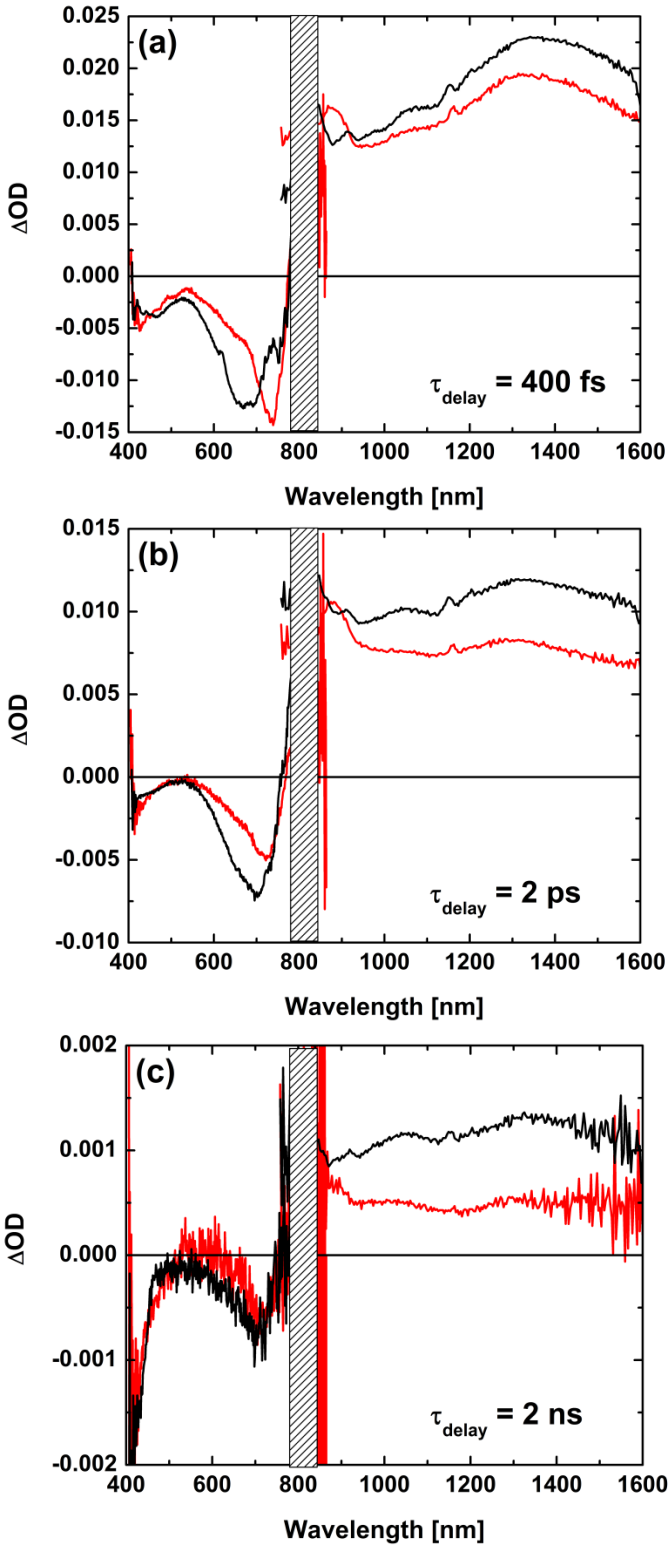

Figure 5.5. Comparison of transient absorption spectra of P(DTP-BThBTD) in toluene (black) and DCM (red) at different time delays. (λ_{ex} = 780 nm, E_{ex} = 420 nJ in toluene and 400 nJ in dichloromethane)

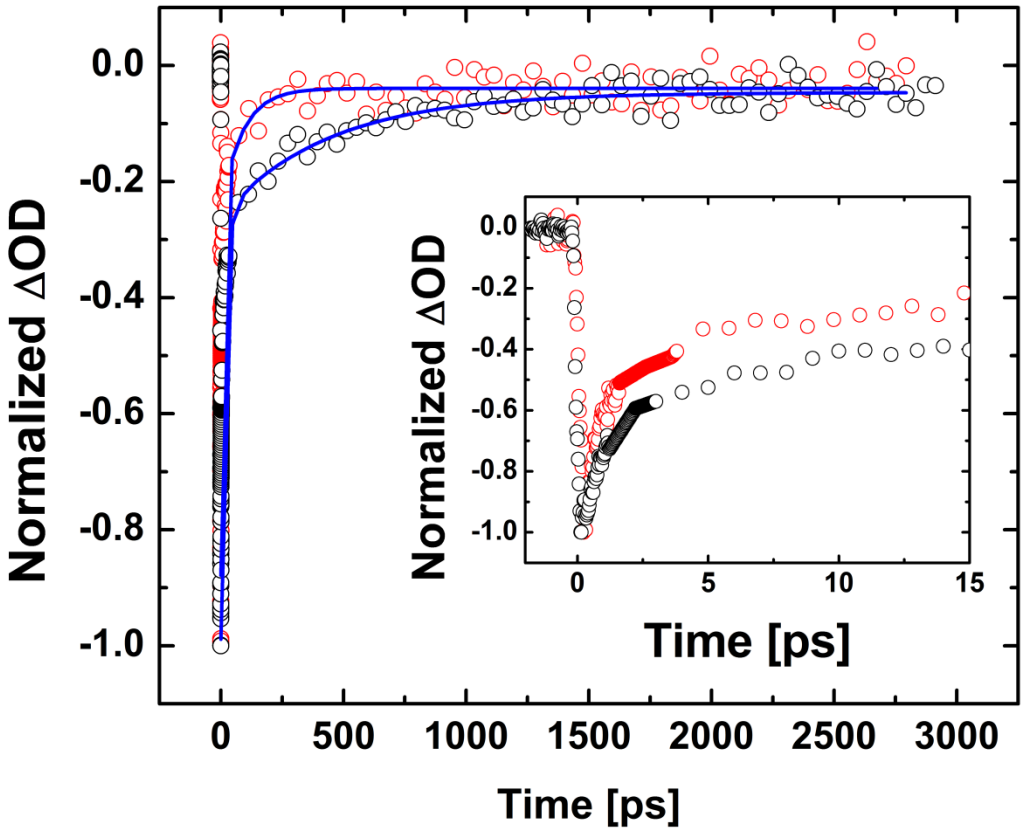

Figure 5.6. Solvent-dependent ground state recovery of P(DTP-BThBTD) in toluene (black) and DCM (red). (λ_{ex} = 780 nm, E_{ex} = 420 nJ in toluene and 400 nJ in dichloromethane)

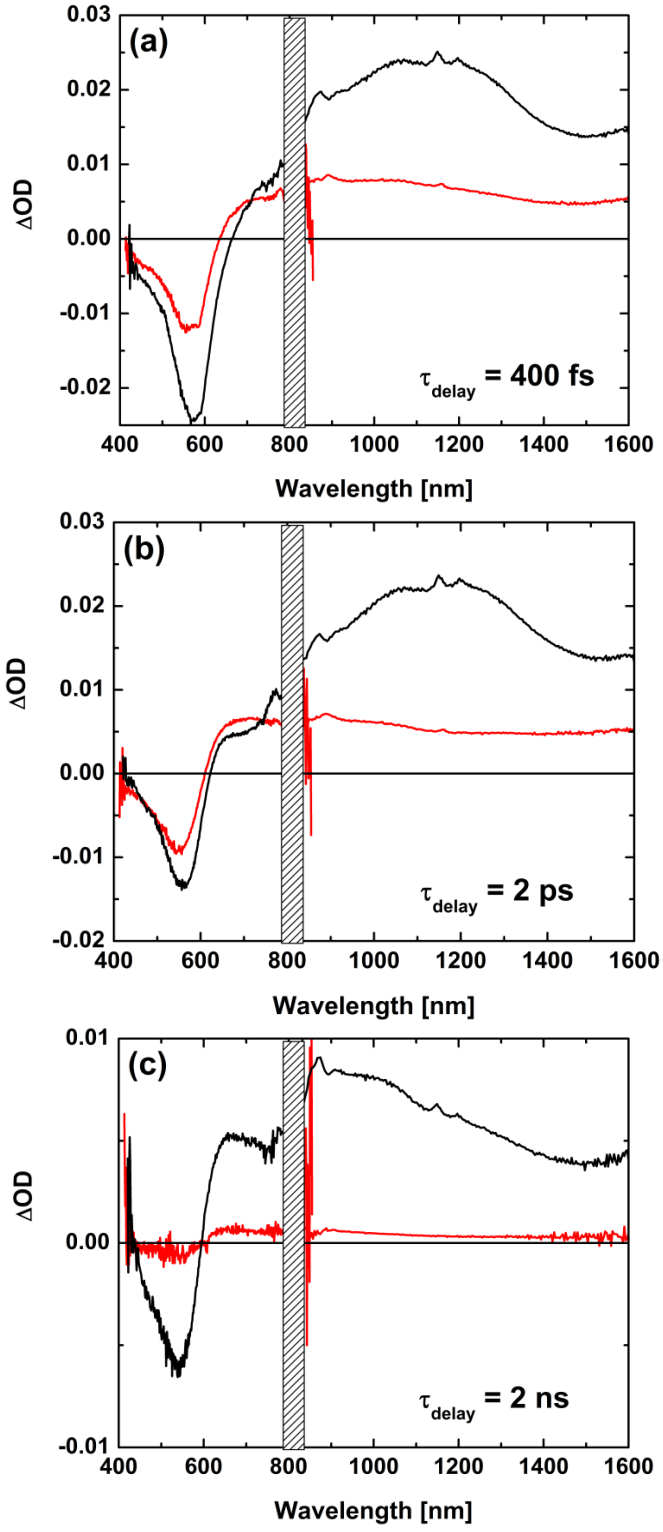

Figure 5.7. Comparison of transient absorption spectra of P(DTP-BHxThBTD) in toluene (black) and DCM (red) at different time delays. (λ_{ex} = 610 nm, E_{ex} = 430 nJ in toluene and 400 nJ in dichloromethane)

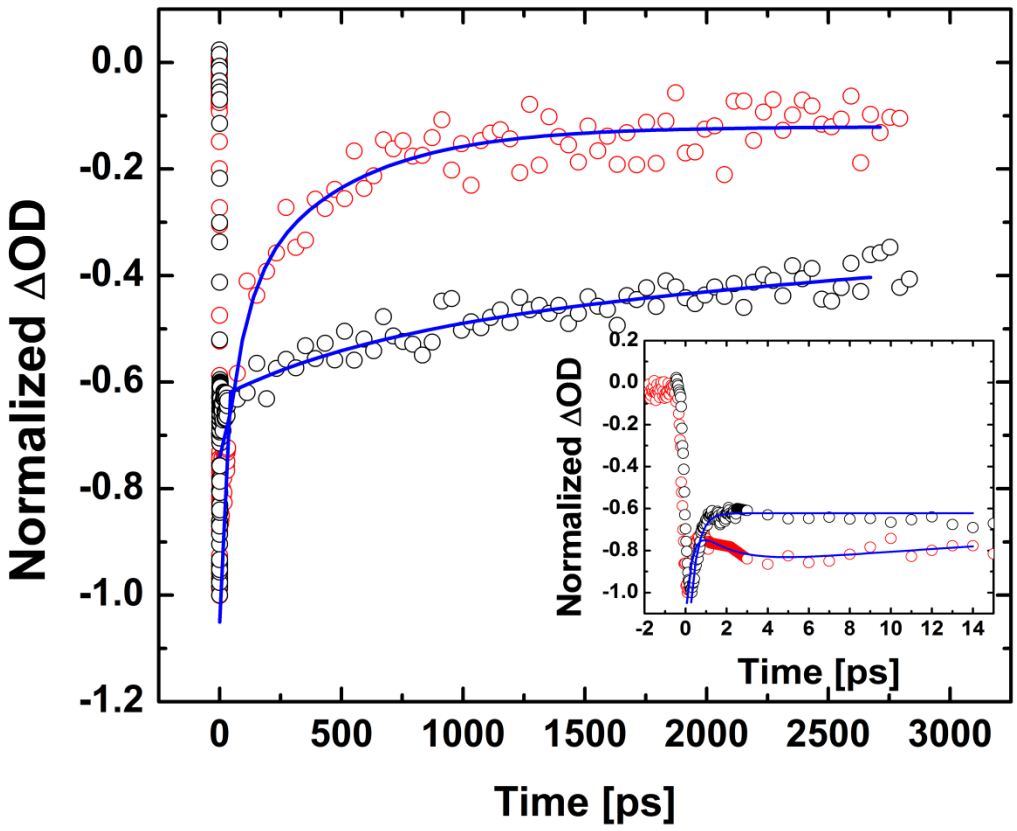

Figure 5.8. Solvent-dependent ground state recovery of P(DTP-BHxThBTD) in toluene (black) and DCM (red). (λ_{ex} = 610 nm, E_{ex} = 430 nJ in toluene and 400 nJ in dichloromethane)

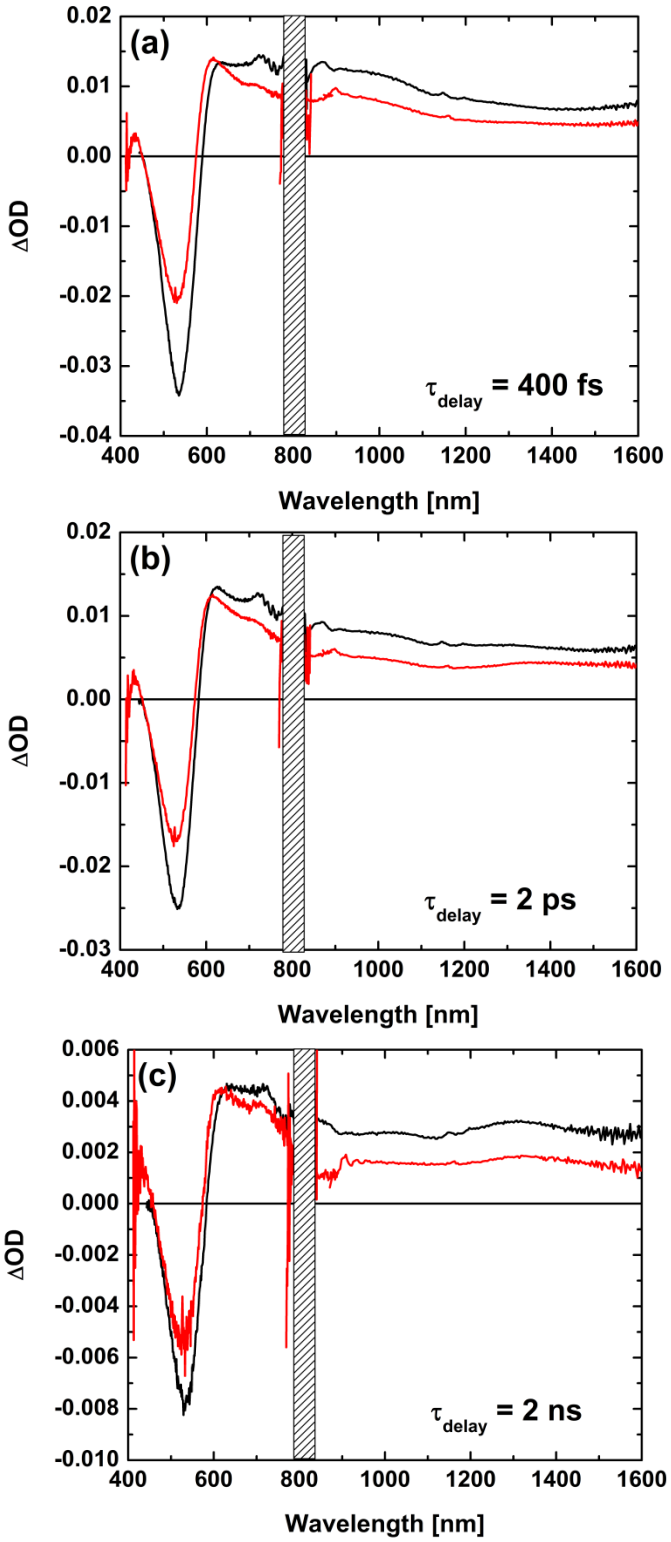

Figure 5.9. Comparison of transient absorption spectra of P(DTP-BPhBTD) in toluene (black) and DCM (red) at different time delays. (λ_{ex} = 585 nm, E_{ex} = 440 nJ in toluene and 400 nJ in dichloromethane)

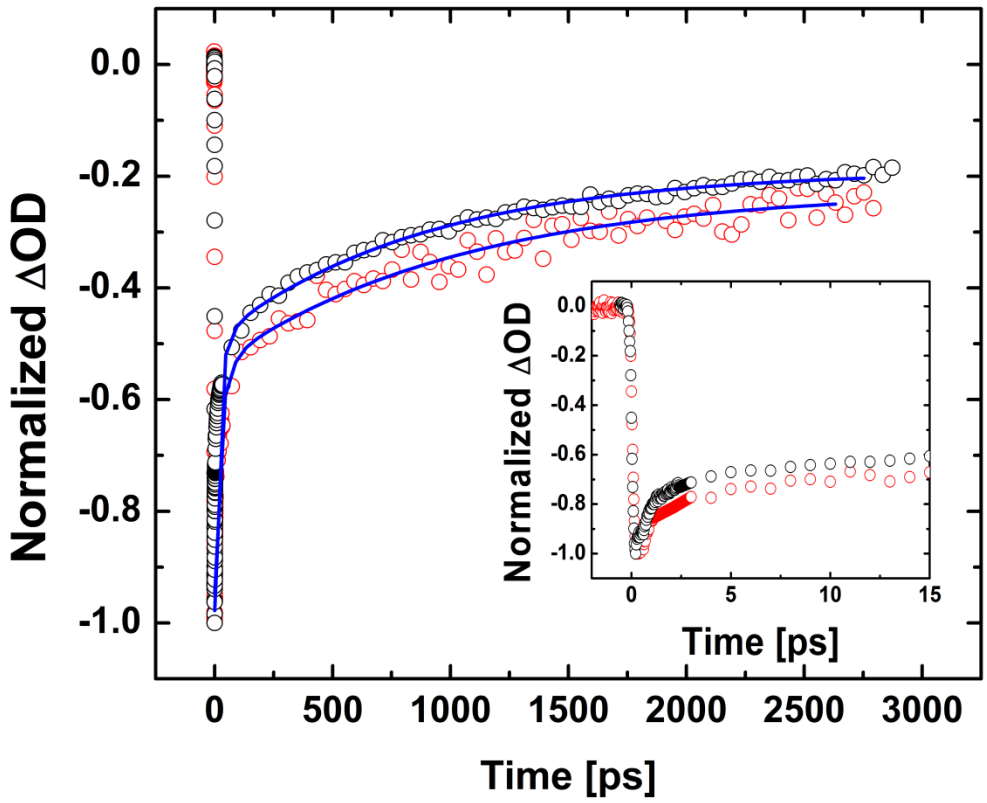

Figure 5.10. Solvent-dependent ground state recovery of P(DTP-BPhBTD) in toluene (black) and DCM (red). (λ_{ex} = 585 nm, E_{ex} = 440 nJ in toluene and 400 nJ in dichloromethane)

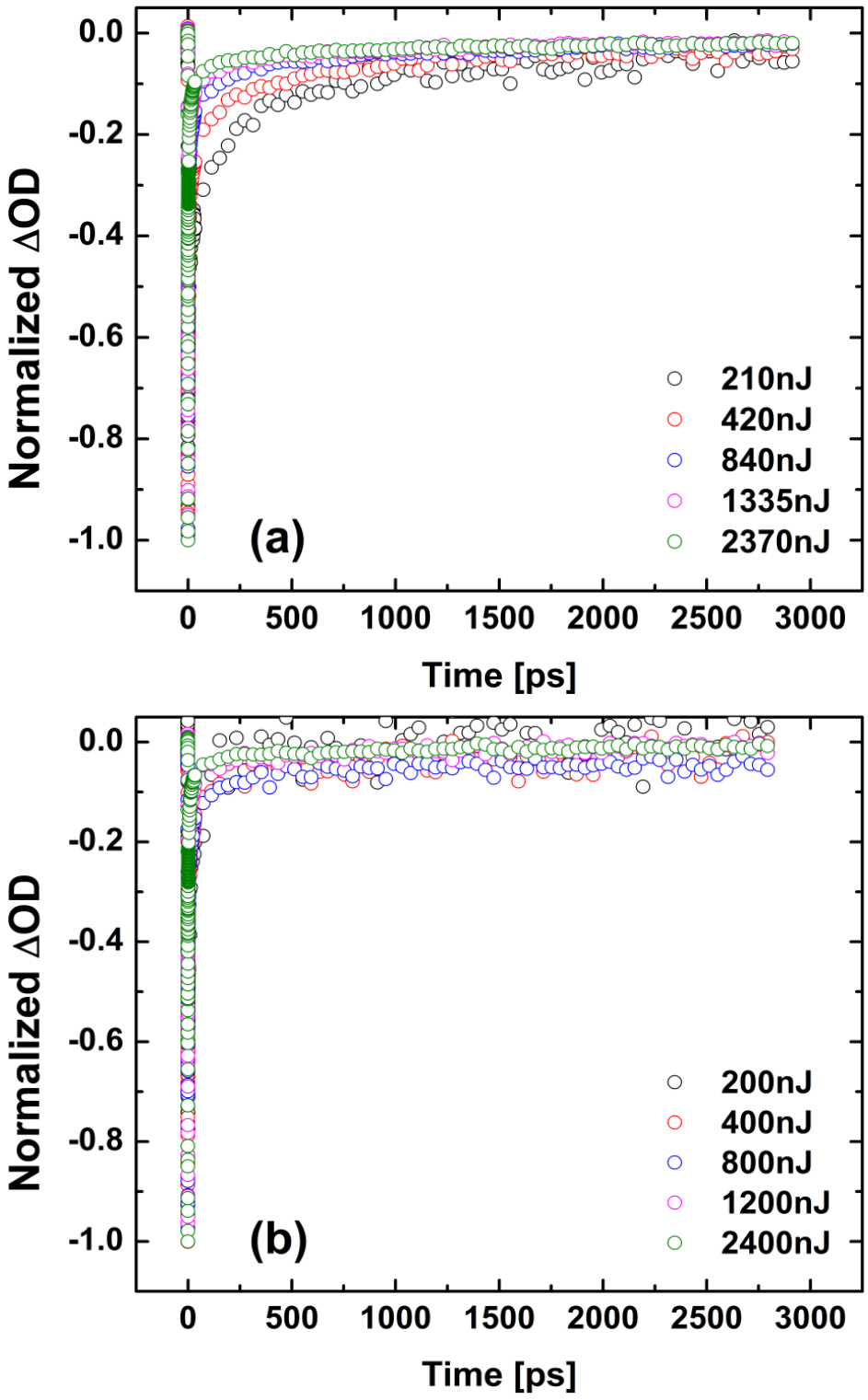

Figure 5.11. Intensity-dependent decay kinetics of P(DTP-BThBTD) in (a) toluene and (b) DCM.

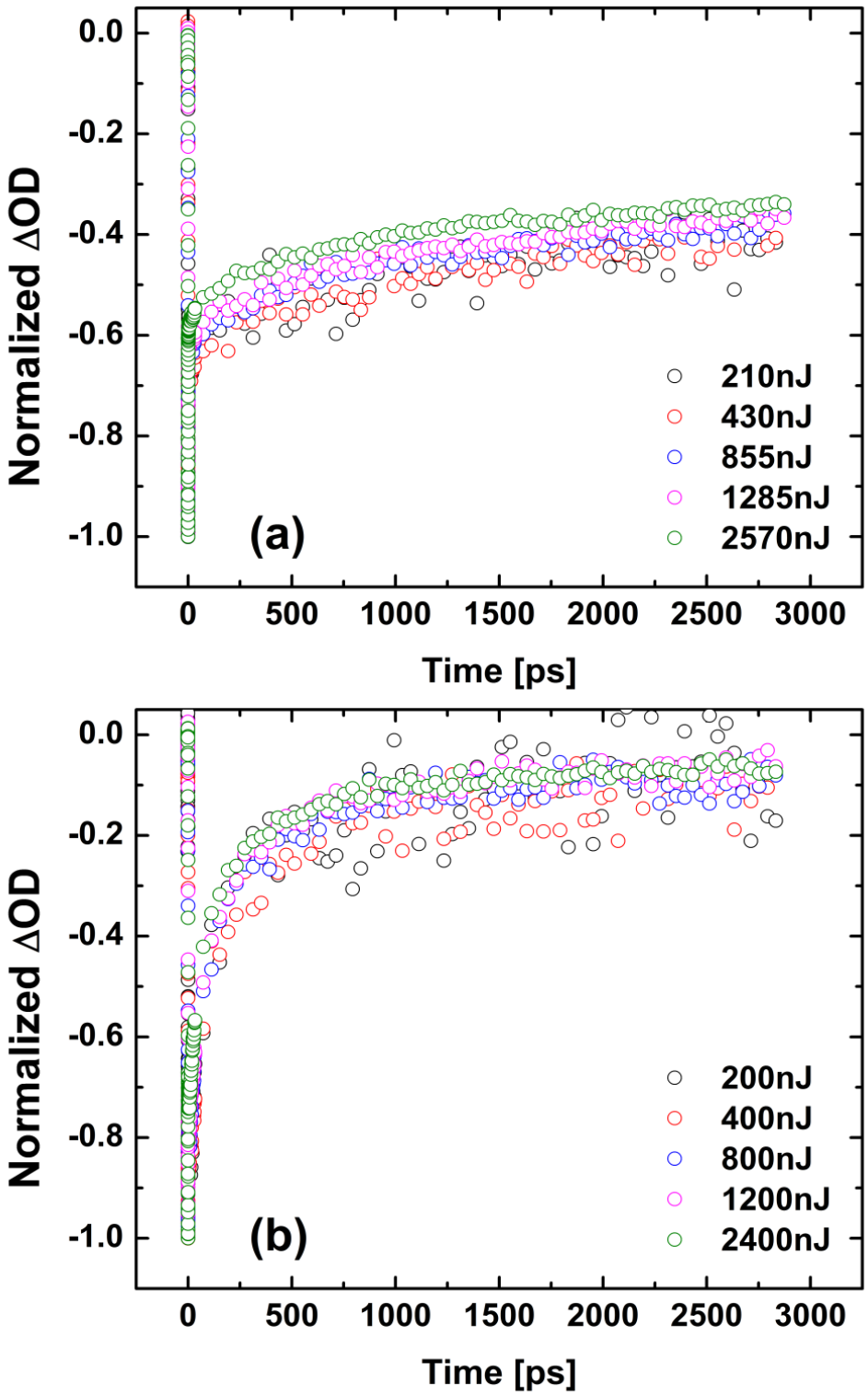

Figure 5.12. Intensity-dependent decay kinetics of P(DTP-BHxThBTD) in (a) toluene and (b) DCM.

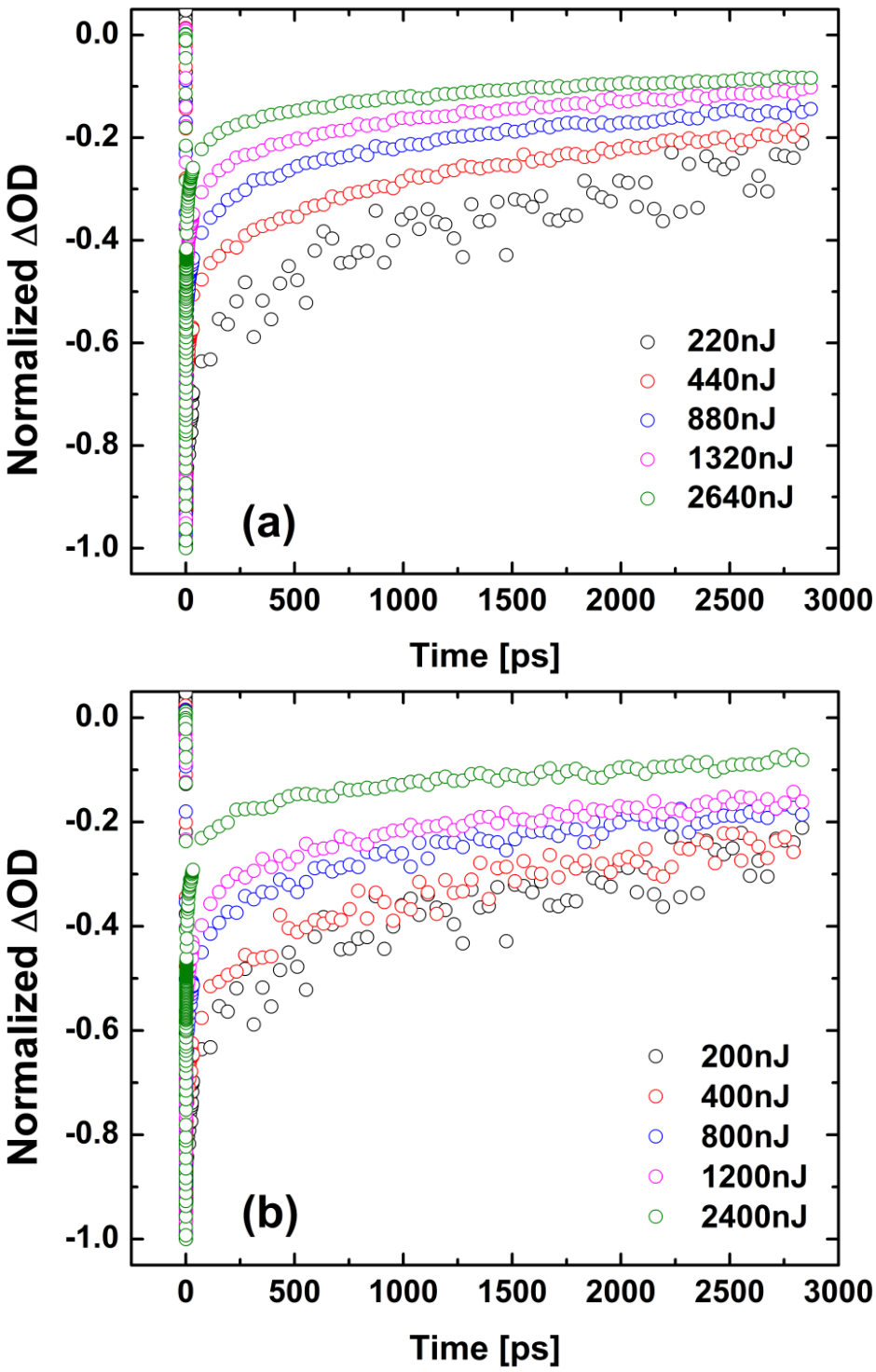

Figure 5.13. Intensity-dependent decay kinetics of P(DTP-BPhBTD) in (a) toluene and (b) DCM.

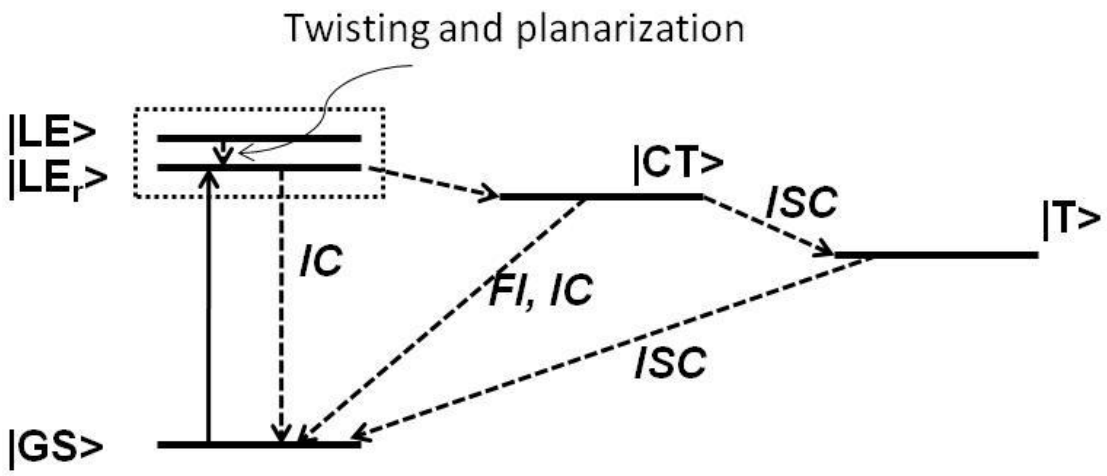

Scheme 5.2. Proposed photophysical mechanism of DTP-based conjugated polymers. (G: ground state; LE: local excited state; LE_r: relaxed local excited state; CT: charge transfer state; T: triplet state; IC: internal conversion; Fl: fluorescence; ISC: intersystem crossing)

5.3.2.4 Proposed Photophysical Mechanism of DTP-based Conjugated Polymers

Based on the transient absorption measurements in different solvents and the observation of ground state recovery kinetics, a potential mechanism for the observed photophysical properties may be proposed (**Scheme 5.2**), though more experimental and theoretical evidence should be obtained to test this hypothesis. The two fast components showed lifetimes on the scales of torsional relaxation, charge transfer and internal conversion. The polymer with the HxTh linker likely exists in the ground state in a twisted conformation of the conjugated polymer backbone structure. The excited state may undergo a planarization (with a moderate degree of charge transfer) or a fully charge separated twisted geometry. The twisted conformation can relax back to the ground state through internal conversion from the minimum of the excited state potential surface to the peak of the ground state potential barrier, with the relaxation occuring within

picoseconds as observed for species 1 and 2. To reach the planarized geometry from the initially excited state may also require some torsional motion especially for P(DTP-BHxThBTD), and this is also expected to have a small or no barrier and be very fast. Upon formation of the relatively long lived CT state, intersystem crossing can occur to the lowest triplet state, with a yield of 5-36%, and decay to the ground state by fluorescence and internal conversion, with a decay time of 150 to 960 ps, depending on the polymer and solvent. The triplet lifetimes are consistent with nonradiative decay via intersystem crossing to the ground state. More detailed transient experiments will be required to obtain solid evidence to resolve the mechanism. Ultrafast time-resolved stimulated Raman spectroscopy might help to clarify the proposed torsional motion about the conjugated backbone. An alternative way to reveal the torsional movement is to perform transient absorption measurements at low temperature or in high viscosity solutions, so the torsional movement of the polymers is slowed down or even frozen. Additionally, performing time-correlated single photon counting (TCSPC) can also help to identify the path and time scale of radiative decay and the assignment of the corresponding transient species.

5.3.3 Nonlinear Absorption

Open-aperature Z-scan measurements on P(DTP-BThBTD), P(DTP-BHxThBTD), and P(DTP-BPhBTD) in toluene were carried out at excitation wavelengths of 1150, 1300, and 1550 nm. As shown in **Figure 5.14**, intensity-dependent, effective two-photon absorption cross sections were observed in all three polymer solutions at each wavelength. Such intensity dependence indicated the existence

of excited state absorptions or higher order nonlinear processes. Based on the assumption that the possible mechanism is a two-photon absorption followed by excited state absorption, a the Z-scan data was simulated (see reference [1]) to obtain a better extraction of two-photon absorption cross sections. Experimentally-determined beam profile and pulse shape parameters were used in the simulations, as were sample-specific parameters (e.g. cuvette pathlength, concentration, linear transmittance, etc.). The excited state absorption cross sections were extracted from femtosecond transient measurements as listed in Table 5.1. Only the measurements performed at the lowest three excitation energies were selected for numerical fitting, in order to minimize the interference of saturable absorption at higher irradiance. The excited state absorption cross sections were allowed to vary within ± 20%, which accounts for instrumental error, and the two-photon absorption cross section that best-fit all three energies was extracted and listed in Table 5.1. These two-photon cross sections should be viewed as upper limits, as described below. As shown in Table 5.1, P(DTP-BThBTD) showed the largest effective two-photon absorption among the three polymers. The magnitude of δ of P(DTP-BThBTD) is about one order magnitude larger than those of P(DTP-BHxThBTD) and P(DTP-BPhBTD). However, as shown in **Figure 5.15**, it should be noted that the numerical simulation of nonlinear absorption based on two-photon absorption with subsequent excited state absorption does not fit the narrow open-aperture curve well. The very narrow open-aperture curve suggests that higher order nonlinear processes may be playing a significant role and the listed two-photon absorption cross sections might be overestimated.

5.3.4 Optical Limiting

Nanosecond-pulsed optical limiting measurements were utilized to test the performance of these DTP-based polymers at 1064 nm. Two sample geometries were used in the test. First, the bulk optical limiting was performed on polymer solutions with a concentration of 2.4 mM in a 1 mm glass cuvette. (**Figure 5.17**) Second, microcapillary based optical limiting was performed on polymer solutions infiltrated into a microcapillary with an inner diameter of 20 μm and pathlength of 18 mm. (**Figure 5.18**) The concentrations of polymer solutions used in microcapillary measurements were adjusted to ensure a minimum transmittance of 70%. As shown in Figure 5.16, the formation of aggregates in P(DTP-BThBTD) and P(DTP-BHxThBTD) was observed. The concentrated P(DTP-BThBTD) showed a broad tail absorption extending into near infrared region and the concentrated P(DTP-BHxThBTD) showed a broad absorption with peak at 1000 nm. Thus, for both P(DTP-BThBTD) and P(DTP-BHxThBTD), dilution is required for microcapillary optical limiting measurements. On the other hand, P(DTP-BPhBTD) showed negligible formation of aggregates. The results of both bulk and microcapillary optical limiting are listed in **Table 5.3**. The performance of optical limiting is strongly dependent on the interaction pathlength as well as the concentration of nonlinear materials. Thus, the dilution of polymer solutions to prevent aggregation might not be preferable, since such dilution could reduce suppression even though the pathlength is increased.

As indicated in Table 5.3, P(DTP-BThBTD) showed the largest suppression and highest FOM in both bulk and microcapillary measurements over the other two polymers. This might be due to the significantly larger estimated two-photon absorption cross

section, as indicated in Table 5.1. Comparing the optical limiting results in both bulk and microcapillary measurements reveals that both P(DTP-BThBTD) (0.5mM) and P(DTP-BPhBTD) (2.4mM) showed significant enhancement of energy suppression in microcapillary measurements, due to the increased interaction pathlength. As indicated by Figure 5.16, the enhanced suppression of P(DTP-BThBTD) in microcapillary geometry might result from the contribution of one-photon absorption, while P(DTP-BPhBTD) result from the high concentration. On the other hand, P(DTP-BHxThBTD) showed a limited increase in energy suppression in the microcapillary geometry compared to the bulk measurements. As mentioned previously, the dilution of nonlinear material could result in a reduction of energy suppression. Thus, even though the interaction pathlength is 18X longer in the microcapillary, the nearly 7X of dilution led to a loss of energy suppression. Furthermore, it must be noted that the microcapillary optical limiting of a diluted P(DTP-BPhBTD) (0.36mM) was also performed in order to have a closer comparison of its performance with the other diluted polymer solutions. However, as indicated by Table 5.3 and **Figure 5.19**, even though the concentration of P(DTP-BPhBTD) was increased nearly 7 fold, the resulting suppression, only increased by less than 2 times.

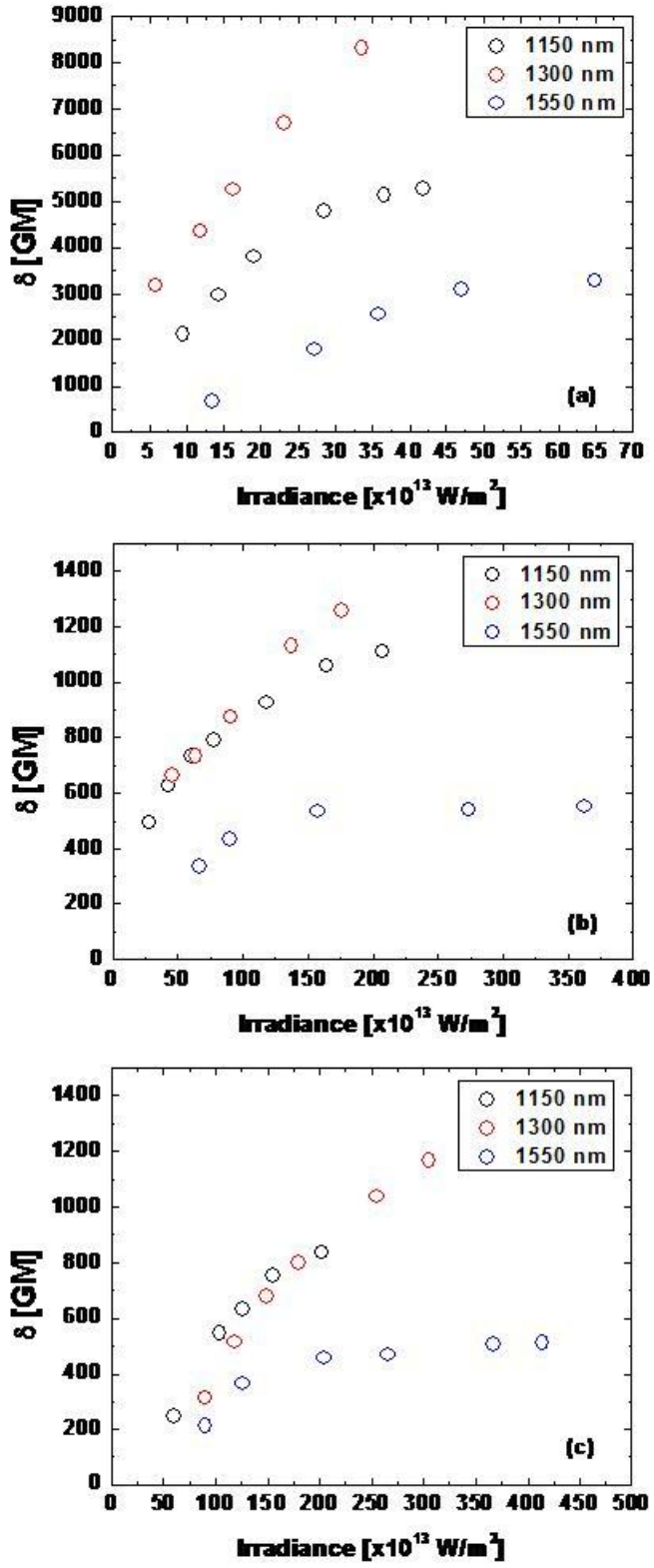

Figure 5.14. Intensity-dependent effective two-photon absorption cross sections of (a) P(DTP-BThBTD), (b) P(DTP-BHxThBTD), and (c) P(DTP-BPhBTD).

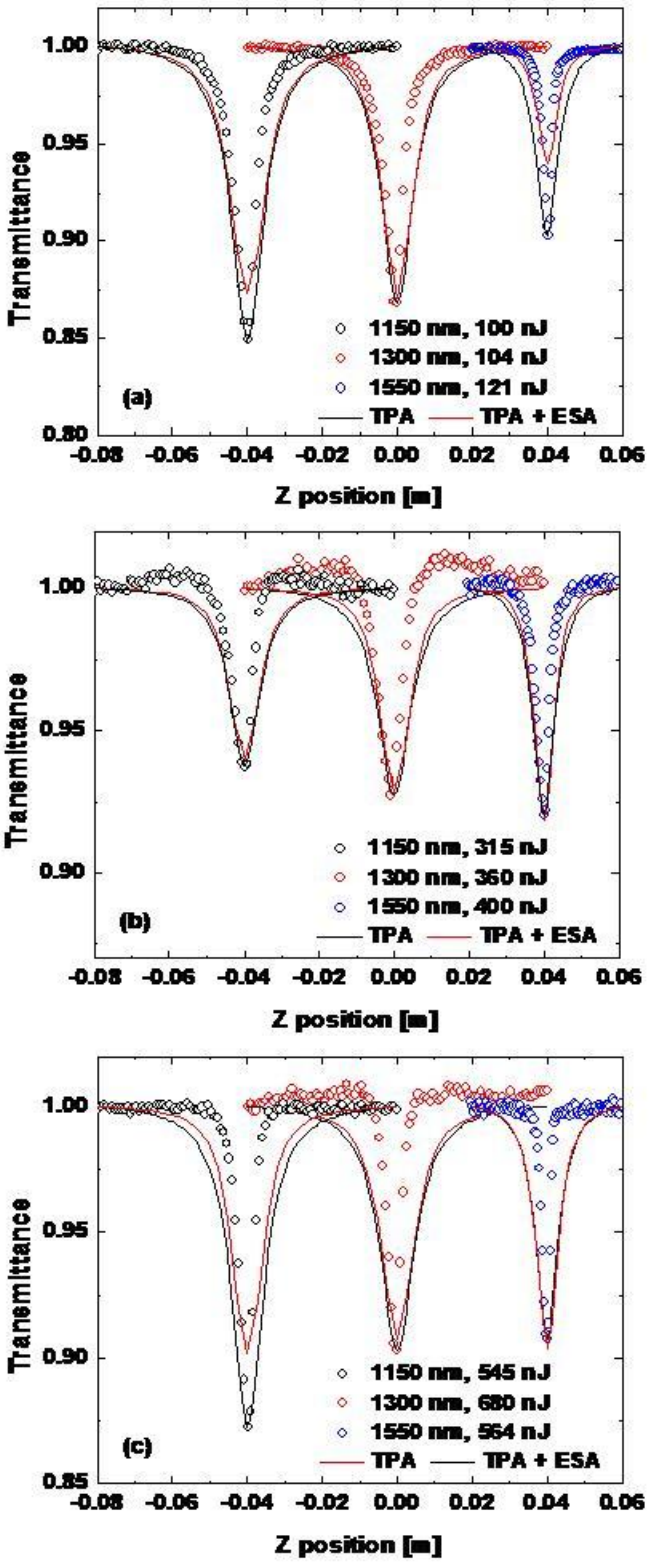

Figure 5.15. Open-aperature Z-scan measurements of (a) P(DTP-BThBTD), (b) P(DTP-BHxThBTD), and (c) P(DTP-BPhBTD) and numerical fitting with two-photon absorption (black line) and two-photon followed by excited state absorptions (red line).

Table 5.3. Nanosecond-pulsed energy suppression of DTP-based polymers at 1064 nm.

Geometry	Polymer	Concentration	T_0	Suppression	FOM
Bulk	P(DTP-BThBTD)	2.4 mM	0.96	7.8X	5.6
	P(DTP-BHxThBTD)	2.4 mM	0.95	2.3X	1.6
	P(DTP-BPhBTD)	2.4 mM	0.97	1.2X	1.3
Microcapillary	P(DTP-BThBTD)	0.5 mM	0.7	17X	35
	P(DTP-BHxThBTD)	0.36 mM	0.73	3.5X	1.7
	P(DTP-BPhBTD)	0.36 mM	0.99	2.7X	1.8
		2.4 mM	0.93	4.8X	2.7

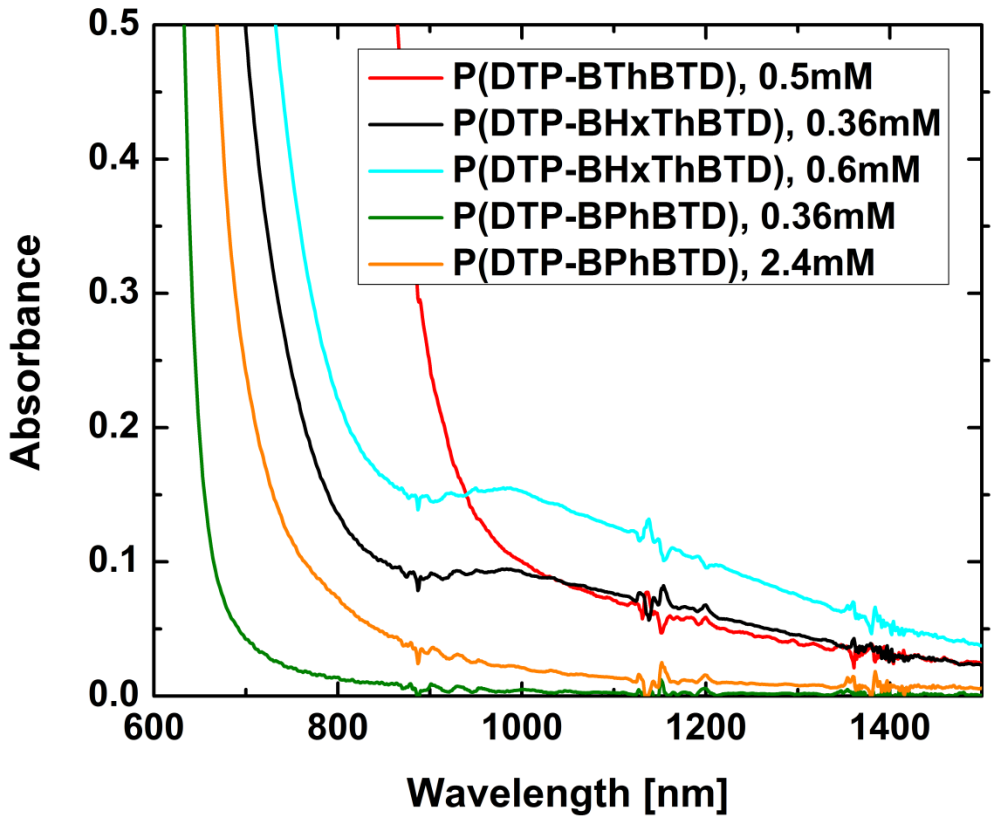

Figure 5.16. Absorption spectra of concentrated DTP-based polymer solutions. (Solvent: Toluene. Optical pathlength: 1 cm)

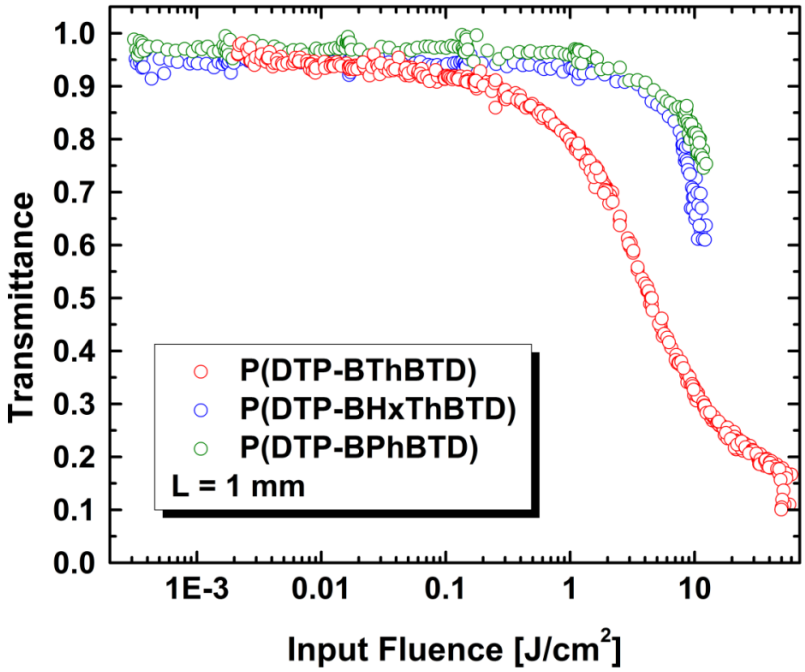

Figure 5.17. Nanosecond-pulsed optical limiting of DTP-based polymers (2.4mM in toluene) in a 1-mm cuvette at 1064 nm. ($\tau_p \sim 4$ns, ω_0 (HW1/e^2) ~ 20μm)

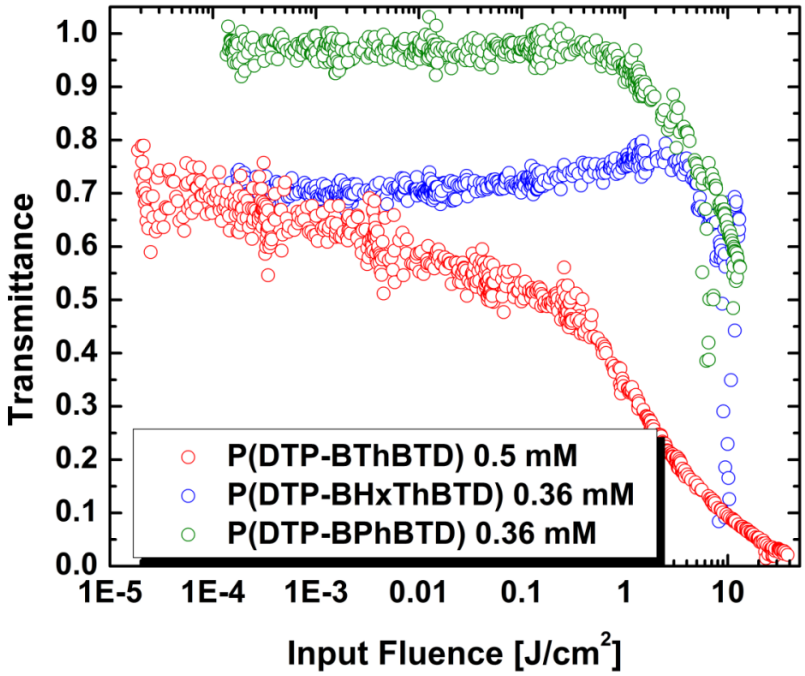

Figure 5.18. Nanosecond-pulsed ($\tau_p \sim 4$ns) optical limiting of DTP-based polymers (in toluene) in an 18-mm MCA (inner diameter of 20 μm) at 1064 nm.

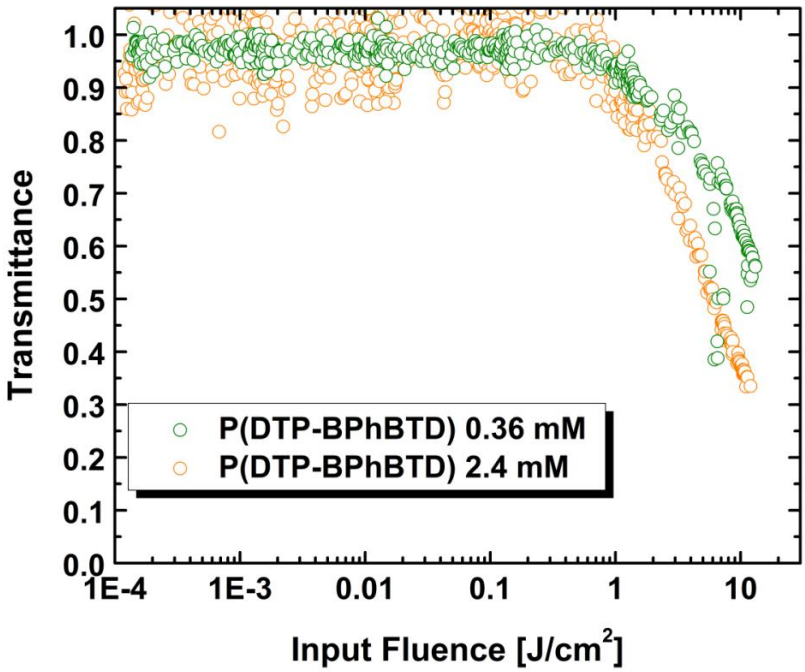

Figure 5.19. Nanosecond-pulsed (τ_p ~ 4ns) optical limiting of P(DTP-BPhBTD) in toluene in an 18-mm MCA (inner diameter of 20 μm) at 1064 nm.

5.4 Future Work

As mentioned previously, further experiments are needed test the proposed photophysical mechanism for the DTP based polymers. Ultrafast stimulated Raman spectroscopy and transient absorption measurements at low temperature or in viscous solution will help to resolve the proposed torsional movement. Theoretical quantum chemistry calculations of the excited state potential energy surface and transient state geometry will also help to clarify aspects of the mechanism. TCSPC will assist in identifying the transient species responsible for radiative decay. Furthermore, nanosecond-pulsed two-photon excitation fluorescence spectroscopy will offer a better

picture of two-photon absorption spectra and cross section of these DTP-based polymers, and thus will help to resolve the results obtained from femtosecond Z-scan, and to identify whether a higher nonlinear process exists in these polymer systems.

Another interesting question remaining in this DTP-based donor-acceptor conjugated polymer system is the effective range of charge delocalization. As indicated by **Scheme 5.3**, the charge separation within a repeat unit will further influence the charge separation in the neighbor units. In particular, it is very important to ascertain whether the effective chromophoric unit in the polymer is of the D-π-A type or of D-π-A-π-D or A-π-D-π-A type. This is fundmentally important because the effective electronic symmetry would be very different between the two types of chromophore classes. Longer charge delocalization range would also have a significant effect on optical and photophysical properties. With different conjugated bridges, the level of mixing between repeat units could be different. Such a different level of mixing may also be an important factor to the various photophysical and nonlinear optical properties observed in these DTP-based polymers. To study the charge delocalization range in these polymers, monomers, dimers and oligomers with various conjugation lengths should be prepared. Experimental variables such as solvent polarity should be studied. Solvent effects (polarity dependence) on the photophysical and nonlinear optical properties should be more pronounced in monomer, dimer or shorter oligomers and the result may give more evidences on the torsional fluctuation proposed in the photophysical mechanism (Scheme 5.2).

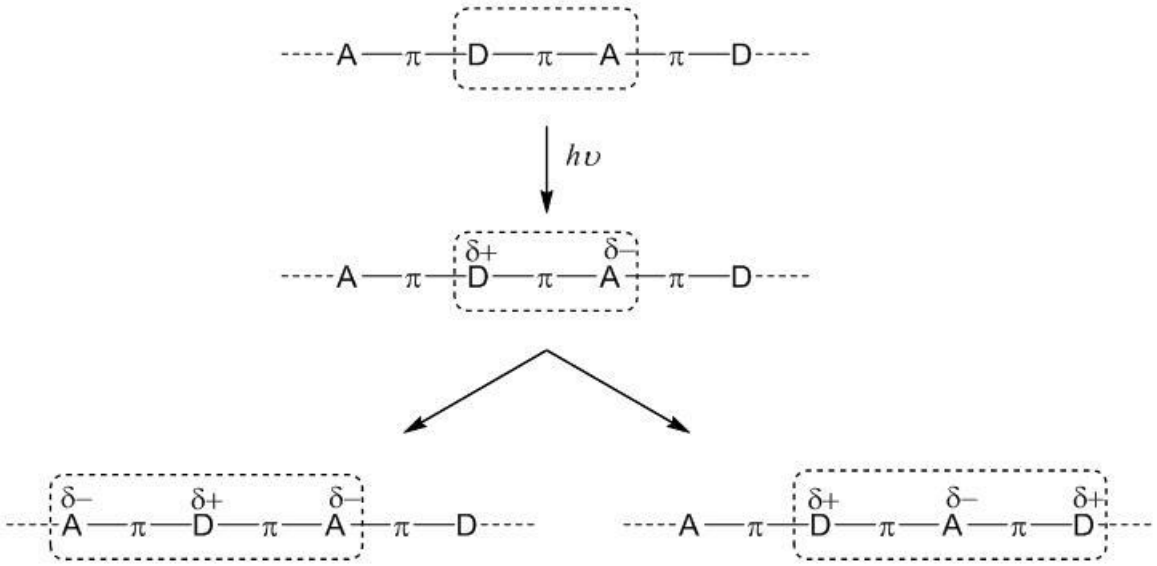

Scheme 5.3. Charge delocalization in donor-acceptor conjugated polymers.

5.5 Conclusion

In this chapter, it has been shown that the substitution of steric hindered or aromatic stabilized p-bridge strongly affects the observed photophysical and nonlinear optical properties. For linear and transient absorption spectroscopy, we show that polymers that are twisted (steric hindered) in the ground state and polymers that are aromatic stabilized have (1) reduced donor-acceptor coupling strength and give blue-shifted linear and excited state absorptions but (2) increased yield of long-lived transient components. From transient kinetic studies, we also show that polymers with large backbone fluctuation have stronger solvent-dependent excited state dynamics but insignificant intensity-dependent decay kinetics. This suggests such backbone fluctuation could reduce the possibility of exciton-exciton annihilation. On the other hand, with

increased aromatic stabilization, the solvent-dependency becomes insignificant while the excition-excition annihilation is promoted due to the increased planarity of conjugated backbones. Further studies on (1) identifying radiative decay process, including fluorescence quantum yields and emission lifetime, (2) mapping two-photon absorption spectra, (3) investigating the influence of backbone fluctuation within viscous medium or under low temperature, (4) theoretical modeling the preferable backbone geometries of all three polymers, (5) numerical simulating the nonlinear absorption mechanisms responsible for optical limiting performance, and (6) photophysical properties of oligomers with various conjugation length are needed and will assist the understanding and revealing of photophysical dynamics of such D-A conjugated copolymers. These results stated in this chapter clearly indicate the interplay of donor-acceptor coupling strength, aromatic stabilization, and torsional conformation are crucial factors in the design of conjugated polymers with strong and well-overlapped nonlinear and excited state absorptions to achieve improved optical limiting performance in selected wavelength ranges.

5.6 Experimental Details

5.6.1 Sample Preparation

The following olymers were received from John Reynolds' research group in the Department of Chemistry at the University of Florida and Seth Marder's research group in the School of Chemistry and Biochemistry at the Georgia Institute of Technology.

(1) P(DTP-BThBTD): Poly(2-(5-(7-(thiophen-2-yl)benzo[c][1,2,5]thiadiazol-4-yl)thiophen-2-yl)-4-(3,4,5-tris(dodecyloxy)phenyl)-4H-dithieno[3,2-b:2',3'-d]pyrrole)

(2) P(DTP-BHxThBTD): Poly(2-(4-hexyl-5-(7-(3-hexylthiophen-2-yl)benzo[c][1,2,5]thiadiazol-4-yl)thiophen-2-yl)-4-(3,4,5-tris(dodecyloxy)phenyl)-4H-dithieno[3,2-b:2',3'-d]pyrrole)

(3) P(DTP-BPhBTD): Poly(2-(4-(7-phenylbenzo[c][1,2,5]thiadiazol-4-yl)phenyl)-4-(3,4,5-tris(dodecyloxy)phenyl)-4H-dithieno[3,2-b:2',3'-d]pyrrole)

Polymers were used as received. Polymer solutions with designated concentrations were prepared with spectral grade toluene or dichloromethane.

5.6.2 Linear and Nonlinear Spectroscopic Measurements

Linear transmission and absorption properties of composite films were determined by Vis-NIR linear absorption spectroscopy using a Shimadzu UV3100 UV-Vis-NIR spectrometer. The two-photon absorption cross sections (δ) were determined at 1150 nm, 1300 nm and 1550 nm using a femtosecond-pulsed (~ 65 fs HW1/e) excitation with the open-aperture Z-scan technique detailed in chapter 2 and elsewhere [1]. The instrumental accuracy associated with these measurements is estimated to be ±15%. The

polymer solutions for Z-scan measurements were prepared at 1.6 mM (per repeat unit) in spectral grade toluene. The optical path length of the quartz cuvette for Z-scan measurements was 1 mm.

5.6.3 Transient Spectroscopic Measurements

Transient measurements were carried out with both femtosecond and nanosecond pulses. Detailed experimental setup was described in chapter 2. The excitation wavelength was chosen at 780 nm for P(DTP-BThBTD), 610 nm for P(DTP-BHxThBTD), and 585 nm for P(DTP-BPhBTD). For femtosecond measurements, the optical path length of the quartz cuvette was 2 mm. The polymer solutions were prepared with spectral grade toluene or dichloromethane, and the concentrations of solutions were chosen to give a linear transmittance between 60-70% at the excitation wavelengths. The excitation energy ranged from 200 to 2400 nJ. The pump beam waists ($HW1/e^2$) were ~480 μm for excitations at 585 and 610 nm and ~509 μm for excitation at 780 nm. The probe beam waist ($HW1/e^2$) was 170 μm. For nanosecond measurements, the optical path length of the quartz cuvette was 1 cm, and the polymer solutions in toluene or dichloromethane were prepared in order to have a linear transmittance ~ 80% at the excitation wavelengths. The excitation energy was around 700 μJ. For de-oxygenated samples, the solutions were bubbled with nitrogen for 20 minutes.

5.6.4 Optical Limiting

Optical limiting measurements were carried out with nanosecond pulses (~ 4 ns HW1/e) at 1064 nm. For bulk optical limiting, polymer solutions with concentration of 2.4 mM (per repeat unit) in spectral grade toluene and 1-mm path length glass cuvette were used. The beam waist was ~ 20μm ($HW1/e^2$), and the foci were placed in the middle of cuvette's pathlength. The excitation energy ranged from 5 nJ to 200 μJ. For optical limiting in an 18 mm microcapillary waveguide, polymer solutions were prepared in spectral grade toluene. The concentrations for solutions were chosen so that the linear transmittance was > 70% over the 18 mm optical path length.

REFERENCES

[1] Hales, J. M., Cozzuol, M., Screen, T. E. O., Anderson, H. L. and Perry, J. W., "Metalloporphyrin polymer with temporally agile, broadband nonlinear absorption for optical pulse suppression in the near infrared," *Optics Express* **17**, 18478-18488 (2009).

[2] Cha, M., Saricftci, N. S., Heeger, A. J., Hummelen, J. C. and Wudl, F., "Enhanced nonlinear absorption and optical limiting in semiconducting polymer/methanofullerene charge transfer films," *Applied Physics Letter* **67**, 3850-3852 (1995).

[3] Tutt, L. W. and Kost, A., "Optical limiting performance of C_{60} and C_{70} solutions," *Nature* **356**, 225-226 (1992).

[4] Perry, J. W., Mansour, K., Lee, I. Y. S., Wu, X. L., Bedworth, P. V., Chen, C. T., Ng, D., Marder, S. R., Miles, P., Wada, T., Tian, M. and Sasabe, H., "Organic optical limiter with a strong nonlinear absorptive response," *Science* **273**, 1533-1536 (1996).

[5] Ehrlich, J. E., Wu, X. L., Lee, I. Y. S., Hu, Z. Y., Rockel, H., Marder, S. R. and Perry, J. W., "Two-photon absorption and broadband optical limiting with bis-donor stilbenes," *Optics Letters* **22**, 1843-1845 (1997).

[6] Perry, J. W., Mansour, K., Marder, S. R., Perry, K. J., Alvarez, D. and Choong, I., "Enhanced reverse saturable absorption and optical limiting in heavy-atom-substituted phthalocyanines," *Optics Letters* **19**, 625-627 (1994).

[7] Chi, S. H., Hales, J. M., Matteo, C., Ochoa, C., Fitzpatrick, M. and Perry, J. W., "Conjugated polymer-fullerene blend with strong optical limiting in the near-infrared," *Optics Express* **accepted** (2009).

[8] Dupuis, B., Michaut, C., Jouanin, I., Delaire, J., Robin, P., Feneyrou, P. and Dentan, V., "Photoinduced intramolecular charge-transfer systems based on porphyrin-viologen dyads for optical limiting," *Chemical Physics Letters* **300**, 169-176 (1999).

[9] Steckler, T. T., Zhang, X., Hwang, J., Honeyager, R., Ohira, S., Zhang, X. H., Grant, A., Ellinger, S., Odom, S. A., Sweat, D., Tanner, D. B., Rinzler, A. G., Barlow, S., Bredas, J. L., Kippelen, B., Marder, S. R. and Reynolds, J. R., "A spray-processable, low bandgap, and ambipolar donor-acceptor conjugated polymer," *Journal of the American Chemical Society* **131**, 2824-2826 (2009).

[10] Zhang, M., Tsao, H. N., Pisula, W., Yang, C. D., Mishra, A. K. and Mullen, K., "Field-effect transistors based on a benzothiadiazole-cyclopentadithiophene copolymer," *Journal of the American Chemical Society* **129**, 3472-+ (2007).

[11] Marder, S. R., Beratan, D. N. and Cheng, L.-T., "Approaches for optimizing the first electronic hyperpolarizability of conjugated organic molecules," *Science* **252**, 103-106 (1991).

[12] Marder, S. R., Perry, J. W., Bourhill, G., Gorman, C. B., Tiemann, B. G. and Mansour, K., "Relation between bond-length alternation and 2nd electronic hyperpolarizability of conjugated organic-molecules," *Science* **261**, 186-189 (1993).

[13] Marder, S. R., Gorman, C. B., Meyers, F., Perry, J. W., Bourhill, G., Bredas, J. L. and Pierce, B. M., "A unified description of linear and nonlinear polarization in organic polymethine dyes," *Science* **265**, 632-635 (1994).

[14] Bourhill, G., Bredas, J. L., Cheng, L.-T., Marder, S. R., Meyers, F., Perry, J. W. and Tiemann, B. G., "Experimental demonstration of the dependence of the first hyperpolarizability of donor-acceptor-substituted polyenes on the ground state polarization and bond length alternation," *Journal of the American Chemistry Society* **116**, 2619-2620 (1994).

[15] Marder, S. R., Cheng, L.-T., Tiemann, B. G., Friedli, A. C., Blanchard-Desce, M., Perry, J. W. and Skindhoj, J., "Large first hyperpolarizabilities in push-pull polyenes by tuning of the bond length alternation and aromaticity," *Science* **263**, 511-514 (1994).

[16] Rumi, M., Ehrlich, J. E., Heikal, A. A., Perry, J. W., Barlow, S., Hu, Z. Y., McCord-Maughon, D., Parker, T. C., Rockel, H., Thayumanavan, S., Marder, S. R., Beljonne, D. and Bredas, J. L., "Structure-property relationships for two-photon absorbing chromophores: Bis-donor diphenylpolyene and

bis(styryl)benzene derivatives," *Journal of the American Chemical Society* **122**, 9500-9510 (2000).

[17] Pond, S. J. K., Rumi, M., Levin, M. D., Parker, T. C., Beljonne, D., Day, M. W., Bredas, J. L., Marder, S. R. and Perry, J. W., "One- and two-photon spectroscopy of donor-acceptor-donor distyrylbenzene derivatives: Effect of cyano substitution and distortion from planarity," *Journal of Physical Chemistry A* **106**, 11470-11480 (2002).

[18] Rumi, M., Pond, S. J. K., Meyer-Friedrichsen, T., Zhang, Q., Bishop, M., Zhang, Y., Barlow, S., Marder, S. R. and Perry, J. W., "Tetrastyrylarene derivatives: Comparison of one- and two-photon spectroscopic properties with distyrylarene analogues," *Journal of Physical Chemistry C* **112**, 8061-8071 (2008).

[19] Yamamoto, T., Zhou, Z.-H., Kanbara, T., Shimura, M., Kizu, K., Maruyama, T., Nakamura, Y., Fukuda, T., Lee, B.-L., Ooba, N., Tomaru, S., Kurihara, T., Kaino, T., Kubota, K. and Sasaki, S., "π-conjugated donor-acceptor copolymers constituted of π-excessive and π-deficient arylene units. Optical and electrochemical properties in relation to ct structure of the polymer," *Journal of the American Chemistry Society* **118**, 10389-10399 (1996).

[20] Zhao, M. T., Singh, B. P. and Prasad, P. N., "A systematic study of polarizability and microscopic 3rd-order optical nonlinearity in thiophene oligomers," *Journal of Chemical Physics* **89**, 5535-5541 (1988).

[21] Zhao, M. T., Samoc, M., Singh, B. P. and Prasad, P. N., "Study of 3rd-order microscopic optical nonlinearities in sequentially built and systematically derivatized structures," *Journal of Physical Chemistry* **93**, 7916-7920 (1989).

[22] Turro, N. J., *Modern molecular photochemistry* (University Science Books, Sausalito, CA, 1991).

[23] Saltiel, J., Waller, A. S. and Sears, D. F., "The temperature and medium dependencies of cis-stilbene fluorescence. The energetics of twisting in the lowest excited singlet state," *Journal of the American Chemical Society* **115**, 2453-2465 (1993).

CHAPTER 6

CONCLUSION

This dissertation presented the investigation of a set of conjugated polymers to understand their processing, photophysical and nonlinear optical responses as well as to show their potential for photonic telecommunication applications.

As described in the very beginning of the introduction, for photonic applications, conjugated polymers possess the advantage of processabilty over their counterpart semiconductors. In chapter 3 and 4, the processing methodology of polyacetylene-based $\chi^{(3)}$ materials and poly(phenylene vinylene)-based fullerene blends has been developed. As shown in chapter 3, the controlled ring-opening metathesis polymerization of polyacetylene-based $\chi^{(3)}$ materials allowed the fabrication of thick, large-area, optical-quality films and the integration into micro-structured photonic crystals. For multi-component system, chapter 4 showed the introduction of plasticizer could improve the miscibility between components and the processability of blends allowing the formation of thick, optical quality blend of poly(phenylene vinylene) and fullerene.

Despite the advantages in processability, conjugated polymers also allow relatively easy engineering of their nonlinear optical responses. In chapter 4, the nonlinear optical responses of poly(phenylene vinylene) was engineered via photo-induced electron transfer. The resulting poly(phenylene vinylene)-fullerene blend showed strong nonlinear absorption and exceeding optical limiting performance over a broad temporal regime in the near IR. In chatper 5, the photophysical and nonlinear optical properties of dithienopyrrole-based donor-acceptor conjugated polymer was

manipulated through the alternation of donor-acceptor strength via molecular engineering. Such structure-property relationship suggests, by molecular engineering, conjugated polymers can be designed to fit the needs of specific photonic applications.

Certainly, there are many interesting topics and questions left out in this dissertation work. In chapter 3, the demonstration of *in situ* polymerization of polyacetylene-based $\chi^{(3)}$ materials showed the potential of these materials for photonic device integration. However, a further study of the nonlinear optical properties of this polyacetylene-integrated photonic crystal was not performed due to the difficulties in the fabrication of defect-free synthetic opal and the availability of proper characterizing equipments. Recently, a femtosecond transient reflection spectrometer has been setup, which might allow some level of investigation of these polyacetylene-integrated photonic crystals.

In chapter 5, as described in section 5.5, the photophysical mechanism of these dithienpyrrole-based donor-acceptor conjugated polymers has not fully resolved. More detailed experimental studies and collaboration with theoretical calculations will proved further evidences to resolve the photophysical mechanism. Also, the structure-property relationship of these donor-acceptor conjugated polymers was not well established yet. Further controlled studies on these donor-acceptor conjugated systems with different conjugation lengths would assist a more comprehensive understanding on the structure-property relationship and prove feedback and guidance for future development of higher performance dithienopyrrole-based donor-acceptor conjugated polymers.

COPYRIGHT INFORMATION

Part of this dissertation work has been published or contributed from students enrolled as REU summer intern. The permissions of using these published data are included following pages.

San-Hui Chi
School of Chemistry and Biochemistry
Georgia Institute of Technology
901 Atlantic Drive NW
Atlanta, Georgia 30318
Fax: 1-404-385-6057

Bettina Loycke
Senior Rights Manager
Wiley-VCH Verlag GmbH & Co. KGaA
Boschstr. 12
69469 Weinheim
Germany

Dear Bettina:

I am completing a doctoral dissertation at Georgia Institute of Technology entitled Ph.D. I would like your permission to reprint in my dissertation excerpts from the following:

Advanced Materials, Volume 20, Issue 17, Page 3199-3203.
The excerpts to be reproduced are Scheme 1, Figure 1, Figure 2, Table 1, Figure S1, Figure S2, Figure S3, Figure S4, and Table S1.

The requested permission extends to any future revisions and editions of my dissertation (Title: Third-Order Nonlinear Optical Properties of Conjugated Polymers and Blends), including non-exclusive world rights in all languages, and to the prospective publication of my dissertation by ProQuest Information and Learning (ProQuest) through its UMI® Dissertation Publishing business. ProQuest may produce and sell copies of my dissertation on demand and may make my dissertation available for free internet download at my request. These rights will in no way restrict republication of the material in any other form by you or by others authorized by you. Your signing of this letter will also confirm that Wiley-VCH Verlag GmbH & Co. owns the copyright to the above-described material.

If these arrangements meet with your approval, please sign this letter where indicated below and return it to me via fax or email in PDF format. Thank you very much.

Sincerely,

San-Hui Chi

We hereby grant permission for the requested use expected that due credit is given to the original source.

WILEY-VCH, STM-Copyright & Licenses

B. Loycke

Weinheim, 13.11.2009

Georgia Tech

Release, Waiver of Liability, and Covenant Not to Sue

For good and valuable consideration, the undersigned hereby grants the GEORGIA INSTITUTE OF TECHNOLOGY ("GIT") and the GEORGIA TECH RESEARCH CORPORATION ("GTRC") the absolute and irrevocable right and permission, in respect to the photographs, video tapes, motion pictures, recordings, or any other media (hereinafter collectively known as "Images") that GIT/GTRC has taken of me or my property, or minors in my care, or in which I may be included with others, to copyright the same, in GIT/GTRC's own name or otherwise, to use, re-use, publish, and re-publish the same in whole or in part, individually or in conjunction with other images, and in conjunction with any printed or electronic matter, in any and all media now or hereafter known, and for any legitimate purpose whatsoever, and to use my name in connection therewith if GIT/GTRC so chooses. I hereby waive any right to inspect or approve the Images or any finished version incorporating the same.

The undersigned does hereby release and forever discharge GIT, GTRC, and the Board of Regents of the University System of Georgia, their members individually, and their officers, agents, and employees of any kind from all claims, demands, rights, and causes of action of whatever kind or nature, arising from and by reason of any and all known and unknown, foreseen, and unforeseen injuries, damages, and the consequences thereof resulting from the use of the Images, including without limitation any and all claims for libel or invasion of privacy.

I understand that the acceptance of this release and waiver of liability by the Board of Regents of the University System of Georgia shall not constitute a waiver, in whole or in part, of sovereign immunity by said Board, its members, officers, agents, and employees.

This authorization and release shall also inure to the benefit of the heirs, legal representatives, licensees, and assigns of GIT, GTRC, and the Board of Regents of the University System of Georgia. I hereby certify that I am suffering under no legal disabilities and that I have read the above carefully before signing. This release shall be binding upon me and my heirs, legal representatives, and assigns. By signing below, I agree to the terms stated above and hereby certify that I am 18 years of age or older.

Charles C. Ochoa

Name (Print)

7691 NW 174th St Miami FL 33015 786 301 4387

Address **Phone Number**

Signature/Date

5/30/07

LICENSE TO PUBLISH

Manuscript: **MDITR Review of Undergraduate Research** ("the Journal")

Title of the contribution: _____ ("the Contribution)

Author(s): Charles C. Ochoa ("the Authors")

To: University of Washington Science and Technology Center Materials and Devices for Information Technology Research ("STC")

1. In consideration of STC agreeing to publish the Contribution, the Authors grant to STC for the full term of copyright in the Contribution and any extensions thereto, subject to clause 2 below, the license (a) to publish, reproduce, distribute, display and store the Contribution in all forms, formats and media (including without limitation in print, digital and electronic form) throughout the world; (b) to create adaptations, summaries or extracts of the Contribution or other derivative works based on the Contribution and exercise all of the rights set forth in (a) above in such adaptations, summaries, extracts and derivative works; and (c) to license others to do any or all of the above.

2. Ownership of copyright remains with the Authors and the Authors retain the following non-exclusive rights:

a) To reproduce the Contribution in whole or in part in any work of which they are the author(s);
b) To grant the right to reproduce the Contribution to any academic institution where they work; and
c) To post a copy of the Contribution on the Authors' own web site.

3. The Authors warrant and represent that:

a) The Authors are the sole authors of and sole owners of the copyright in the Contribution. If the Contribution includes materials of others, the Authors have obtained the permission of the owners of the copyright in all such materials to enable them to grant the rights contained herein. Copies of all such permissions are attached to this license.
b) The Author who has signed this Agreement has full right, power and authority to enter into this Agreement on behalf of all of the Authors.
c) Nothing in the Contribution is obscene, defamatory, libelous, violates any right of privacy or infringes any intellectual property rights (including without limitation copyright, patent or trademark) or any other rights of any person or entity or is otherwise unlawful.
d) Nothing in the Contribution infringes any duty of confidentiality which any of the Authors may owe to anyone else or violates any contract, express or implied, of any of the Authors, and all of the institutions in which work recorded in the Contribution was carried out have authorized publication of the Contribution.

This Agreement, and the rights and liabilities of the parties with respect to this Agreement and its subject matter, shall be governed by the laws of the State of Washington, without reference to the principles of conflicts of laws thereof.

Signed for and on behalf of the Authors .....

Date 5/30/07

Please print name Charles C. Ochoa

Mailing address (to send hardcopy of Publication) 7691 NW 179th st Miami FL 33015

REU 2004

Release, Waiver of Liability, and Covenant Not to Sue

For good and valuable consideration, the undersigned hereby grants the GEORGIA INSTITUTE OF TECHNOLOGY ("GIT") and the GEORGIA TECH RESEARCH CORPORATION ("GTRC") the absolute and irrevocable right and permission, in respect to the photographs, video tapes, motion pictures, recordings, or any other media (hereinafter collectively known as "Images") that GIT/GTRC has taken of me or my property, or minors in my care, or in which I may be included with others, to copyright the same, in GIT/GTRC's own name or otherwise, to use, re-use, publish, and re-publish the same in whole or in part, individually or in conjunction with other images, and in conjunction with any printed or electronic matter, in any and all media now or hereafter known, and for any legitimate purpose whatsoever, and to use my name in connection therewith if GIT/GTRC so chooses. I hereby waive any right to inspect or approve the Images or any finished version incorporating the same.

The undersigned does hereby release and forever discharge GIT, GTRC, and the Board of Regents of the University System of Georgia, their members individually, and their officers, agents, and employees of any kind from all claims, demands, rights, and causes of action of whatever kind or nature, arising from and by reason of any and all known and unknown, foreseen, and unforeseen injuries, damages, and the consequences thereof resulting from the use of the Images, including without limitation any and all claims for libel or invasion of privacy.

I understand that the acceptance of this release and waiver of liability by the Board of Regents of the University System of Georgia shall not constitute a waiver, in whole or in part, of sovereign immunity by said Board, its members, officers, agents, and employees.

This authorization and release shall also inure to the benefit of the heirs, legal representatives, licensees, and assigns of GIT, GTRC, and the Board of Regents of the University System of Georgia. I hereby certify that I am suffering under no legal disabilities and that I have read the above carefully before signing. This release shall be binding upon me and my heirs, legal representatives, and assigns. By signing below, I agree to the terms stated above and hereby certify that I am 18 years of age or older.

MENG KANG
Name (Print)

4124 W. CARROUSEL LANE, PEORIA, IL 61615
Address

309-256-6020
Phone Number

Meng Kang / 5/20/08
Signature/Date

Jenna Tomlinson 5/20/08
Witness/Date

LICENSE TO PUBLISH

Manuscript: **MDITR Review of Undergraduate Research** ("the Journal")

Title of the contribution: _____ ("the Contribution)

Author(s): MENG KANG ("the Authors")

To: University of Washington Science and Technology Center Materials and Devices for Information Technology Research ("STC")

1. In consideration of STC agreeing to publish the Contribution, the Authors grant to STC for the full term of copyright in the Contribution and any extensions thereto, subject to clause 2 below, the license (a) to publish, reproduce, distribute, display and store the Contribution in all forms, formats and media (including without limitation in print, digital and electronic form) throughout the world; (b) to create adaptations, summaries or extracts of the Contribution or other derivative works based on the Contribution and exercise all of the rights set forth in (a) above in such adaptations, summaries, extracts and derivative works; and (c) to license others to do any or all of the above.

2. Ownership of copyright remains with the Authors and the Authors retain the following non-exclusive rights:

a) To reproduce the Contribution in whole or in part in any work of which they are the author(s);
b) To grant the right to reproduce the Contribution to any academic institution where they work; and
c) To post a copy of the Contribution on the Authors' own web site.

3. The Authors warrant and represent that:

a) The Authors are the sole authors of and sole owners of the copyright in the Contribution. If the Contribution includes materials of others, the Authors have obtained the permission of the owners of the copyright in all such materials to enable them to grant the rights contained herein. Copies of all such permissions are attached to this license.
b) The Author who has signed this Agreement has full right, power and authority to enter into this Agreement on behalf of all of the Authors.
c) Nothing in the Contribution is obscene, defamatory, libelous, violates any right of privacy or infringes any intellectual property rights (including without limitation copyright, patent or trademark) or any other rights of any person or entity or is otherwise unlawful.
d) Nothing in the Contribution infringes any duty of confidentiality which any of the Authors may owe to anyone else or violates any contract, express or implied, of any of the Authors, and all of the institutions in which work recorded in the Contribution was carried out have authorized publication of the Contribution.

This Agreement, and the rights and liabilities of the parties with respect to this Agreement and its subject matter, shall be governed by the laws of the State of Washington, without reference to the principles of conflicts of laws thereof.

Signed for and on behalf of the Authors Meng Kang

Date 5/20/08

Please print name MENG KANG

Mailing address (to send hardcopy of Publication) 4124 W. CARROUSEL LANE,
PEORIA, IL 61615

REU 2004

VITA

SAN-HUI CHI

San-Hui Chi was born in Taichung City, Taiwan, Republic of China. She attended Stella Matutina Girls' High School (Taichung City, Taiwan) from 1989-1995, received a B.S. in Chemistry from National Tsing Hua University (Hsinchu City, Taiwan) in 1999, and a M.S. in Chemistry from National Tsing Hua University (Hsinchu City, Taiwan) in 2001. She worked as an engineer of process and production technology in Taiwan Semiconductor Manufacturing Company (TSMC, Hsinchu City, Taiwan) in 2001 and as a research associate with Prof. I-Chia Chen in the Department of Chemistry, National Tsing Hua University (Hsinchu City, Taiwan) from 2001-2003. In 2003, she came to Georgia Tech to pursue a doctorate in Chemistry.